



Deposited via The University of Sheffield.

White Rose Research Online URL for this paper:

<https://eprints.whiterose.ac.uk/id/eprint/218457/>

Version: Published Version

Article:

Aad, G., Aakvaag, E., Abbott, B. et al. (2024) Search for low-mass resonances decaying into two jets and produced in association with a photon or a jet at $s = 13\text{TeV}$ with the ATLAS detector. *Physical Review D*, 110. 032002. ISSN: 2470-0010

<https://doi.org/10.1103/physrevd.110.032002>

Reuse

This article is distributed under the terms of the Creative Commons Attribution (CC BY) licence. This licence allows you to distribute, remix, tweak, and build upon the work, even commercially, as long as you credit the authors for the original work. More information and the full terms of the licence here:


<https://creativecommons.org/licenses/>

Takedown

If you consider content in White Rose Research Online to be in breach of UK law, please notify us by emailing eprints@whiterose.ac.uk including the URL of the record and the reason for the withdrawal request.

Search for low-mass resonances decaying into two jets and produced in association with a photon or a jet at $\sqrt{s} = 13$ TeV with the ATLAS detector

G. Aad *et al.**
(ATLAS Collaboration)

 (Received 14 March 2024; accepted 5 June 2024; published 2 August 2024)

A search is performed for localized excesses in the low-mass dijet invariant mass distribution, targeting a hypothetical new particle decaying into two jets and produced in association with either a high transverse momentum photon or a jet. The search uses the full Run 2 data sample from LHC proton-proton collisions collected by the ATLAS experiment at a center-of-mass energy of 13 TeV during 2015–2018. Two variants of the search are presented for each type of initial-state radiation: one that makes no jet flavor requirements and one that requires both of the jets to have been identified as containing b -hadrons. No excess is observed relative to the Standard Model prediction, and the data are used to set upper limits on the production cross section for a benchmark Z' model and, separately, for generic, beyond the Standard Model scenarios which might produce a Gaussian-shaped contribution to dijet invariant mass distributions. The results extend the current constraints on dijet resonances to the mass range between 200 and 650 GeV.

DOI: [10.1103/PhysRevD.110.032002](https://doi.org/10.1103/PhysRevD.110.032002)

I. INTRODUCTION

The Standard Model of particle physics (SM) successfully describes a wide range of phenomena across many orders of magnitude of energy at colliders, astrophysical observatories, and other experiments [1]. Nevertheless it fails to account for many observed phenomena, such as the presence of dark matter (DM) [2–4] and the imbalance of matter over antimatter in the observable universe [5]. While there are a wide range of proposed models of physics beyond the SM (BSM) to explain these effects [6–17], this paper focuses on a search for a hadronically decaying resonance.

Z' bosons are hypothetical spin-1 vector bosons that are singlets under electric and color charge [1], predicted in a variety of BSM models as a potential mediator to dark matter particles [14,17–22]. Direct Z' searches have shown to be an effective way of constraining BSM models [19–21]. Searches at the Large Hadron Collider (LHC) for Z' decays into pairs of charged leptons set strong constraints [21,23], but may be eluded by choosing the couplings of the Z' such that it is *leptophobic*, meaning it does not couple to

SM leptons. However, constraints from searches for hadronically decaying Z' resonances cannot be avoided in this way, since the same Z' - q - q decay vertex would also be responsible for Z' production at the LHC for any kind of resonance or search for topologies with a single reconstructed object recoiling against a large missing transverse energy. Additionally, the Z' - q - q vertex would be necessary for the dark matter self-annihilation cross section that drives the relic-density for weakly interacting massive particles [2].

The ATLAS and CMS Collaborations at the LHC have published several searches that are sensitive to hadronic Z' production using a variety of strategies. Searches for excesses in the invariant mass of the two jets with the highest transverse momentum (p_T) in the event constrain Z' production at high masses [24–38]. The lower reach of these searches are limited by the bandwidth available to single- and multijet triggers, and so different strategies must be used to gain sensitivity to Z' masses below around twice the p_T threshold where these triggers become fully efficient, around 1 TeV. One strategy is to record only minimal information, but at a higher rate than the standard triggers, enabling lower trigger thresholds [31,39]. A complementary approach, explored in this paper, relies on the production of high- p_T initial-state-radiation (ISR), such as a jet or a photon, which recoils against the Z' , enabling access to lower dijet masses without trigger bias. This type of search was performed by the ATLAS and CMS Collaborations in topologies where the two Z' decay

*Full author list given at the end of the article.

Published by the American Physical Society under the terms of the [Creative Commons Attribution 4.0 International license](https://creativecommons.org/licenses/by/4.0/). Further distribution of this work must maintain attribution to the author(s) and the published article's title, journal citation, and DOI. Funded by SCOAP³.

products can be resolved as individual jets [40,41] and the case where the decay products are sufficiently boosted to be reconstructed into a single large-radius jet [42–46].

This paper explores the resolved case, where the resonance decay products are reconstructed into two jets, covering a resonance mass range of 200 to 650 GeV. In total, four different channels are studied, based on the type of ISR particle and the flavor composition of the Z' decay products. The first channel, γjj , selects events in which the ISR is a photon and applies an inclusive selection on the jets that form the Z' . The second channel, γbb , focuses on the case where the ISR is a photon and both jets are identified as containing b -hadrons (b -tagged). The third and fourth channels focus on the case where the ISR is a jet, both in the inclusive case (jjj), and the case where both jets from the candidate resonance decay are b -tagged (jbb). While b -tagging requirements impose assumptions on the Z' decay products, they also provide significant background suppression, resulting in a more powerful search for some models. The cross sections for the jjj and jbb processes are higher than for γjj and γbb . However, the jjj channel has the additional challenge of identifying which jets might correspond to the Z' decay products, and which correspond to the ISR. Furthermore, different trigger thresholds apply for recorded events triggered by a photon or a jet. Hence a different kinematic acceptance is imposed on the ISR object for the various channels. The two channels where the ISR is a photon are collectively called the *photon* channels, while the two where the ISR is a jet are referred to as the *trijet* channels.

In addition to the increased luminosity, this analysis features several improvements over the previous analysis targeting the same signature [40], including a better b -tagging algorithm that reduces the background and the inclusion of the trijet channels. The dominant backgrounds for this search are multijet and single-photon production, which are estimated from data using a functional form fit to the m_{jj} distribution. For each channel, estimates for background and signal are combined into a likelihood function, where the signal yields are controlled by a free multiplicative parameter. The signal is interpreted as either a Z' boson or a generic narrow resonance producing a Gaussian-shaped bump in the measured mass spectrum.

The paper is organized as follows. The ATLAS detector at the LHC and the data and simulated samples used in this search are described in Secs. II–III. The object and event selection for the four channels are summarized in Sec. IV. The methodology of the search is introduced in Sec. V and the systematic uncertainties are discussed in Sec. VI. The results are presented in Sec. VII and conclusions are drawn in Sec. VIII.

II. THE ATLAS DETECTOR

The ATLAS detector [47] at the LHC covers nearly the entire solid angle around the collision point.¹ It consists of an inner tracking detector surrounded by a thin superconducting solenoid, electromagnetic and hadron calorimeters, and a muon spectrometer incorporating three large superconducting air-core toroidal magnets.

The inner-detector system is immersed in a 2 T axial magnetic field and provides charged-particle tracking in the range of $|\eta| < 2.5$. The high-granularity silicon pixel detector covers the vertex region and typically provides four measurements per track, the first hit normally being in the insertable B-layer installed before Run 2 [48,49]. It is followed by the silicon microstrip tracker, which usually provides eight measurements per track. These silicon detectors are complemented by the transition radiation tracker (TRT), which enables radially extended track reconstruction up to $|\eta| = 2.0$. The TRT also provides electron identification information based on the fraction of hits (typically 30 in total) above a higher energy-deposit threshold corresponding to transition radiation.

The calorimeter system covers the pseudorapidity range $|\eta| < 4.9$. Within the region $|\eta| < 3.2$, electromagnetic calorimetry is provided by barrel and end cap high-granularity lead/liquid-argon (LAr) calorimeters, with an additional thin LAr presampler covering $|\eta| < 1.8$ to correct for energy loss in material upstream of the calorimeters. Hadron calorimetry is provided by the steel/scintillator-tile calorimeter, segmented into three barrel structures within $|\eta| < 1.7$, and two copper/LAr hadron end cap calorimeters. The solid angle coverage is completed with forward copper/LAr and tungsten/LAr calorimeter modules optimized for electromagnetic and hadronic energy measurements respectively.

The muon spectrometer comprises separate trigger and high-precision tracking chambers measuring the deflection of muons in a magnetic field generated by the superconducting air-core toroidal magnets. The field integral of the toroids ranges between 2.0 and 6.0 T m across most of the detector. Three layers of precision chambers, each consisting of layers of monitored drift tubes, cover the region $|\eta| < 2.7$, complemented by cathode-strip chambers in the forward region, where the background is highest. The muon trigger system covers the range $|\eta| < 2.4$ with

¹ATLAS uses a right-handed coordinate system with its origin at the nominal interaction point (IP) in the center of the detector and the z -axis along the beam pipe. The x -axis points from the IP to the center of the LHC ring, and the y -axis points upward. Cylindrical coordinates (r, ϕ) are used in the transverse plane, ϕ being the azimuthal angle around the z -axis. The pseudorapidity is defined in terms of the polar angle θ as $\eta = -\ln \tan(\theta/2)$. Angular distance is measured in units of $\Delta R \equiv \sqrt{(\Delta y)^2 + (\Delta \phi)^2}$, where $y = (1/2)[(E + p_z)/(E - p_z)]$ is the object's rapidity defined by its energy and longitudinal momentum.

resistive-plate chambers in the barrel, and thin-gap chambers in the end cap regions.

Interesting events are selected by the first-level trigger system implemented in custom hardware, followed by selections made by algorithms implemented in software in the high-level trigger [50]. The first-level trigger accepts events from the 40 MHz bunch crossings at a rate below 100 kHz, which the high-level trigger further reduces to record events to disk at about 1 kHz.

An extensive software suite [51] is used in data simulation, in the reconstruction and analysis of real and simulated data, in detector operations, and in the trigger and data acquisition systems of the experiment.

III. DATA AND MONTE CARLO SIMULATED SAMPLES

This analysis is performed using data from proton-proton (pp) collisions at $\sqrt{s} = 13$ TeV at the LHC, collected during 2015–2018 with the ATLAS detector. The total integrated luminosity of this data sample is 140 fb^{-1} [52], obtained using the LUCID-2 detector [53] for the primary luminosity measurements. Due to the high instantaneous luminosity and the large total inelastic pp cross section, there are, on average, 33.7 collisions in each bunch crossing. The additional collisions not selected as the hard-scatter process are referred to as pileup collisions. Data in this analysis are required to satisfy standard quality requirements [54].

Samples of Monte Carlo (MC) simulated signal and background events are used in this analysis for optimization, estimate of possible signal contributions, and validation of background estimation strategies.

The main benchmark model is a simplified leptophobic Z' axial-vector mediator signal, which is used to test the sensitivity to potential resonant signals. The choice of this benchmark signal is motivated by the role that dijet resonance searches play in constraining possible interactions between dark matter and SM particles. This simplified model considers an s -channel mediator with axial-vector interactions, as described in Refs. [18,55]. Two relevant parameters of this model in the dijet search are the Z' mass, and the coupling of the Z' to quarks (g_q), which affect the intrinsic width of the resonance. The mass of the dark matter fermion is set to be much heavier than the Z' mass, such that the decay width into dark matter is zero. In all channels, signal samples are generated for Z' masses between 200 and 650 GeV, with the coupling of the mediator to non-top-quarks set to 0.2, regardless of the quark flavor. Such a choice for the coupling value is a benchmark model already used in other analyses [40]. Also, given the Z' intrinsic width for $g_q = 0.2$ is much smaller than the experimental resolution, such a sample is adequate to also model the shape of signals with slightly different or smaller g_q values. Signal samples are generated separately for a Z' decaying into u, d, s

and c quark flavors and Z' decaying into b -quarks, in order to enhance the signal statistical precision for the b -tagged channels.

The signal samples are simulated using the MadGraph generator [56] at leading-order (LO) in perturbative quantum chromodynamics (QCD) with the NNPDF[2.3lo] parton distribution function (PDF) set [57]. The events are interfaced to PYTHIA8.244 [58,59] to model the parton shower, hadronization, and underlying event, with parameter values set according to the A14 tune [60]. EvtGen [61] is used to model decays of heavy flavor hadrons. To further increase statistical precision in the γjj channel, a generator-level filter is applied on the photon p_T . Two sets of samples are produced: one set with this filter defined to be $p_{T,\gamma} \geq 130$ GeV and a second with the filter at $p_{T,\gamma} \geq 65$ GeV. For the trijet channels, a generator-level jet filter of 370 GeV is applied on the leading- p_T $R = 0.4$ jet, which is fully efficient for the reconstructed jet p_T threshold. The generator-level filters are chosen based on the triggers used in the two different analyses, to ensure high statistical precision for each mass point without introducing kinematic biases.

While the final background estimate is performed using a data-driven approach, background multijet and photon-plus-jets samples are used to optimize the event selection and validate the background estimation strategy. For the photon channels, prompt single-photon production is simulated with the Sherpa[2.2] [62] generator. In this arrangement and thanks to the Comix [63] and OpenLoops [64–66] libraries, matrix elements for up to two partons are calculated to next-to-leading-order (NLO) accuracy, while matrix elements for up to four partons are calculated at LO in QCD. They are matched with the Sherpa parton shower [67] using the MEPS@NLO prescription [68–71] with a dynamic merging scale cut [72] of 20 GeV. Photons are required to be isolated according to a smooth-cone isolation criterion [73]. Samples are simulated using the NNPDF[3.0nnlo] PDF set [74], along with the dedicated set of tuned parton-shower parameters developed by the Sherpa authors.

For the trijet channels, background samples of simulated multijet processes are generated using PYTHIA 8.230 with the $2 \rightarrow 2$ matrix element, and additional jets are produced through the parton shower. Events are simulated using the A14 tune [60], the Lund string hadronization model and the NNPDF2.3lo PDF set. The PYTHIA parton shower algorithm uses a dipole-style p_T -ordered evolution, and its renormalization and factorization scales are set to the geometric mean of the squared transverse masses of the outgoing particles.

The generated background and signal events are passed through a detailed detector simulation [75] based on Geant4 [76]. Additional minimum-bias interactions simulated using PYTHIA8 with the A3 tune [77] and the NNPDF[2.3lo] PDF set [57] are overlaid to the background and signal events, to model pileup interactions. The distribution of the average

number of pileup interactions in simulation is reweighted during data analysis to match that observed in Run 2 data.

IV. EVENT RECONSTRUCTION AND SELECTION

A. Object reconstruction

While the four different channels use different combinations of objects, the object reconstruction is standardized across all of the different channels. Three different objects are used: jets, b -tagged jets, and photons.

Selected events are required to contain a primary vertex with at least two associated tracks with transverse momentum $p_T > 0.5$ GeV [78]. The vertex with the highest sum of p_T^2 of the associated tracks is taken as the primary vertex.

Jets in this analysis are reconstructed from particle flow objects [79] using the anti- k_r algorithm [80] as implemented in FastJet [81], using a jet radius parameter $R = 0.4$. The ATLAS particle flow algorithm combines measurements from the ATLAS inner detector and calorimeter systems [82] to improve the jet energy resolution, reduce sensitivity to pileup effects, and improve jet reconstruction efficiency, especially at low jet p_T . The jet energy scale of particle flow jets is calibrated with a combination of simulation-based and *in situ* corrections [83]. Calibrated jets are required to have a $p_T > 25$ GeV and satisfy $|\eta| < 2.5$. To reduce the effects of pileup, jets with $p_T < 60$ GeV and $|\eta| < 2.4$ are required to satisfy the “tight” working point of the jet vertex tagger criteria [84], which selects jets originating from the selected primary vertex. A set of quality criteria is also applied to reject events containing at least one jet arising from noncollision sources or detector noise [85].

Reconstructed jets are b -tagged using the DL1r multivariate algorithm [86]. Jets are considered b -tagged if they satisfy the 77% b -tag efficiency working point, as measured in inclusive $t\bar{t}$ events. The corresponding rejection factors for gluon/light-quark jets and charm-quark jets are approximately 200 and 5, respectively. This working point was found to result in optimal signal sensitivity for both the γbb and jbb channels.

Photons are reconstructed from energy deposits in the electromagnetic calorimeter [87]. Reconstructed photon candidates are required to have $p_T > 25$ GeV, and only central photons with $|\eta| < 2.5$ are considered, excluding the barrel/end cap calorimeter transition region ($1.37 < |\eta| < 1.52$). Only photons that satisfy the *tight* identification requirement are considered, and additional *tight* isolation requirements are imposed to further suppress contamination from jets [87].

An overlap removal procedure is applied to avoid any double-counting between the reconstructed photons and jets, by removing any jet with an angular distance $\sqrt{\Delta\eta^2 + \Delta\phi^2} < 0.4$ to any photon.

B. Photon channel selection

The two photon channels (γjj and γbb) are required to satisfy the single-photon trigger [88] with the lowest threshold where all events passing it are saved (unprescaled), and a single photon with $p_T > 150$ GeV is required in order for the trigger selection to be fully efficient. In addition, the event is required to have two reconstructed jets passing the selection in Sec. IV A, and the two highest- p_T (leading) jets are used to reconstruct the resonance candidate. Several dijet and γ -jet kinematic variables were studied to enhance the $Z' \rightarrow q\bar{q}$ signal over the expected background, and the strongest discriminating variable was found to be the asymmetry $y^* = \frac{|y_1 - y_2|}{2}$, where y_1 and y_2 are the rapidities of the two selected jets. It is expected that a signal from Z' production produces isotropic jets while forward jets are more common in background events, causing the signal to have smaller values of y^* than the background. The shape of the y^* variable is found to be well described by the background simulation, with maximum differences of a few percent. A cut of $y^* < 0.825$ is applied to maximize the signal sensitivity across the different mass ranges. For the γbb channel, in addition to satisfying the selection for the γjj channel, the two leading jets in the event are required to satisfy the b -tagging requirements described in Sec. IV A.

C. Trijet channel selection

In both the jjj and jbb channels, events are required to have at least three reconstructed jets, where the leading jet is required to be above 475 GeV to be fully efficient for the lowest unprescaled single jet trigger [89]. When considering only the three leading- p_T jets in a given event, there are three possible choices to assign two jets as corresponding to the resonance decay product candidates.² In the case where the resonance decays into two b -quarks, the combinatorial problem can be in principle trivially solved by identifying the two b -tagged-jets in the event. While possible, this causes challenges in background modeling, and so this trivial solution is not used. To illustrate the combinatorial problem more clearly, Fig. 1 shows the particle-level dijet mass spectrum of different jet pairs for three different Z' signal samples. Each jet is assigned a number based on its p_T ordering, e.g., m_{12} is the dijet mass distribution (m_{jj}) of the leading and subleading jets. For lower Z' mass, the m_{23} contribution clearly peaks near the Z' mass, while at higher Z' mass, contributions from m_{13} become more important.

The combinatorial challenge is further complicated by the background estimate, which relies on a functional fit to a smoothly falling m_{jj} spectrum, meaning that any additional selection to solve the combinatorial problem must

²While a fourth jet can contribute, it is typically not the dominant contribution, and so it is not considered, to simplify the combinatorics.

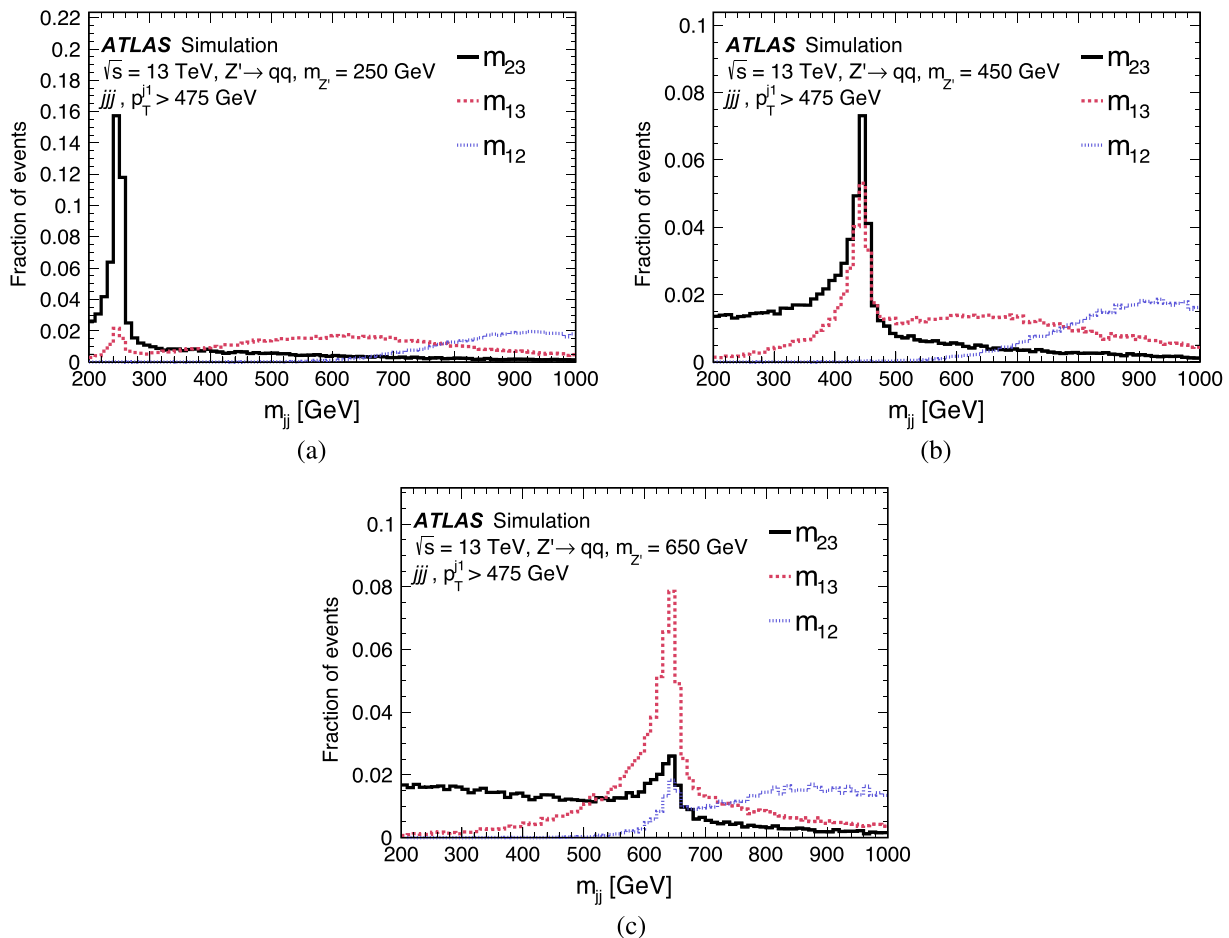


FIG. 1. Distributions of particle-level dijet mass in simulated $Z' \rightarrow qq$ events corresponding to different combinations of two jets, where jets 1,2 and 3 correspond to the leading, subleading and third-leading jets. Signal events generated with (a) $m_{Z'} = 250$ GeV, (b) $m_{Z'} = 450$ GeV, and (c) $m_{Z'} = 650$ GeV are shown.

also result in a smooth m_{jj} spectrum. The dominant background for these channels may be simplistically modeled as balanced high- p_T dijet events where one jet emits a softer jet, resulting in a trijet event. Since the emitting jet loses some energy to its emission, the three jets are roughly p_T ordered from low to high as the emitted jet, the emitting jet, and the nonemitting jet, it is possible to roughly map m_{23} to $m_{\text{emitted,emitting}}$, m_{13} to $m_{\text{nonemitting,emitted}}$ and m_{12} to $m_{\text{nonemitting,emitting}}$. In reality, this description of the background does not fully describe the observed background. Multiple emissions may occur, and various detector effects can spoil the p_T balance of the reconstructed jets, meaning that the assumption that m_{23} corresponds to the mass of the emitting and emitted jet may not hold in some events.

The mass spectra of the three possible pairings have different shapes, since different underlying physics contributes to each of them. This is illustrated in Fig. 2(a), which shows the m_{jj} distribution for m_{12} , m_{13} , and m_{23} distributions. Any generic combination of the different pairings will result in nonsmoothness in the spectrum,

roughly corresponding to the turn-ons in these different pairings. Hence instead of pairing jets based solely on p_T -ordering, a different pairing method based on the kinematics of the three leading jets need to be used in the analysis.

Three similar options for choosing the dijet pairing were compared to determine which one results in the smoothest spectrum, each roughly corresponding to the mass of the emitting and emitted jet: the second- and third-leading jets (as described above), the jet pair with the minimum $|\Delta\phi|$, and the pair of jets with the lowest mass. The smoothness of the m_{jj} spectrum at low masses determines the fit range therefore limiting the lowest Z' mass reach covered by the search. The signal efficiencies of these three m_{jj} selection options are similar. However, selecting jet pairs with the minimum $|\Delta\phi|$ between them results in the smoothest low-mass spectrum in studies of multijet MC simulation.

One final aspect to consider is that in dijet-like topologies, where one of the high- p_T jets radiates a low- p_T gluon reconstructed as a jet, the gluon radiation tends to happen at small angles, while the two high- p_T jets are produced back-to-back. This means that the $|\Delta\phi|$ selection

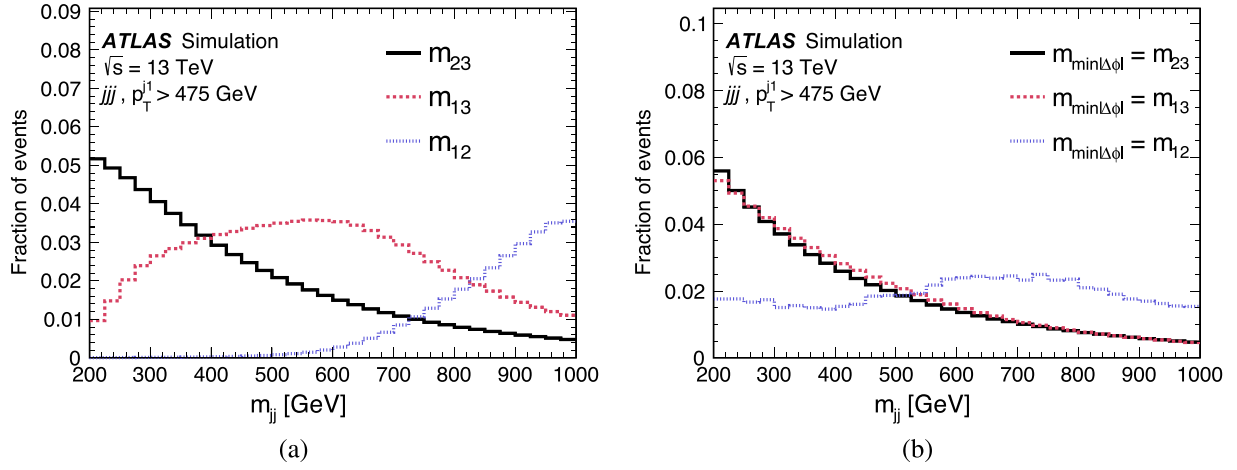


FIG. 2. (a) Distributions of reconstructed dijet mass in simulated background events corresponding to different combinations of two jets, where jets 1,2 and 3 correspond to the leading, subleading and third-leading jets, and (b) comparison of the shape of the normalized selected dijet m_{jj} spectra in the case where the selected jets are the second and third leading jets ($m_{\min|\Delta\phi|} = m_{23}$), the first and third leading jets ($m_{\min|\Delta\phi|} = m_{13}$), or the first and second leading jets ($m_{\min|\Delta\phi|} = m_{12}$). Events are simulated with PYTHIA.

tends to identify the radiating jet and the gluon. Depending on which jet radiates the gluon, this selection can identify either the second- and third-leading jets or the first- and third-leading jets. In a small fraction of events, the $|\Delta\phi|$ selection identifies the two leading jets in the events as trijets, but where the underlying topological assumptions break down. These events, comprising around 0.2% of background events, do not produce a smooth m_{jj} spectrum, as shown in Fig. 2(b). Based on this, events where the $|\Delta\phi|$ selection identifies the two leading jets are rejected to avoid biasing the fit.

To summarize, the algorithm selected to identify the Z' decay candidates takes the jet pair with the minimum $|\Delta\phi|$ between them and rejects the event if such jets correspond to the two p_T -leading jets. The pair of jets passing such requirements are referred to as the *selected jets* and, as explained above, produces the smoothest low-mass spectrum in studies of multijet MC simulation. No additional background suppression is applied, since cuts on observables such as y^* can sculpt the background distribution. For the jbb channel, in addition to passing the same jet requirements as the j_{jj} channel, the two jets with the minimum $|\Delta\phi|$ between them are also required to be b -tagged.

The resulting signal m_{jj} distributions after the event selection are shown for each channel in Fig. 3. The j_{jj} channel, at higher masses, has a clear tail in the m_{jj} distribution resulting from the incorrect selection of the dijet pair. This tail is less pronounced for the jbb channel, owing to the additional b -tagging requirement imposed on the selected jets. The signal efficiency for the jbb selection gets smaller at high masses, as the selected dijet pair is often not b -tagged there. Such an effect is considered less relevant than obtaining a smoothly falling m_{jj} distribution

for the background at lower m_{jj} values, as the more energetic part of the m_{jj} spectrum is better studied by other analyses [31,39].

V. METHODOLOGY

The numbers of signal and background events are estimated channel-by-channel by binned profile likelihood fits of a signal-plus-background model to the measured m_{jj} distributions. The number of selected events as a function of m_{jj} is parametrized in the fit as

$$n_{\text{tot}}(m_{jj}) = n_S \times f_S(m_{jj}) + n_B \times f_B(m_{jj}),$$

where n_S and n_B are the number of signal and background events, respectively, and $f_S(m_{jj})$ and $f_B(m_{jj})$ are their probability distribution functions. All the distributions entering the fit are binned finely in bins of 1 GeV width, to minimize the loss of information and the typical biases of binned likelihood fits [90].

A. Signal templates

The likelihood fit results are interpreted using model-independent and model-dependent strategies. For the model-independent limits, the signal probability distribution functions are taken as Gaussian distributions, with a mean equal to the resonance mass, with widths ranging from 5% to 15%. The upper end of the template width is determined based on the results of the spurious signal test and signal injection test described in Sec. V B.

For the model-dependent limits, the shape of the m_{jj} distributions from simulated samples are used directly. Signal samples are produced with a limited set of signal masses, and these templates are used as inputs to an

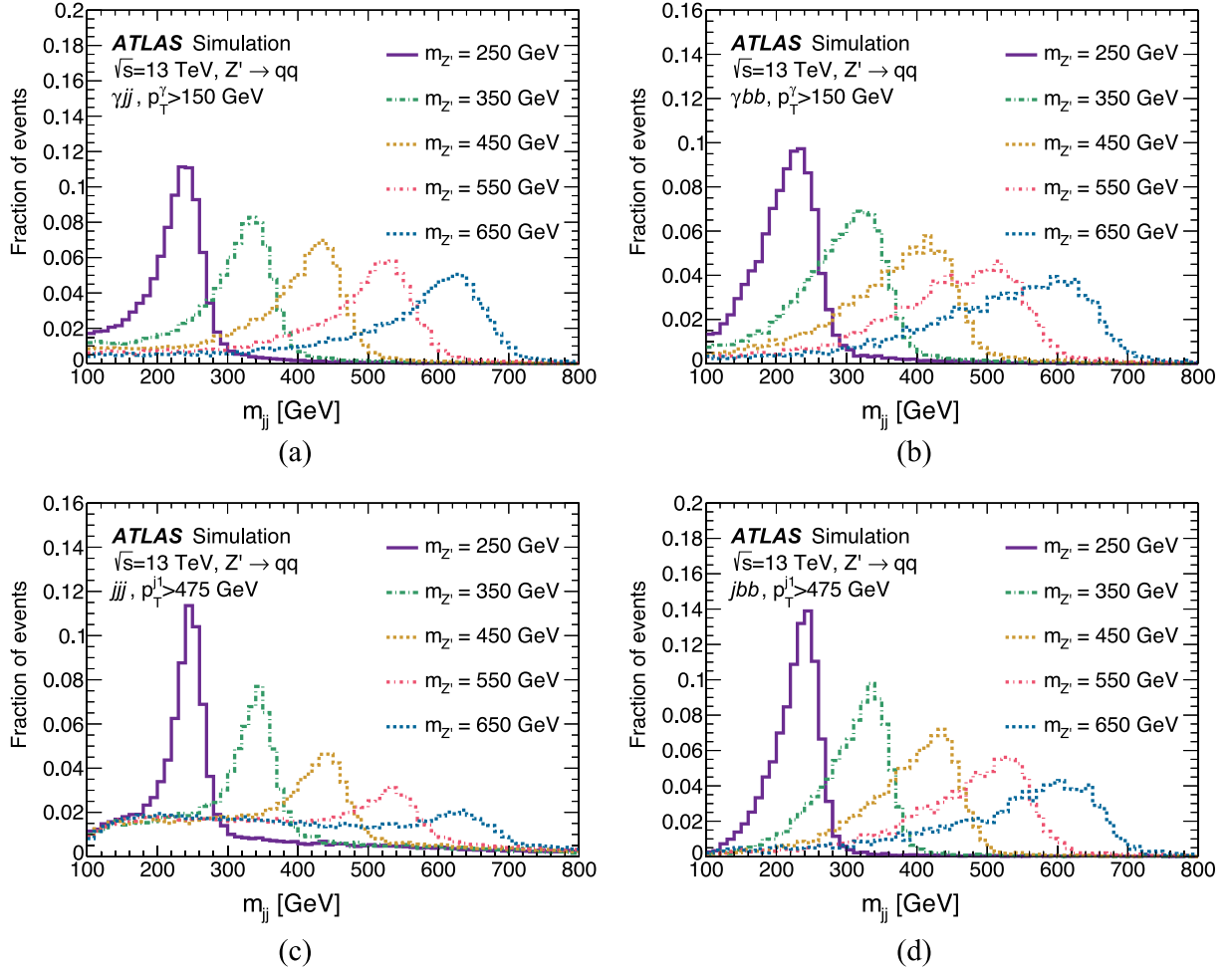


FIG. 3. Distributions of reconstructed dijet mass in simulated $Z' \rightarrow qq$ events with different $m_{Z'}$ values in the (a) γjj , (b) γbb , (c) jjj , and (d) jbb channels after full event selection.

interpolation between mass points to provide a finer signal grid using the method described in Ref. [91].

B. Background estimate

The selected jets in nonresonant QCD processes, which constitute the SM background for this search, result in dijet systems with smoothly-falling invariant mass distributions. In order to estimate this background in the search regions, a class of parametric functions is fit to the m_{jj} distributions:

$$f_B(x) = p_1(1-x)^{p_2} x^{p_3+p_4 \ln(x)+p_5 \ln^2(x)+p_6 \ln^3(x)},$$

where $x = m_{jj}/\sqrt{s}$, and p_1, p_2, p_3, p_4, p_5 , and p_6 are the fitted parameters. For an N -parameter fit, only the first N parameters are allowed to vary, while the higher- N terms are fixed to zero. Such functions were successfully used by a wide variety of dijet and multijet resonance searches by the CDF, CMS, and ATLAS Collaborations [25,27,32,34,92–97].

The data-driven background fitting procedure employs a 5-parameter function and was validated using several cross-checks, including spurious signal tests and signal injection tests. These tests were performed using simulated samples, with a subset of checks performed on a partial data sample.

The spurious signal test evaluates whether the fitting procedure is biased such that it produces a nonzero extracted signal when fitting a data sample with no true signal. This test is performed using many pseudodata distributions which are generated from background-only fits to the simulated m_{jj} distribution with a 6-parameter function, which has more flexibility than the final fit function. Each distribution is tested by performing signal + background fits with a 5-parameter fit function and various signal hypotheses. Gaussian-shaped signals with widths ranging from 5 to 15% of the signal mean are tested, as well as using the signal templates from the Z' simulated samples directly. For each pseudodata distribution and signal hypothesis n_S is determined, and the median value and standard deviation of the n_S distribution are taken to be S_{spur} and σ_{spur} respectively. To satisfy the spurious signal

requirements, $S_{\text{spur}}/\sigma_{\text{spur}}$ is required to be less than 0.5 for every signal hypothesis mass point. This requirement is satisfied for all channels for Z' masses between 250 GeV and 650 GeV. While the fits extend to m_{jj} values beyond 650 GeV, higher signal masses do not always satisfy the spurious signal tests, and are not considered further. In addition, for the jjj channel, the signal shape degrades significantly at higher signal masses, since the selected jets often do not correspond to the resonance decay products. Finally, the jbb channel passes this requirement for resonance masses down to 200 GeV, which is possible since the m_{jj} spectrum in this channel is smooth down to lower masses than the other channels.

The signal injection test is performed to ensure that the fit is able to extract a signal component with the expected signal strength. Simulated signal models, with both Gaussian shapes and in a range of widths and signal templates, are included in the fitted background distribution with a given signal cross section selected to be in the range $0 - 5\sigma$, where $\sigma = n_S/\sqrt{n_B}$ and the number of signal and background events are determined using a 2σ window around the injected signal peak in each test. The injected signals in this study were extracted for pseudodata distributions, with the requirement that the median of the extracted significances is within 0.5σ of the injected significance, for all the signal hypotheses and mass points individually. These tests were satisfied for all channels for the same range of resonance masses and widths as with the spurious signal tests, while they failed for Gaussian-shaped signals with widths above 15%.

The fitted m_{jj} region is determined separately for each channel. For the chosen range, the fit quality, spurious signal, and signal injection tests are must be satisfied for the MC simulation. The fitted m_{jj} region is chosen to prioritize a fit that starts as low in m_{jj} as possible while maintaining a wide enough fit range to study the relevant signal models. The lowest part of the m_{jj} spectrum does not have a smoothly falling shape because of trigger inefficiency and analysis selection effects, such as the y^* cut, and such a behavior cannot be fit by the class of functions considered. The γjj and γbb channels are found to have a smoothly falling behavior starting from $m_{jj} = 200$ GeV, while the jjj and jbb channels from $m_{jj} = 225$ GeV and $m_{jj} = 160$ GeV respectively. The upper fit ranges are defined from the edges of bins defined by the m_{jj} resolution, and are taken to be the highest among those where the background fit functions to the simulated m_{jj} distributions have a $\chi^2 p$ -value above 0.05. The procedure to determine the fit range is repeated on the measured data, to ensure the fit ranges estimated from the MC simulation are adequate. If they are not, the upper limit of the fit range is reduced by one m_{jj} resolution bin, and all the tests are repeated.

For the γbb channel, the background estimate is further validated using an ABCD method with simulated samples,

following the strategy of Ref. [40]. Such method allows a test of the background estimate in the γbb channel with a higher statistical precision than available in the existing simulated sample and also serves as a test for potential biases in the m_{jj} spectrum introduced by b -tagging. The ABCD re-weighting method defines different regions based on whether events satisfy or fail to meet the y^* selection and the b -tagging requirements, providing an estimate for the b -tagged spectrum which is based on the untagged distribution. The ABCD-reweighted m_{jj} spectrum is found to be compatible with the one obtained by applying the γbb event selection, within the statistical precision of the reweighted and high-statistics spectrum. Given the level of agreement, no uncertainty related to b -tagging is considered to affect the background fit. The resulting distribution is found to satisfy the spurious signal and signal injection tests described above, providing further confirmation of the fit strategy. Since this method relies on the y^* selection, the technique cannot easily be applied to the jbb channel, but the conclusions on the possible b -tagging biases from γbb apply to the jbb channel as well.

VI. SYSTEMATIC UNCERTAINTIES

When interpreting the analysis in terms of candidate signal models, the impact of various experimental and theoretical sources of uncertainty is considered.

Luminosity. The uncertainty in the combined 2015–2018 integrated luminosity is 0.83% [52], obtained using the LUCID-2 detector [53] for the primary luminosity measurements. It is treated as a single normalization uncertainty applied as a scale factor to the signal models.

Jets. Systematic uncertainties in the $R = 0.4$ jet energy scale and resolution are evaluated using a series of *in situ* measurements and simulation-based techniques, thoroughly documented in Ref. [83]. The most significant source of uncertainty in the JES originates from uncertainties on the flavor of the jet. Uncertainties on the JVT are also included, but are negligible, since the uncertainties are applied only to the signal. For the photon channels, these uncertainties have a negligible impact on the efficiency, and around a 2% impact on the location of the Z' mass. For the trijet channels, the impact on the location of the Z' mass is around 1%, while the impact on the selection efficiency is around 3%.

Photons. The systematic uncertainties in the photon identification and isolation efficiencies are estimated following the prescriptions in Ref. [87]. They are evaluated by varying the correction factors for photon selection efficiencies in simulation by the corresponding uncertainties and affect the diphoton selection efficiency. The experimental uncertainties in the photon energy scale and resolution are obtained from Ref. [87], and are only applied to the γjj and γbb channels. These systematic uncertainties primarily impact the selection efficiency of the signal events, with a total impact on the efficiency of around 2%.

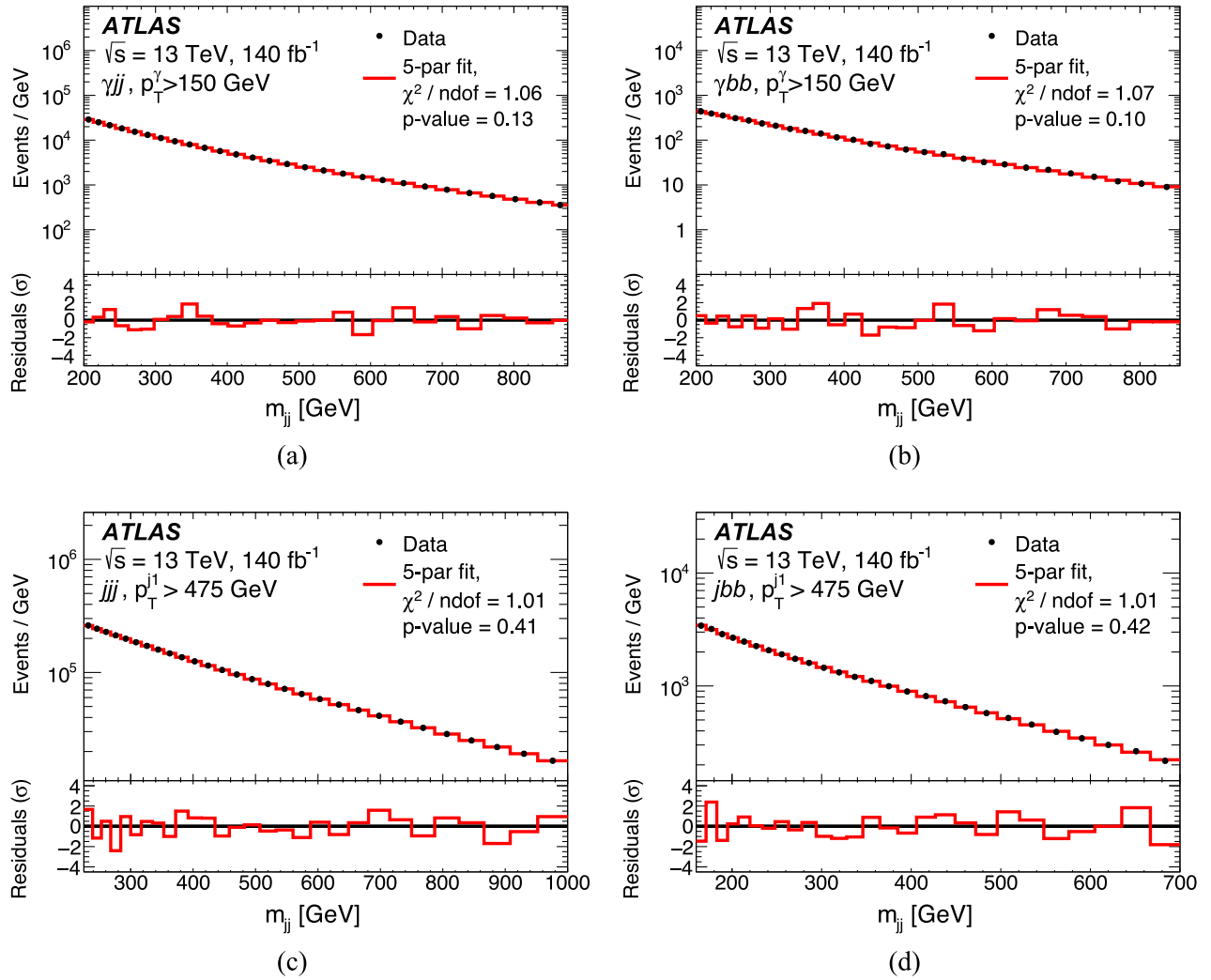


FIG. 4. Dijet invariant mass distributions data compared to the fitted background estimates for the (a) γjj , (b) γbb , (c) jjj , and (d) jbb channels. Bottom panel shows the fit residuals in terms of standard deviations (σ). The distributions are shown here with the m_{jj} resolution binning.

B-tagging. For final states with requirements on the number of b -tagged jets, additional systematic uncertainties are applied. The systematic uncertainty in the b -tagging efficiency is measured using data enriched in $t\bar{t}$ events for jet $p_T < 400 \text{ GeV}$ and extrapolated to higher p_T regions using a method similar to the one described in Ref. [98]. The impact of this systematic uncertainty in the efficiency of the event selection of signal events ranges from 2%–3%.

Parton distribution functions. The theoretical uncertainty envelope associated with the NNPDF[2.31_o] PDF set is propagated through the analysis, where their impact is primarily on the normalization of the signal events. The change in analysis selection efficiency is recalculated for each provided PDF variation, and the standard deviation of all such variations is taken as a measure of the systematic uncertainty due to PDFs. This uncertainty affects signal samples and ranges from 1%–5% across the different

channels, with larger effects on the photon channels than on the dijet channels.

Background modeling. A systematic uncertainty to cover potential biases in modeling the background shape is accounted for using the spurious signal S_{modeling} . The value of S_{modeling} is determined as the envelope of $|S_{\text{spur}}|$ over m_{jj} and is considered to cover features of the m_{jj} background spectrum which are not modeled by the background parametrization chosen. This is implemented in the likelihood fit as an additional signal contribution, such that

$$N_{\text{signal}}(m_{Z'}) = \sigma \times A \times BR \times \mathcal{L} + S_{\text{modeling}}(m_{Z'})\theta_{\text{modeling}},$$

where $N_{\text{signal}}(m_{Z'})$ is the number of extracted signal events at a given $m_{Z'}$, σ , A , BR , and \mathcal{L} are the signal cross section, acceptance, signal branching ratio, and integrated luminosity, respectively; and θ_{modeling} is a nuisance parameter

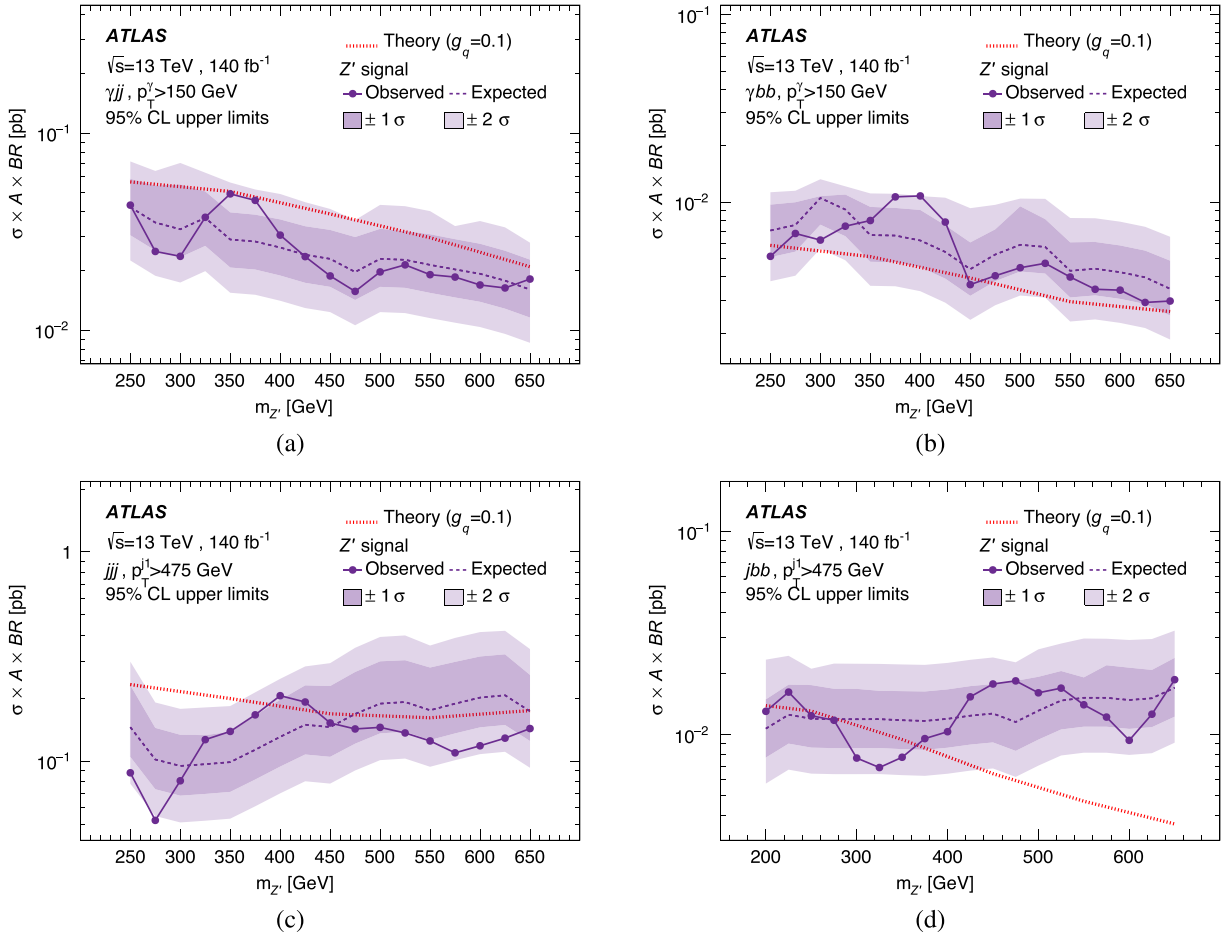


FIG. 5. Expected and observed 95% CL upper limits on the product of the cross section, acceptance and branching ratio ($\sigma \times A \times BR$) as a function of the Z' mass for the (a) γjj , (b) γbb , (c) jjj , and (d) jbb channels with the background and signal contributions modeled by a 5-parameter fit function and templates from the signal samples, respectively. Observed limits are indicated with markers and a solid line, and expected limits are indicated with a dashed line. The shaded bands around the expected limit indicates the (darker band) 1σ and (lighter band) 2σ uncertainty range. The dotted line represents the expected $\sigma \times A \times BR$ assuming $g_q = 0.1$, as obtained from the MadGraph signal samples.

associated with the background modeling uncertainty. The signal acceptance is defined as the fraction of simulated events at detector level that pass the analysis selection cuts.

The spurious signal uncertainty is found to be, together with the statistical uncertainty, the leading source of uncertainty on the extracted number of signal events.

VII. RESULTS

The dijet invariant mass distributions in data, together with the corresponding fitted background estimates, are shown in Fig. 4 for all four channels. The data are well described by the 5-parameter fit function in all channels, and the global χ^2 p -value ranges from 0.10 to 0.42 for the different channels. Fit ranges are chosen such that the fits satisfy the tests explained in Sec. VB. For the photon channels, the background fit spans the m_{jj} range of 200 to 875 GeV for the γjj channel and of 200 to 854 GeV for the

γbb channel, while for the jjj and jbb channels, the fit spans 225 to 1000 GeV and 160 to 700 GeV respectively.

The BumpHunter [99,100] algorithm, as implemented in pyBumpHunter [101,102], is used to measure the statistical significance of localized excesses of the measured data relative to the estimated background in the m_{jj} distributions, which could be due to the presence of resonant signals. This is done using mass bins with a bin width determined by the mass resolution of m_{jj} as a function of the mass, where the mass resolution is determined using a Gaussian function fit to the m_{jj} response distribution. Windows are allowed to have a width of up to three mass-resolution bins, hence corresponding to three times the m_{jj} resolution, and for each scanned window BumpHunter evaluates the statistical significance of the observed difference between the data distribution and the background fit. The BumpHunter p -value is defined as the smallest observed probability for the data in a given window to deviate from the background prediction by

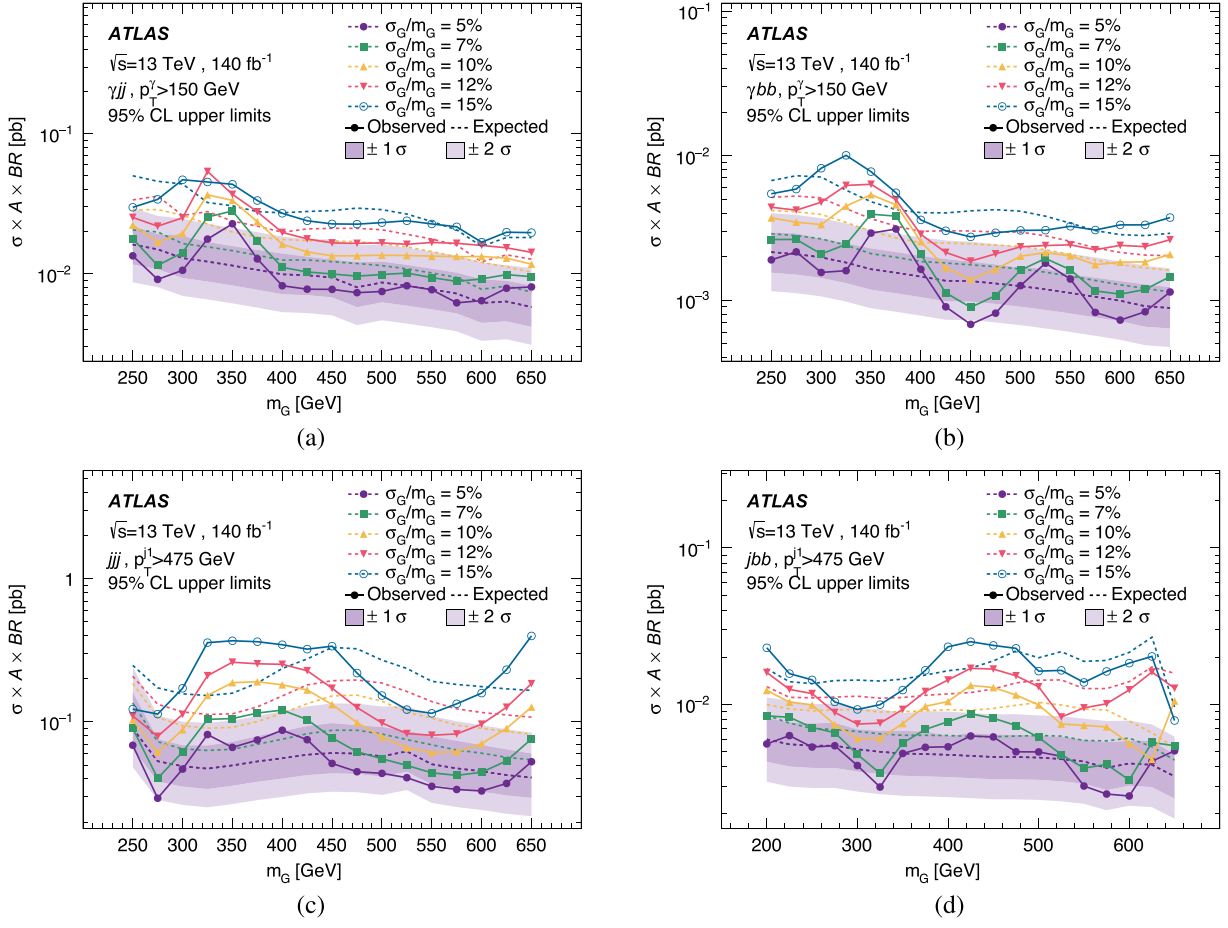


FIG. 6. Expected and observed 95% CL upper limits on the product of the cross section, acceptance and branching ratio ($\sigma \times A \times BR$) for the (a) γjj , (b) γbb , (c) jjj , and (d) jbb channels with the background and signal contributions modeled by a 5-parameter fit function and Gaussian distributed signal templates with a mass m_G and width σ_G , respectively. Observed limits are indicated with markers and a solid line, and expected limits are indicated with a dashed line. Observed and expected limits corresponding to different choices of template widths (5%, 7%, 10%, 12% and 15%) are indicated as different sets of markers or line styles, respectively. The shaded bands around the expected limit for templates with 5% width indicate the (darker band) 1σ and (lighter band) 2σ uncertainty range.

the observed amount due to a Poissonian fluctuation of the background, using pseudoexperiments generated from the background prediction, and without considering systematic uncertainties. The most significant localized excesses identified by the BumpHunter algorithm are found at 348 GeV with a local significance of 1.9σ for the γjj channel, at 380 GeV with a local significance of 1.8σ for the γbb channel, at 404 GeV with a local significance of 1.8σ for the jjj channel and at 522 GeV with a local significance of 1.5σ for the jbb channel.

As no significant deviation from the background expectation is observed, upper limits are set on the signal production rate as a function of the hypothesized resonance mass. The numbers of signal and background events are estimated from maximum-likelihood fits of the signal-plus-background models to the corresponding m_{jj} distributions. Systematic uncertainties described in Sec. VI are included in the fits via nuisance parameters constrained by Gaussian-distributed penalty terms. Systematic uncertainties affecting

the signal shape have only a small impact on the result, and the dominant uncertainties arise from the statistical and spurious signal uncertainties. The p -value is determined from a profile-likelihood-ratio-test statistic [103]. The local p -value for compatibility with the background-only hypothesis when testing a given signal hypothesis (p_0) is evaluated based on the asymptotic approximation [103]. Global significance values are computed from background-only pseudoexperiments to account for the trial factors due to scanning both the signal mass and the width hypotheses. The expected and observed 95% confidence level (CL) exclusion limits on the product of the cross section, branching ratio, and acceptance are computed using a modified frequentist-approach [104], in an asymptotic approximation to the test-statistic distribution [103].

Figure 5 shows the 95% CL upper limits on the $\sigma \times A \times BR$ of the Z' axial-vector dark-matter mediator as a function of its mass, derived using the signal templates. Results are interpolated linearly in the log of the cross section. Similar

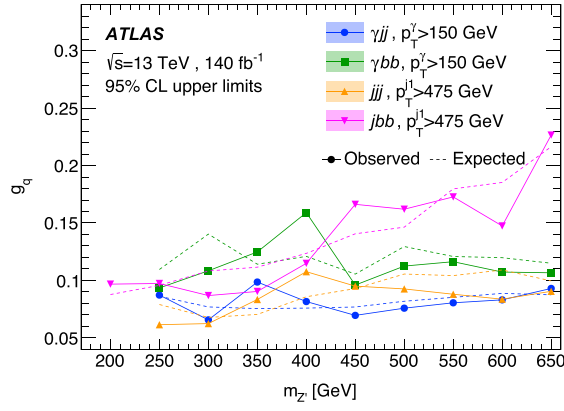


FIG. 7. Expected and observed 95% CL upper limits on the g_q coupling as a function of the Z' mass on the γjj , γbb , jjj , and jbb channels with the background and signal contributions modeled by a 5-parameter fit function and templates from the signal samples, respectively. Observed limits are indicated with markers and a solid line, and expected limits are indicated with a dashed line.

results are shown in Fig. 6 for generic signals with Gaussian function shapes with 5%, 7%, 10%, 12%, and 15% signal widths.

Given the relation between couplings and cross section, the limits on the Z' cross sections can be translated to constraints on the g_q coupling, by taking into account the values of the simulated sample cross sections and the analysis acceptance. A comparison of the limits on the g_q coupling as a function of the Z' mass for all channels is shown in Fig. 7. For the flavor-inclusive channels, the cross section combines the contributions from the signal samples where the Z' decays are restricted to light flavors with the samples where the Z' decay products decay into b -quarks. While the limits on $\sigma \times A \times \text{BR}$ are much stronger for the γbb and jbb channels than for the γjj and jjj channels, the cross sections and branching ratios are much lower, meaning that the limits on g_q are more similar across channels. Overall, the jjj and γjj channels set the strongest limits on the g_q coupling.

The limits on the g_q coupling obtained from the γjj and jjj channels are similar in value and there is only a small overlap in the selected events across the two categories. Hence a combination of the two channels can further strengthen the constraints on g_q . No combination of the b -tagged channel is considered, as the constraints on g_q from such channels are weaker than the flavor-inclusive ones.

Events passing both the γjj and jjj selections are removed from the jjj channel, to have two statistically independent measurements. Such double-counted events amount to 0.2% of all the jjj -selected events and their impact on the jjj channel fits were found to be negligible. A combined likelihood function, which is the product of the γjj and jjj likelihood functions, is used to obtain 95% CL

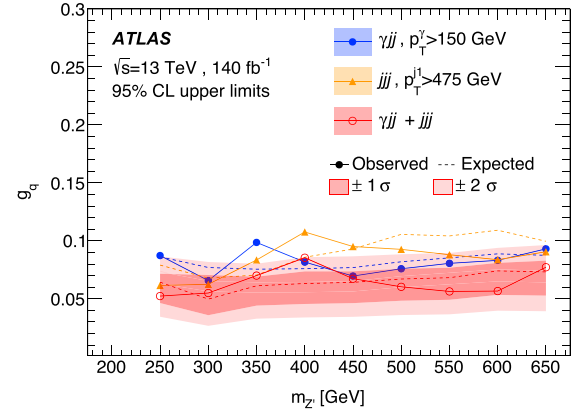


FIG. 8. Expected and observed 95% CL upper limits on the g_q coupling as a function of the Z' mass on the γjj channel, the jjj channel and the combination of the two. The background and signal contributions are modeled by a 5-parameter fit function and templates from the signal samples, respectively. Observed limits are indicated with markers and a solid line, and expected limits are indicated with a dashed line. The shaded bands indicate the (darker band) 1σ and (lighter band) 2σ uncertainty range on the combined result.

upper limits on g_q . In the combined likelihood, the jet and luminosity systematic uncertainties are taken as correlated among the channels. Spurious signal and PDF systematic uncertainties are instead taken as uncorrelated, as the background fit functions and production mechanisms of the two processes are independent across channels. Photon systematic uncertainties only affect the γjj part of the combined likelihood. The combination improves the limits on g_q relative to the individual channels, as shown in Fig. 8, with both the expected and observed limits excluding coupling values down to 0.05–0.07.

VIII. CONCLUSION

Dijet resonances with a width up to 15% of the mass, produced in association with a photon or jet, were searched for in 140 fb^{-1} of LHC pp collisions recorded by the ATLAS experiment at $\sqrt{s} = 13 \text{ TeV}$. This search expands on previous similar searches by using the full Run 2 data samples, and by including the case where the initial-state radiation is a jet. It considers the cases where no flavor requirements are placed on the resonance decay products, and the case where both of the decay products are required to be b -tagged, resulting in four channels, depending on the type of initial-state radiation and the flavor requirements. In all four channels, the observed m_{jj} distribution is well-described by a smooth functional fit without contributions from such resonances. No significant excess of events beyond the Standard Model expectation is observed, and so upper limits are set on two models: Z' axial-vector dark-matter mediators and Gaussian-shape signal contributions for resonant masses between 200 and 650 GeV. Relative to

already published results using a similar analysis technique, this search improves the limits on the $Z'-q-q$ coupling g_q by up to 50%, with the most stringent limits on g_q set by the jjj channel for lower Z' candidate masses and by the γjj channel for higher Z' masses. A further combination of the jjj and γjj channels is performed, which set limits on g_q down to 0.05–0.07.

ACKNOWLEDGMENTS

We thank CERN for the very successful operation of the LHC and its injectors, as well as the support staff at CERN and at our institutions worldwide without whom ATLAS could not be operated efficiently. The crucial computing support from all WLCG partners is acknowledged gratefully, in particular from CERN, the ATLAS Tier-1 facilities at TRIUMF/SFU (Canada), NDGF (Denmark, Norway, Sweden), CC-IN2P3 (France), KIT/GridKA (Germany), INFN-CNAF (Italy), NL-T1 (Netherlands), PIC (Spain), RAL (UK) and BNL (USA), the Tier-2 facilities worldwide and large non-WLCG resource providers. Major contributors of computing resources are listed in Ref. [105]. We gratefully acknowledge the support of ANPCyT, Argentina; YerPhI, Armenia; ARC, Australia; BMWFW and FWF, Austria; ANAS, Azerbaijan; CNPq and FAPESP, Brazil; NSERC, NRC and CFI, Canada; CERN; ANID, Chile; CAS, MOST and NSFC, China; Minciencias, Colombia; MEYS CR, Czech Republic; DNRF and DNSRC, Denmark; IN2P3-CNRS and CEA-DRF/IRFU, France; SRNSFG, Georgia; BMBF, HGF and MPG, Germany; GSRI, Greece; RGC and Hong Kong SAR, China; ISF and Benoziyo Center, Israel; INFN, Italy; MEXT and JSPS, Japan; CNRST, Morocco; NWO, Netherlands; RCN, Norway; MEiN, Poland; FCT, Portugal; MNE/IFA, Romania; MESTD, Serbia; MSSR, Slovakia; ARRS and MIZŠ, Slovenia; DSI/NRF, South Africa; MICINN, Spain; SRC and Wallenberg Foundation, Sweden; SERI, SNSF and Cantons of Bern and Geneva, Switzerland; MOST, Taipei; TENMAK, Türkiye; STFC, United Kingdom; DOE and NSF, USA. Individual groups and members have received support from BCKDF, CANARIE, CRC and DRAC, Canada; PRIMUS 21/SCI/017 and UNCE SCI/013, Czech Republic; COST, ERC, ERDF, Horizon 2020, ICSC-NextGenerationEU and Marie Skłodowska-Curie Actions, European Union; Investissements d'Avenir Labex, Investissements d'Avenir Idex and ANR, France; DFG and AvH Foundation, Germany; Herakleitos, Thales and Aristeia programmes co-financed by EU-ESF and the Greek NSRF, Greece; BSF-NSF and MINERVA, Israel; Norwegian Financial Mechanism 2014–2021, Norway; NCN and

NAWA, Poland; La Caixa Banking Foundation, CERCA Programme Generalitat de Catalunya and PROMETEO and GenT Programmes Generalitat Valenciana, Spain; Göran Gustafssons Stiftelse, Sweden; The Royal Society and Leverhulme Trust, United Kingdom. In addition, individual members wish to acknowledge support from CERN: European Organization for Nuclear Research (CERN PJAS); Chile: Agencia Nacional de Investigación y Desarrollo (FONDECYT 1190886, FONDECYT 1210400, FONDECYT 1230987); China: National Natural Science Foundation of China (NSFC—12175119, NSFC 12275265); European Union: European Research Council (ERC—948254, ERC 101089007), Horizon 2020 Framework Programme (MUCCA—CHIST-ERA-19-XAI-00), Italian Center for High Performance Computing, Big Data and Quantum Computing (ICSC, NextGenerationEU); France: Agence Nationale de la Recherche (ANR-20-CE31-0013, ANR-21-CE31-0022), Investissements d'Avenir Labex (ANR-11-LABX-0012); Germany: Baden-Württemberg Stiftung (BW Stiftung-Postdoc Eliteprogramme), Deutsche Forschungsgemeinschaft (DFG—469666862, DFG—CR 312/5-2); Italy: Istituto Nazionale di Fisica Nucleare (ICSC, NextGenerationEU); Japan: Japan Society for the Promotion of Science (JSPS KAKENHI 22H01227, JSPS KAKENHI 22KK0227, JSPS KAKENHI JP21H05085, JSPS KAKENHI JP22H04944); Netherlands: Netherlands Organisation for Scientific Research (NWO Veni 2020—VI.Veni.202.179); Norway: Research Council of Norway (RCN-314472); Poland: Polish National Agency for Academic Exchange (PPN/PPO/2020/1/00002/U/00001), Polish National Science Centre (NCN 2021/42/E/ST2/00350, NCN OPUS nr 2022/47/B/ST2/03059, NCN UMO-2019/34/E/ST2/00393, UMO-2020/37/B/ST2/01043, UMO-2022/47/O/ST2/00148); Slovenia: Slovenian Research Agency (ARIS Grant No. J1-3010); Spain: BBVA Foundation (LEO22-1-603), Generalitat Valenciana (Computer resources at Artemisa, co-funded by the European Union 2014-2020 FEDER Operative Programme of Comunitat Valenciana IDIFEDER/2018/048), Ministry of Science and Innovation (RYC2019-028510-I, RYC2020-030254-I), PROMETEO and GenT Programmes Generalitat Valenciana (CIDEAGENT/2019/023, CIDEAGENT/2019/027); Sweden: Swedish Research Council (VR 2022-03845), Knut and Alice Wallenberg Foundation (KAW 2022.0358); Switzerland: Swiss National Science Foundation (SNSF—PCEFP2_194658); United Kingdom: Leverhulme Trust (Leverhulme Trust RPG-2020-004); USA: Neubauer Family Foundation.

- [1] P. Zyla *et al.* (Particle Data Group), Review of particle physics, *Prog. Theor. Exp. Phys.* **2020**, 083C01 (2020).
- [2] G. Bertone, D. Hooper, and J. Silk, Particle dark matter: Evidence, candidates and constraints, *Phys. Rep.* **405**, 279 (2005).
- [3] L. Bergström, Non-baryonic dark matter: Observational evidence and detection methods, *Rep. Prog. Phys.* **63**, 793 (2000).
- [4] D. Clowe, M. Bradač, A. H. Gonzalez, M. Markevitch, S. W. Randall, C. Jones, and D. Zaritsky, A direct empirical proof of the existence of dark matter, *Astrophys. J. Lett.* **648**, L109 (2006).
- [5] L. Canetti, M. Drewes, and M. Shaposhnikov, Matter and antimatter in the Universe, *New J. Phys.* **14**, 095012 (2012).
- [6] S. P. Martin, A supersymmetry primer, *Adv. Ser. Dir. High Energy Phys.* **18**, 1 (1998).
- [7] J. A. Aguilar-Saavedra, Identifying top partners at LHC, *J. High Energy Phys.* **11** (2009) 030.
- [8] G. F. Giudice, Y. Kats, M. McCullough, R. Torre, and A. Urbano, Clockwork/linear dilaton: Structure and phenomenology, *J. High Energy Phys.* **06** (2018) 009.
- [9] M. J. Strassler and K. M. Zurek, Echoes of a hidden valley at hadron colliders, *Phys. Lett. B* **651**, 374 (2007).
- [10] J. Fan, M. Reece, and J. T. Ruderman, Stealth supersymmetry, *J. High Energy Phys.* **11** (2011) 012.
- [11] D. Ghosh, R. Godbole, M. Guchait, K. Mohan, and D. Sengupta, Looking for an invisible Higgs signal at the LHC, *Phys. Lett. B* **725**, 344 (2013).
- [12] P. Konar, K. T. Matchev, M. Park, and G. K. Sarangi, How to look for supersymmetry under the LHC lamppost, *Phys. Rev. Lett.* **105**, 221801 (2010).
- [13] A. Flórez, A. Gurrrola, W. Johns, J. Maruri, P. Sheldon, K. Sinha, and Savanna Rae Starko, Anapole dark matter via vector boson fusion processes at the LHC, *Phys. Rev. D* **100**, 016017 (2019).
- [14] J. Abdallah *et al.*, Simplified models for dark matter searches at the LHC, *Phys. Dark Universe* **9–10**, 8 (2015).
- [15] N. Bernal, M. Heikinheimo, T. Tenkanen, K. Tuominen, and V. Vaskonen, The dawn of FIMP dark matter: A review of models and constraints, *Int. J. Mod. Phys. A* **32**, 1730023 (2017).
- [16] P. Arias, D. Cadamuro, M. Goodsell, J. Jaeckel, J. Redondo, and A. Ringwald, WISPy cold dark matter, *J. Cosmol. Astropart. Phys.* **06** (2012) 013.
- [17] F. Kahlhoefer, K. Schmidt-Hoberg, T. Schwetz, and S. Vogl, Implications of unitarity and gauge invariance for simplified dark matter models, *J. High Energy Phys.* **02** (2016) 016.
- [18] D. Abercrombie *et al.*, Dark matter benchmark models for early LHC Run-2 searches: Report of the ATLAS/CMS dark matter forum, *Phys. Dark Universe* **27**, 100371 (2020).
- [19] F. Kahlhoefer, Review of LHC dark matter searches, *Int. J. Mod. Phys. A* **32**, 1730006 (2017).
- [20] M. Fairbairn, J. Heal, F. Kahlhoefer, and P. Tunney, Constraints on Z' models from LHC dijet searches and implications for dark matter, *J. High Energy Phys.* **09** (2016) 018.
- [21] ATLAS Collaboration, Constraints on mediator-based dark matter and scalar dark energy models using $\sqrt{s} = 13$ TeV pp collision data collected by the ATLAS detector, *J. High Energy Phys.* **05** (2019) 142.
- [22] O. Buchmueller, M. J. Dolan, and C. McCabe, Beyond effective field theory for dark matter searches at the LHC, *J. High Energy Phys.* **01** (2014) 025.
- [23] ATLAS Collaboration, Dark matter summary plots for s -channel, 2HDM + a and dark Higgs models, ATLAS-PHYS-PUB-2023-018, <https://cds.cern.ch/record/2865335> (2023).
- [24] ATLAS Collaboration, Search for new physics in the dijet mass distribution using 1 fb^{-1} of pp collision data at $\sqrt{s} = 7$ TeV collected by the ATLAS detector, *Phys. Lett. B* **708**, 37 (2012).
- [25] ATLAS Collaboration, Search for new phenomena in the dijet mass distribution using pp collision data at $\sqrt{s} = 8$ TeV with the ATLAS detector, *Phys. Rev. D* **91**, 052007 (2015).
- [26] CMS Collaboration, Search for dijet resonances in 7 TeV pp collisions at CMS, *Phys. Rev. Lett.* **105**, 211801 (2010).
- [27] CMS Collaboration, Search for resonances in the dijet mass spectrum from 7 TeV pp collisions at CMS, *Phys. Lett. B* **704**, 123 (2011).
- [28] CMS Collaboration, Search for narrow resonances and quantum black holes in inclusive and b -tagged dijet mass spectra from pp collisions at $\sqrt{s} = 7$ TeV, *J. High Energy Phys.* **01** (2013) 013.
- [29] CMS Collaboration, Search for narrow resonances using the dijet mass spectrum in pp collisions at $\sqrt{s} = 8$ TeV, *Phys. Rev. D* **87**, 114015 (2013).
- [30] CMS Collaboration, Search for resonances and quantum black holes using dijet mass spectra in proton-proton collisions at $\sqrt{s} = 8$ TeV, *Phys. Rev. D* **91**, 052009 (2015).
- [31] CMS Collaboration, Search for narrow resonances in dijet final states at $\sqrt{s} = 8$ TeV with the novel CMS technique of data scouting, *Phys. Rev. Lett.* **117**, 031802 (2016).
- [32] ATLAS Collaboration, Search for new phenomena in dijet mass and angular distributions from pp collisions at $\sqrt{s} = 13$ TeV with the ATLAS detector, *Phys. Lett. B* **754**, 302 (2016).
- [33] CMS Collaboration, Search for narrow resonances decaying to dijets in proton-proton collisions at $\sqrt{s} = 13$ TeV, *Phys. Rev. Lett.* **116**, 071801 (2016).
- [34] CMS Collaboration, Search for dijet resonances in proton-proton collisions at $\sqrt{s} = 13$ TeV and constraints on dark matter and other models, *Phys. Lett. B* **769**, 520 (2017).
- [35] CMS Collaboration, Search for narrow and broad dijet resonances in proton-proton collisions at $\sqrt{s} = 13$ TeV and constraints on dark matter mediators and other new particles, *J. High Energy Phys.* **08** (2018) 130.
- [36] CMS Collaboration, Search for narrow resonances in the b -tagged dijet mass spectrum in proton-proton collisions at $\sqrt{s} = 8$ TeV, *Phys. Rev. Lett.* **120**, 201801 (2018).
- [37] CMS Collaboration, Search for high mass dijet resonances with a new background prediction method in proton-proton collisions at $\sqrt{s} = 13$ TeV, *J. High Energy Phys.* **05** (2020) 033.

- [38] CMS Collaboration, Search for narrow resonances in the b -tagged dijet mass spectrum in proton-proton collisions at $\sqrt{s} = 13$ TeV, *Phys. Rev. D* **108**, 012009 (2023).
- [39] ATLAS Collaboration, Search for low-mass dijet resonances using trigger-level jets with the ATLAS detector in pp collisions at $\sqrt{s} = 13$ TeV, *Phys. Rev. Lett.* **121**, 081801 (2018).
- [40] ATLAS Collaboration, Search for low-mass resonances decaying into two jets and produced in association with a photon using pp collisions at $\sqrt{s} = 13$ TeV with the ATLAS detector, *Phys. Lett. B* **795**, 56 (2019).
- [41] CMS Collaboration, Search for dijet resonances using events with three jets in proton-proton collisions at $\sqrt{s} = 13$ TeV, *Phys. Lett. B* **805**, 135448 (2020).
- [42] CMS Collaboration, Search for low-mass quark–antiquark resonances produced in association with a photon at $\sqrt{s} = 13$ TeV, *Phys. Rev. Lett.* **123**, 231803 (2019).
- [43] CMS Collaboration, Search for low mass vector resonances decaying into quark–antiquark pairs in proton-proton collisions at $\sqrt{s} = 13$ TeV, *Phys. Rev. D* **100**, 112007 (2019).
- [44] CMS Collaboration, Search for low mass vector resonances decaying into quark–antiquark pairs in proton-proton collisions at $\sqrt{s} = 13$ TeV, *J. High Energy Phys.* **01** (2018) 097.
- [45] CMS Collaboration, Search for low mass vector resonances decaying to quark–antiquark pairs in proton-proton collisions at $\sqrt{s} = 13$ TeV, *Phys. Rev. Lett.* **119**, 111802 (2017).
- [46] ATLAS Collaboration, Search for light resonances decaying to boosted quark pairs and produced in association with a photon or a jet in proton-proton collisions at $\sqrt{s} = 13$ TeV with the ATLAS detector, *Phys. Lett. B* **788**, 316 (2019).
- [47] ATLAS Collaboration, The ATLAS experiment at the CERN Large Hadron Collider, *J. Instrum.* **3**, S08003 (2008).
- [48] ATLAS Collaboration, ATLAS insertable B-layer: Technical design report, ATLAS-TDR-19; CERN-LHCC-2010-013, <https://cds.cern.ch/record/1291633> (2010); Addendum: ATLAS-TDR-19-ADD-1; CERN-LHCC-2012-009, <https://cds.cern.ch/record/1451888> (2012).
- [49] B. Abbott *et al.*, Production and integration of the ATLAS insertable B-layer, *J. Instrum.* **13**, T05008 (2018).
- [50] ATLAS Collaboration, Performance of the ATLAS trigger system in 2015, *Eur. Phys. J. C* **77**, 317 (2017).
- [51] ATLAS Collaboration, The ATLAS Collaboration software and firmware, ATL-SOFT-PUB-2021-001, <https://cds.cern.ch/record/2767187> (2021).
- [52] ATLAS Collaboration, Luminosity determination in pp collisions at $\sqrt{s} = 13$ TeV using the ATLAS detector at the LHC, *Eur. Phys. J. C* **83**, 982 (2023).
- [53] G. Avoni *et al.*, The new LUCID-2 detector for luminosity measurement and monitoring in ATLAS, *J. Instrum.* **13**, P07017 (2018).
- [54] ATLAS Collaboration, ATLAS data quality operations and performance for 2015–2018 data-taking, *J. Instrum.* **15**, P04003 (2020).
- [55] A. Albert *et al.*, Recommendations of the LHC dark matter working group: Comparing LHC searches for dark matter mediators in visible and invisible decay channels and calculations of the thermal relic density, *Phys. Dark Universe* **26**, 100377 (2019).
- [56] J. Alwall, R. Frederix, S. Frixione, V. Hirschi, F. Maltoni, O. Mattelaer, H.-S. Shao, T. Stelzer, P. Torrielli, and M. Zaro, The automated computation of tree-level and next-to-leading order differential cross sections, and their matching to parton shower simulations, *J. High Energy Phys.* **07** (2014) 079.
- [57] R. D. Ball *et al.* (NNPDF Collaboration), Parton distributions with LHC data, *Nucl. Phys.* **B867**, 244 (2013).
- [58] T. Sjöstrand, S. Ask, J. R. Christiansen, R. Corke, N. Desai, P. Ilten, S. Mrenna, S. Prestel, Christine O. Rasmussen, and P. Z. Skands, An introduction to PYTHIA 8.2, *Comput. Phys. Commun.* **191**, 159 (2015).
- [59] T. Sjöstrand, S. Mrenna, and P. Skands, PYTHIA 6.4 physics and manual, *J. High Energy Phys.* **05** (2006) 026.
- [60] ATLAS Collaboration, ATLAS PYTHIA8 tunes to 7 TeV data, ATL-PHYS-PUB-2014-021, <https://cds.cern.ch/record/1966419> (2014).
- [61] D. J. Lange, The EvtGen particle decay simulation package, *Nucl. Instrum. Methods Phys. Res., Sect. A* **462**, 152 (2001).
- [62] E. Bothmann *et al.*, Event generation with Sherpa 2.2, *SciPost Phys.* **7**, 034 (2019).
- [63] T. Gleisberg and S. Höche, Comix, A new matrix element generator, *J. High Energy Phys.* **12** (2008) 039.
- [64] F. Buccioni, J.-N. Lang, J. M. Lindert, P. Maierhöfer, S. Pozzorini, H. Zhang, and M. F. Zoller, OpenLoops 2, *Eur. Phys. J. C* **79**, 866 (2019).
- [65] F. Cascioli, P. Maierhöfer, and S. Pozzorini, Scattering amplitudes with OpenLoops, *Phys. Rev. Lett.* **108**, 111601 (2012).
- [66] A. Denner, S. Dittmaier, and L. Hofer, Collier: A Fortran-based complex one-loop library in extended regularizations, *Comput. Phys. Commun.* **212**, 220 (2017).
- [67] S. Schumann and F. Krauss, A parton shower algorithm based on Catani–Seymour dipole factorisation, *J. High Energy Phys.* **03** (2008) 038.
- [68] S. Höche, F. Krauss, M. Schönherr, and F. Siegert, A critical appraisal of NLO + PS matching methods, *J. High Energy Phys.* **09** (2012) 049.
- [69] S. Höche, F. Krauss, M. Schönherr, and F. Siegert, QCD matrix elements + parton showers. The NLO case, *J. High Energy Phys.* **04** (2013) 027.
- [70] S. Catani, F. Krauss, B. R. Webber, and R. Kuhn, QCD matrix elements + parton showers, *J. High Energy Phys.* **11** (2001) 063.
- [71] S. Höche, F. Krauss, S. Schumann, and F. Siegert, QCD matrix elements and truncated showers, *J. High Energy Phys.* **05** (2009) 053.
- [72] F. Siegert, A practical guide to event generation for prompt photon production with Sherpa, *J. Phys. G* **44**, 044007 (2017).
- [73] S. Frixione, Isolated photons in perturbative QCD, *Phys. Lett. B* **429**, 369 (1998).
- [74] R. D. Ball *et al.* (NNPDF Collaboration), Parton distributions for the LHC run II, *J. High Energy Phys.* **04** (2015) 040.
- [75] ATLAS Collaboration, The ATLAS simulation infrastructure, *Eur. Phys. J. C* **70**, 823 (2010).

- [76] S. Agostinelli *et al.*, Geant4—A simulation toolkit, *Nucl. Instrum. Methods Phys. Res., Sect. A* **506**, 250 (2003).
- [77] ATLAS Collaboration, The PYTHIA8 A3 tune description of ATLAS minimum bias and inelastic measurements incorporating the Donnachie–Landshoff diffractive model, ATL-PHYS-PUB-2016-017, <https://cds.cern.ch/record/2206965> (2016).
- [78] ATLAS Collaboration, Vertex reconstruction performance of the ATLAS detector at $\sqrt{s} = 13$ TeV, ATL-PHYS-PUB-2015-026, <https://cds.cern.ch/record/2037717> (2015).
- [79] ATLAS Collaboration, Jet reconstruction and performance using particle flow with the ATLAS detector, *Eur. Phys. J. C* **77**, 466 (2017).
- [80] M. Cacciari, G. P. Salam, and G. Soyez, The anti- k_r jet clustering algorithm, *J. High Energy Phys.* **04** (2008) 063.
- [81] M. Cacciari, G. P. Salam, and G. Soyez, FastJet user manual, *Eur. Phys. J. C* **72**, 1896 (2012).
- [82] ATLAS Collaboration, Topological cell clustering in the ATLAS calorimeters and its performance in LHC Run 1, *Eur. Phys. J. C* **77**, 490 (2017).
- [83] ATLAS Collaboration, Jet energy scale and resolution measured in proton-proton collisions at $\sqrt{s} = 13$ TeV with the ATLAS detector, *Eur. Phys. J. C* **81**, 689 (2021).
- [84] ATLAS Collaboration, Performance of pile-up mitigation techniques for jets in pp collisions at $\sqrt{s} = 8$ TeV using the ATLAS detector, *Eur. Phys. J. C* **76**, 581 (2016).
- [85] ATLAS Collaboration, Selection of jets produced in 13 TeV proton-proton collisions with the ATLAS detector, ATL-CONF-2015-029, <https://cds.cern.ch/record/2037702> (2015).
- [86] ATLAS Collaboration, ATLAS flavour-tagging algorithms for the LHC Run 2 pp collision dataset, *Eur. Phys. J. C* **83**, 681 (2023).
- [87] ATLAS Collaboration, Electron and photon performance measurements with the ATLAS detector using the 2015–2017 LHC proton-proton collision data, *J. Instrum.* **14**, P12006 (2019).
- [88] ATLAS Collaboration, Performance of electron and photon triggers in ATLAS during LHC Run 2, *Eur. Phys. J. C* **80**, 47 (2020).
- [89] ATLAS Collaboration, The performance of the jet trigger for the ATLAS detector during 2011 data taking, *Eur. Phys. J. C* **76**, 526 (2016).
- [90] H. Dembinski, M. Schmelling, and R. Waldi, Application of the iterated weighted least-squares fit to counting experiments, *Nucl. Instrum. Methods Phys. Res., Sect. A* **940**, 135 (2019).
- [91] M. Baak, S. Gadatsch, R. Harrington, and W. Verkerke, Interpolation between multi-dimensional histograms using a new non-linear moment morphing method, *Nucl. Instrum. Methods Phys. Res., Sect. A* **771**, 39 (2015).
- [92] CDF Collaboration, Search for new particles decaying into dijets in proton-antiproton collisions at $\sqrt{s} = 1.96$ TeV, *Phys. Rev. D* **79**, 112002 (2009).
- [93] ATLAS Collaboration, Search for new particles in two-jet final states in 7 TeV proton-proton collisions with the ATLAS detector at the LHC, *Phys. Rev. Lett.* **105**, 161801 (2010).
- [94] ATLAS Collaboration, Search for new phenomena in multi-body invariant masses in events with at least one isolated lepton and two jets using $\sqrt{s} = 13$ TeV proton-proton collision data collected by the ATLAS detector, *J. High Energy Phys.* **07** (2023) 202.
- [95] ATLAS Collaboration, Search for new resonances in mass distributions of jet pairs using 139 fb^{-1} of pp collisions at $\sqrt{s} = 13$ TeV with the ATLAS detector, *J. High Energy Phys.* **03** (2020) 145.
- [96] CMS Collaboration, Search for resonant and nonresonant production of pairs of dijet resonances in proton-proton collisions at $\sqrt{s} = 13$ TeV, *J. High Energy Phys.* **07** (2023) 161.
- [97] ATLAS Collaboration, Pursuit of paired dijet resonances in the Run 2 dataset with ATLAS, *Phys. Rev. D* **108**, 112005 (2023).
- [98] ATLAS Collaboration, Simulation-based extrapolation of b -tagging calibrations towards high transverse momenta in the ATLAS experiment, ATL-PHYS-PUB-2021-003, <https://cds.cern.ch/record/2753444> (2021).
- [99] CDF Collaboration, Global search for new physics with 2.0 fb^{-1} at CDF, *Phys. Rev. D* **79**, 011101 (2009).
- [100] G. Choudalakis, On hypothesis testing, trials factor, hypertests and the BumpHunter, [arXiv:1101.0390](https://arxiv.org/abs/1101.0390).
- [101] L. Vaslin, S. Calvet, V. Barra, and J. Donini, pyBumpHunter: A model independent bump hunting tool in Python for High Energy Physics analyses, *SciPost Phys. Codebases* **15** (2023).
- [102] pyBumpHunter, <https://github.com/scikit-hep/pyBumpHunter>.
- [103] G. Cowan, K. Cranmer, E. Gross, and O. Vitells, Asymptotic formulae for likelihood-based tests of new physics, *Eur. Phys. J. C* **71**, 1554 (2011); **73**, 2501(E) (2013).
- [104] A. L. Read, Presentation of search results: The CL_s technique, *J. Phys. G* **28**, 2693 (2002).
- [105] ATLAS Collaboration, ATLAS computing acknowledgements, ATL-SOFT-PUB-2023-001, <https://cds.cern.ch/record/2869272> (2023).

G. Aad¹⁰³, E. Aakvaag¹⁶, B. Abbott¹²¹, K. Abeling⁵⁵, N. J. Abicht⁴⁹, S. H. Abidi²⁹, M. Aboelela⁴⁴, A. Abouhorma^{35e}, H. Abramowicz¹⁵², H. Abreu¹⁵¹, Y. Abulaiti¹¹⁸, B. S. Acharya^{69a,69b,b}, A. Ackermann^{63a}, C. Adam Bourdarios⁴, L. Adamczyk^{86a}, S. V. Addepalli²⁶, M. J. Addison¹⁰², J. Adelman¹¹⁶, A. Adiguzel^{21c}, T. Adye¹³⁵, A. A. Affolder¹³⁷, Y. Afik³⁹, M. N. Agaras¹³, J. Agarwala^{73a,73b}, A. Aggarwal¹⁰¹, C. Agheorghiesei^{27c}, A. Ahmad³⁶, F. Ahmadov^{38,c}, W. S. Ahmed¹⁰⁵, S. Ahuja⁹⁶, X. Ai^{62e}, G. Aielli^{76a,76b}, A. Aikot¹⁶⁴, M. Ait Tamlahat^{35e}, B. Aitbenkhik^{35a}, I. Aizenberg¹⁷⁰, M. Akbiyik¹⁰¹, T. P. A. Åkesson⁹⁹

A. V. Akimov³⁷ D. Akiyama¹⁶⁹ N. N. Akolkar²⁴ S. Aktas^{21a} K. Al Khoury⁴¹ G. L. Alberghi^{23b} J. Albert¹⁶⁶
P. Albicocco⁵³ G. L. Albouy⁶⁰ S. Alderweireldt⁵² Z. L. Alegria¹²² M. Aleksa³⁶ I. N. Aleksandrov³⁸
C. Alexa^{27b} T. Alexopoulos¹⁰ F. Alfonsi^{23b} M. Algren⁵⁶ M. Alhroob¹⁴² B. Ali¹³³ H. M. J. Ali⁹² S. Ali¹⁴⁹
S. W. Alibocus⁹³ M. Aliev^{33c} G. Alimonti^{71a} W. Alkakhki⁵⁵ C. Allaire⁶⁶ B. M. M. Allbrooke¹⁴⁷ J. F. Allen⁵²
C. A. Allendes Flores^{138f} P. P. Allport²⁰ A. Aloisio^{72a,72b} F. Alonso⁹¹ C. Alpigiani¹³⁹ M. Alvarez Estevez¹⁰⁰
A. Alvarez Fernandez¹⁰¹ M. Alves Cardoso⁵⁶ M. G. Alviggi^{72a,72b} M. Aly¹⁰² Y. Amaral Coutinho^{83b}
A. Ambler¹⁰⁵ C. Amelung³⁶ M. Amerl¹⁰² C. G. Ames¹¹⁰ D. Amidei¹⁰⁷ K. J. Amirie¹⁵⁶
S. P. Amor Dos Santos^{131a} K. R. Amos¹⁶⁴ S. An⁸⁴ V. Ananiev¹²⁶ C. Anastopoulos¹⁴⁰ T. Andeen¹¹
J. K. Anders³⁶ S. Y. Andreato^{47a,47b} A. Andreazza^{71a,71b} S. Angelidakis⁹ A. Angerami^{41,d} A. V. Anisenkov³⁷
A. Annovi^{74a} C. Antel⁵⁶ M. T. Anthony¹⁴⁰ E. Antipov¹⁴⁶ M. Antonelli⁵³ F. Anulli^{75a} M. Aoki⁸⁴
T. Aoki¹⁵⁴ J. A. Aparisi Pozo¹⁶⁴ M. A. Aparo¹⁴⁷ L. Aperio Bella⁴⁸ C. Appelt¹⁸ A. Apyan²⁶ S. J. Arbiol Val⁸⁷
C. Arcangeletti⁵³ A. T. H. Arce⁵¹ E. Arena⁹³ J-F. Arguin¹⁰⁹ S. Argyropoulos⁵⁴ J.-H. Arling⁴⁸ O. Arnaez⁴
H. Arnold¹¹⁵ G. Artoni^{75a,75b} H. Asada¹¹² K. Asai¹¹⁹ S. Asai¹⁵⁴ N. A. Asbah³⁶ K. Assamagan²⁹
R. Astalos^{28a} K. S. V. Astrand⁹⁹ S. Atashi¹⁶⁰ R. J. Atkin^{33a} M. Atkinson¹⁶³ H. Atmani^{35f} P. A. Atmasiddha¹²⁹
K. Augsten¹³³ S. Auricchio^{72a,72b} A. D. Auriol²⁰ V. A. Austrup¹⁰² G. Avolio³⁶ K. Axiotis⁵⁶ G. Azuelos^{109,e}
D. Babal^{28b} H. Bachacou¹³⁶ K. Bachas^{153,f} A. Bachi³⁴ F. Backman^{47a,47b} A. Badea³⁹ T. M. Baer¹⁰⁷
P. Bagnaia^{75a,75b} M. Bahmani¹⁸ D. Bahner⁵⁴ K. Bai¹²⁴ J. T. Baines¹³⁵ L. Baines⁹⁵ O. K. Baker¹⁷³
E. Bakos¹⁵ D. Bakshi Gupta⁸ V. Balakrishnan¹²¹ R. Balasubramanian¹¹⁵ E. M. Baldin³⁷ P. Balek^{86a}
E. Ballabene^{23b,23a} F. Balli¹³⁶ L. M. Baltes^{63a} W. K. Balunas³² J. Balz¹⁰¹ E. Banas⁸⁷ M. Bandieramonte¹³⁰
A. Bandyopadhyay²⁴ S. Bansal²⁴ L. Barak¹⁵² M. Barakat⁴⁸ E. L. Barberio¹⁰⁶ D. Barberis^{57b,57a}
M. Barbero¹⁰³ M. Z. Barel¹¹⁵ K. N. Barends^{33a} T. Barillari¹¹¹ M-S. Barisits³⁶ T. Barklow¹⁴⁴ P. Baron¹²³
D. A. Baron Moreno¹⁰² A. Baroncelli^{62a} G. Barone²⁹ A. J. Barr¹²⁷ J. D. Barr⁹⁷ F. Barreiro¹⁰⁰
J. Barreiro Guimarães da Costa^{14a} U. Barron¹⁵² M. G. Barros Teixeira^{131a} S. Barsov³⁷ F. Bartels^{63a}
R. Bartoldus¹⁴⁴ A. E. Barton⁹² P. Bartos^{28a} A. Basan¹⁰¹ M. Baselga⁴⁹ A. Bassalat^{66,g} M. J. Basso^{157a}
R. Bate¹⁶⁵ R. L. Bates⁵⁹ S. Batlamous¹⁰⁰ B. Batool¹⁴² M. Battaglia¹³⁷ D. Battulga¹⁸ M. Bauge^{75a,75b}
M. Bauer³⁶ P. Bauer²⁴ L. T. Bazzano Hurrell³⁰ J. B. Beacham⁵¹ T. Beau¹²⁸ J. Y. Beaucamp⁹¹
P. H. Beauchemin¹⁵⁹ P. Bechtel²⁴ H. P. Beck^{19,h} K. Becker¹⁶⁸ A. J. Beddall⁸² V. A. Bednyakov³⁸
C. P. Bee¹⁴⁶ L. J. Beemster¹⁵ T. A. Beermann³⁶ M. Begalli^{83d} M. Begel²⁹ A. Behera¹⁴⁶ J. K. Behr⁴⁸
J. F. Beirer³⁶ F. Beisiegel²⁴ M. Belfkir^{117b} G. Bella¹⁵² L. Bellagamba^{23b} A. Bellerive³⁴ P. Bellos²⁰
K. Beloborodov³⁷ D. Benckekroun^{35a} F. Bendebba^{35a} Y. Benhammou¹⁵² K. C. Benkendorfer⁶¹ L. Beresford⁴⁸
M. Beretta⁵³ E. Bergeas Kuutmann¹⁶² N. Berger⁴ B. Bergmann¹³³ J. Beringer^{17a} G. Bernardi⁵
C. Bernius¹⁴⁴ F. U. Bernlochner²⁴ F. Bernon^{36,103} A. Berrocal Guardia¹³ T. Berry⁹⁶ P. Berta¹³⁴
A. Berthold⁵⁰ S. Bethke¹¹¹ A. Betti^{75a,75b} A. J. Bevan⁹⁵ N. K. Bhalla⁵⁴ M. Bhanjee^{33c} S. Bhatta¹⁴⁶
D. S. Bhattacharya¹⁶⁷ P. Bhattarai¹⁴⁴ K. D. Bhide⁵⁴ V. S. Bhopatkar¹²² R. M. Bianchi¹³⁰ G. Bianco^{23b,23a}
O. Biebel¹¹⁰ R. Bielski¹²⁴ M. Biglietti^{77a} C. S. Billingsley⁴⁴ M. Bindi⁵⁵ A. Bingul^{21b} C. Bini^{75a,75b}
A. Biondini⁹³ C. J. Birch-sykes¹⁰² G. A. Bird³² M. Birman¹⁷⁰ M. Biros¹³⁴ S. Biryukov¹⁴⁷ T. Bisanz⁴⁹
E. Bisceglie^{43b,43a} J. P. Biswal¹³⁵ D. Biswas¹⁴² I. Bloch⁴⁸ A. Blue⁵⁹ U. Blumenschein⁹⁵ J. Blumenthal¹⁰¹
V. S. Bobrovnikov³⁷ M. Boehler⁵⁴ B. Boehm¹⁶⁷ D. Bogavac³⁶ A. G. Bogdanchikov³⁷ C. Bohm^{47a}
V. Boisvert⁹⁶ P. Bokač³⁶ T. Bold^{86a} M. Bomben⁵ M. Bona⁹⁵ M. Boonekamp¹³⁶ C. D. Booth⁹⁶
A. G. Borbély⁵⁹ I. S. Bordulev³⁷ H. M. Borecka-Bielska¹⁰⁹ G. Borissov⁹² D. Bortoletto¹²⁷ D. Boscherini^{23b}
M. Bosman¹³ J. D. Bossio Sola³⁶ K. Bouaouda^{35a} N. Bouchhar¹⁶⁴ J. Boudreau¹³⁰ E. V. Bouhova-Thacker⁹²
D. Boumediene⁴⁰ R. Bouquet^{57b,57a} A. Boveia¹²⁰ J. Boyd³⁶ D. Boye²⁹ I. R. Boyko³⁸ J. Bracinik²⁰
N. Brahimi⁴ G. Brandt¹⁷² O. Brandt³² F. Braren⁴⁸ B. Brau¹⁰⁴ J. E. Brau¹²⁴ R. Brenner¹⁷⁰ L. Brenner¹¹⁵
R. Brenner¹⁶² S. Bressler¹⁷⁰ D. Britton⁵⁹ D. Britzger¹¹¹ I. Brock²⁴ G. Brooijmans⁴¹ E. Brost²⁹
L. M. Brown¹⁶⁶ L. E. Bruce⁶¹ T. L. Bruckler¹²⁷ P. A. Bruckman de Renstrom⁸⁷ B. Brüers⁴⁸ A. Bruni^{23b}
G. Bruni^{23b} M. Bruschi^{23b} N. Bruscinò^{75a,75b} T. Buanes¹⁶ Q. Buat¹³⁹ D. Buchin¹¹¹ A. G. Buckley⁵⁹
O. Bulekov³⁷ B. A. Bullard¹⁴⁴ S. Burdin⁹³ C. D. Burgard⁴⁹ A. M. Burger³⁶ B. Burghgrave⁸
O. Burlayenko⁵⁴ J. T. P. Burr³² C. D. Burton¹¹ J. C. Burzynski¹⁴³ E. L. Busch⁴¹ V. Büscher¹⁰¹ P. J. Bussey⁵⁹
J. M. Butler²⁵ C. M. Buttar⁵⁹ J. M. Butterworth⁹⁷ W. Buttinger¹³⁵ C. J. Buxo Vazquez¹⁰⁸ A. R. Buzykaev³⁷

S. Cabrera Urbán¹⁶⁴ L. Cadamuro⁶⁶ D. Caforio⁵⁸ H. Cai¹³⁰ Y. Cai^{14a,14e} Y. Cai^{14c} V. M. M. Cairo³⁶
O. Cakir^{3a} N. Calace³⁶ P. Calafiura^{17a} G. Calderini¹²⁸ P. Calfayan⁶⁸ G. Callea⁵⁹ L. P. Caloba^{83b} D. Calvet⁴⁰
S. Calvet⁴⁰ M. Calvetti^{74a,74b} R. Camacho Toro¹²⁸ S. Camarda³⁶ D. Camarero Munoz²⁶ P. Camarri^{76a,76b}
M. T. Camerlingo^{72a,72b} D. Cameron³⁶ C. Camincher¹⁶⁶ M. Campanelli⁹⁷ A. Camplani⁴² V. Canale^{72a,72b}
A. C. Canbay^{3a} E. Canonero⁹⁶ J. Cantero¹⁶⁴ Y. Cao¹⁶³ F. Capocasa²⁶ M. Capua^{43b,43a} A. Carbone^{71a,71b}
R. Cardarelli^{76a} J. C. J. Cardenas⁸ F. Cardillo¹⁶⁴ G. Carducci^{43b,43a} T. Carli³⁶ G. Carlino^{72a} J. I. Carlotto¹³
B. T. Carlson^{130,i} E. M. Carlson^{166,157a} L. Carminati^{71a,71b} A. Carnelli¹³⁶ M. Carnesale^{75a,75b} S. Caron¹¹⁴
E. Carquin^{138f} S. Carrá^{71a} G. Carratta^{23b,23a} A. M. Carroll¹²⁴ T. M. Carter⁵² M. P. Casado^{13j} M. Caspar⁴⁸
F. L. Castillo⁴ L. Castillo Garcia¹³ V. Castillo Gimenez¹⁶⁴ N. F. Castro^{131a,131e} A. Catinaccio³⁶
J. R. Catmore¹²⁶ T. Cavaliere⁴ V. Cavaliere²⁹ N. Cavalli^{23b,23a} Y. C. Cekmecelioglu⁴⁸ E. Celebi^{21a} S. Cella³⁶
F. Celli¹²⁷ M. S. Centonze^{70a,70b} V. Cepaitis⁵⁶ K. Cerny¹²³ A. S. Cerqueira^{83a} A. Cerri¹⁴⁷ L. Cerrito^{76a,76b}
F. Cerutti^{17a} B. Cervato¹⁴² A. Cervelli^{23b} G. Cesarini⁵³ S. A. Cetin⁸² D. Chakraborty¹¹⁶ J. Chan^{17a}
W. Y. Chan¹⁵⁴ J. D. Chapman³² E. Chapon¹³⁶ B. Chargeishvili^{150b} D. G. Charlton²⁰ M. Chatterjee¹⁹
C. Chauhan¹³⁴ Y. Che^{14c} S. Chekanov⁶ S. V. Chekulaev^{157a} G. A. Chelkov^{38,k} A. Chen¹⁰⁷ B. Chen¹⁵²
B. Chen¹⁶⁶ H. Chen^{14c} H. Chen²⁹ J. Chen^{62c} J. Chen¹⁴³ M. Chen¹²⁷ S. Chen¹⁵⁴ S. J. Chen^{14c}
X. Chen^{62c,136} X. Chen^{14b,l} Y. Chen^{62a} C. L. Cheng¹⁷¹ H. C. Cheng^{64a} S. Cheong¹⁴⁴ A. Cheplakov³⁸
E. Cheremushkina⁴⁸ E. Cherepanova¹¹⁵ R. Cherkaoui El Moursli^{35e} E. Cheu⁷ K. Cheung⁶⁵ L. Chevalier¹³⁶
V. Chiarella⁵³ G. Chiarelli^{74a} N. Chiedde¹⁰³ G. Chiodini^{70a} A. S. Chisholm²⁰ A. Chitan^{27b} M. Chitishvili¹⁶⁴
M. V. Chizhov³⁸ K. Choi¹¹ Y. Chou¹³⁹ E. Y. S. Chow¹¹⁴ K. L. Chu¹⁷⁰ M. C. Chu^{64a} X. Chu^{14a,14e}
J. Chudoba¹³² J. J. Chwastowski⁸⁷ D. Cieri¹¹¹ K. M. Ciesla^{86a} V. Cindro⁹⁴ A. Ciocio^{17a} F. Ciotto^{72a,72b}
Z. H. Citron¹⁷⁰ M. Citterio^{71a} D. A. Ciubotaru^{27b} A. Clark⁵⁶ P. J. Clark⁵² C. Clarry¹⁵⁶
J. M. Clavijo Columbie⁴⁸ S. E. Clawson⁴⁸ C. Clement^{47a,47b} J. Clercx⁴⁸ Y. Coadou¹⁰³ M. Cobal^{69a,69c}
A. Coccaro^{57b} R. F. Coelho Barrue^{131a} R. Coelho Lopes De Sa¹⁰⁴ S. Coelli^{71a} B. Cole⁴¹ J. Collot⁶⁰
P. Conde Muiño^{131a,131g} M. P. Connell^{33c} S. H. Connell^{33c} E. I. Conroy¹²⁷ F. Conventi^{72a,m} H. G. Cooke²⁰
A. M. Cooper-Sarkar¹²⁷ F. A. Corchia^{23b,23a} A. Cordeiro Oudot Choi¹²⁸ L. D. Corpe⁴⁰ M. Corradi^{75a,75b}
F. Corriveau^{105,n} A. Cortes-Gonzalez¹⁸ M. J. Costa¹⁶⁴ F. Costanza⁴ D. Costanzo¹⁴⁰ B. M. Cote¹²⁰
G. Cowan⁹⁶ K. Cranmer¹⁷¹ D. Cremonini^{23b,23a} S. Crépe-Renaudin⁶⁰ F. Crescioli¹²⁸ M. Cristinziani¹⁴²
M. Cristoforetti^{78a,78b} V. Croft¹¹⁵ J. E. Crosby¹²² G. Crosetti^{43b,43a} A. Cueto¹⁰⁰ H. Cui^{14a,14e} Z. Cui⁷
W. R. Cunningham⁵⁹ F. Curcio¹⁶⁴ J. R. Curran⁵² P. Czodrowski³⁶ M. M. Czurylo³⁶
M. J. Da Cunha Sargedas De Sousa^{57b,57a} J. V. Da Fonseca Pinto^{83b} C. Da Via¹⁰² W. Dabrowski^{86a} T. Dado⁴⁹
S. Dahbi¹⁴⁹ T. Dai¹⁰⁷ D. Dal Santo¹⁹ C. Dallapiccola¹⁰⁴ M. Dam⁴² G. D'amen²⁹ V. D'Amico¹¹⁰
J. Damp¹⁰¹ J. R. Dandoy³⁴ M. Danninger¹⁴³ V. Dao³⁶ G. Darbo^{57b} S. J. Das^{29,o} F. Dattola⁴⁸
S. D'Auria^{71a,71b} A. D'avanzo^{72a,72b} C. David^{33a} T. Davidek¹³⁴ B. Davis-Purcell³⁴ I. Dawson⁹⁵
H. A. Day-hall¹³³ K. De⁸ R. De Asmundis^{72a} N. De Biase⁴⁸ S. De Castro^{23b,23a} N. De Groot¹¹⁴ P. de Jong¹¹⁵
H. De la Torre¹¹⁶ A. De Maria^{14c} A. De Salvo^{75a} U. De Sanctis^{76a,76b} F. De Santis^{70a,70b} A. De Santo¹⁴⁷
J. B. De Vivie De Regie⁶⁰ D. V. Dedovich³⁸ J. Degens⁹³ A. M. Deiana⁴⁴ F. Del Corso^{23b,23a} J. Del Peso¹⁰⁰
F. Del Rio^{63a} L. Delagrangé¹²⁸ F. Deliot¹³⁶ C. M. Delitzsch⁴⁹ M. Della Pietra^{72a,72b} D. Della Volpe⁵⁶
A. Dell'Acqua³⁶ L. Dell'Asta^{71a,71b} M. Delmastro⁴ P. A. Delsart⁶⁰ S. Demers¹⁷³ M. Demichev³⁸
S. P. Denisov³⁷ L. D'Eramo⁴⁰ D. Derendarz⁸⁷ F. Derue¹²⁸ P. Dervan⁹³ K. Desch²⁴ C. Deutsch²⁴
F. A. Di Bello^{57b,57a} A. Di Ciaccio^{76a,76b} L. Di Ciaccio⁴ A. Di Domenico^{75a,75b} C. Di Donato^{72a,72b}
A. Di Girolamo³⁶ G. Di Gregorio³⁶ A. Di Luca^{78a,78b} B. Di Micco^{77a,77b} R. Di Nardo^{77a,77b}
M. Diamantopoulou³⁴ F. A. Dias¹¹⁵ T. Dias Do Vale¹⁴³ M. A. Diaz^{138a,138b} F. G. Diaz Capriles²⁴
M. Didenko¹⁶⁴ E. B. Diehl¹⁰⁷ S. Díez Cornell⁴⁸ C. Díez Pardos¹⁴² C. Dimitriadi^{162,24} A. Dimitrievska²⁰
J. Dingfelder²⁴ I-M. Dinu^{27b} S. J. Dittmeier^{63b} F. Dittus³⁶ M. Divisek¹³⁴ F. Djama¹⁰³ T. Djobava^{150b}
C. Doglioni^{102,99} A. Dohnalova^{28a} J. Dolejsi¹³⁴ Z. Dolezal¹³⁴ K. M. Dona³⁹ M. Donadelli^{83c} B. Dong¹⁰⁸
J. Donini⁴⁰ A. D'Onofrio^{72a,72b} M. D'Onofrio⁹³ J. Dopke¹³⁵ A. Doria^{72a} N. Dos Santos Fernandes^{131a}
P. Dougan¹⁰² M. T. Dova⁹¹ A. T. Doyle⁵⁹ M. A. Draguet¹²⁷ E. Dreyer¹⁷⁰ I. Drivas-koulouris¹⁰
M. Dnevich¹¹⁸ M. Drozdova⁵⁶ D. Du^{62a} T. A. du Pree¹¹⁵ F. Dubinin³⁷ M. Dubovsky^{28a} E. Duchovni¹⁷⁰
G. Duckeck¹¹⁰ O. A. Ducu^{27b} D. Duda⁵² A. Dudarev³⁶ E. R. Duden²⁶ M. D'uffizi¹⁰² L. Duflost⁶⁶

M. Dührssen³⁶ I. Duminica^{27g} A. E. Dumitriu^{27b} M. Dunford^{63a} S. Dungs⁴⁹ K. Dunne^{47a,47b} A. Duperrin¹⁰³
 H. Duran Yildiz^{3a} M. Düren⁵⁸ A. Durglishvili^{150b} B. L. Dwyer¹¹⁶ G. I. Dyckes^{17a} M. Dyndal^{86a}
 B. S. Dziedzic⁸⁷ Z. O. Earnshaw¹⁴⁷ G. H. Eberwein¹²⁷ B. Eckerova^{28a} S. Eggebrecht⁵⁵
 E. Egidio Purcino De Souza¹²⁸ L. F. Ehrke⁵⁶ G. Eigen¹⁶ K. Einsweiler^{17a} T. Ekelof¹⁶² P. A. Ekman⁹⁹
 S. El Farkh^{35b} Y. El Ghazali^{35b} H. El Jarrari³⁶ A. El Moussaouy¹⁰⁹ V. Ellajosyula¹⁶² M. Ellert¹⁶²
 F. Ellinghaus¹⁷² N. Ellis³⁶ J. Elmsheuser²⁹ M. Elsayy^{117a} M. Elsing³⁶ D. Emeliyanov¹³⁵ Y. Enari¹⁵⁴
 I. Ene^{17a} S. Epari¹³ P. A. Erland⁸⁷ M. Errenst¹⁷² M. Escalier⁶⁶ C. Escobar¹⁶⁴ E. Etzion¹⁵² G. Evans^{131a}
 H. Evans⁶⁸ L. S. Evans⁹⁶ A. Ezhilov³⁷ S. Ezzarqtouni^{35a} F. Fabbri^{23b,23a} L. Fabbri^{23b,23a} G. Facini⁹⁷
 V. Fadeyev¹³⁷ R. M. Fakhrtudinov³⁷ D. Fakoudis¹⁰¹ S. Falciano^{75a} L. F. Falda Ulhoa Coelho³⁶ P. J. Falke²⁴
 F. Fallavollita¹¹¹ J. Faltova¹³⁴ C. Fan¹⁶³ Y. Fan^{14a} Y. Fang^{14a,14e} M. Fanti^{71a,71b} M. Faraj^{69a,69b}
 Z. Farazpay⁹⁸ A. Farbin⁸ A. Farilla^{77a} T. Farooque¹⁰⁸ S. M. Farrington⁵² F. Fassi^{35e} D. Fassouliotis⁹
 M. Fauci Giannelli^{76a,76b} W. J. Fawcett³² L. Fayard⁶⁶ P. Federic¹³⁴ P. Federicova¹³² O. L. Fedin^{37,k}
 M. Feickert¹⁷¹ L. Feligioni¹⁰³ D. E. Fellers¹²⁴ C. Feng^{62b} M. Feng^{14b} Z. Feng¹¹⁵ M. J. Fenton¹⁶⁰
 L. Ferencz⁴⁸ R. A. M. Ferguson⁹² S. I. Fernandez Luengo^{138f} P. Fernandez Martinez¹³ M. J. V. Fernoux¹⁰³
 J. Ferrando⁹² A. Ferrari¹⁶² P. Ferrari^{115,114} R. Ferrari^{73a} D. Ferrere⁵⁶ C. Ferretti¹⁰⁷ F. Fiedler¹⁰¹
 P. Fiedler¹³³ A. Filipčić⁹⁴ E. K. Filmer¹ F. Filthaut¹¹⁴ M. C. N. Fiolhais^{131a,131c,p} L. Fiorini¹⁶⁴
 W. C. Fisher¹⁰⁸ T. Fitschen¹⁰² P. M. Fitzhugh¹³⁶ I. Fleck¹⁴² P. Fleischmann¹⁰⁷ T. Flick¹⁷² M. Flores^{33d,q}
 L. R. Flores Castillo^{64a} L. Flores Sanz De Acedo³⁶ F. M. Follega^{78a,78b} N. Fomin¹⁶ J. H. Foo¹⁵⁶ A. Formica¹³⁶
 A. C. Forti¹⁰² E. Fortin³⁶ A. W. Fortman^{17a} M. G. Foti^{17a} L. Fountas^{9,r} D. Fournier⁶⁶ H. Fox⁹²
 P. Francavilla^{74a,74b} S. Francescato⁶¹ S. Franchellucci⁵⁶ M. Franchini^{23b,23a} S. Franchino^{63a} D. Francis³⁶
 L. Franco¹¹⁴ V. Franco Lima³⁶ L. Franconi⁴⁸ M. Franklin⁶¹ G. Frattari²⁶ W. S. Freund^{83b} Y. Y. Frid¹⁵²
 J. Friend⁵⁹ N. Fritzsche⁵⁰ A. Froch⁵⁴ D. Froidevaux³⁶ J. A. Frost¹²⁷ Y. Fu^{62a} S. Fuenzalida Garrido^{138f}
 M. Fujimoto¹⁰³ K. Y. Fung^{64a} E. Furtado De Simas Filho^{83e} M. Furukawa¹⁵⁴ J. Fuster¹⁶⁴ A. Gabrielli^{23b,23a}
 A. Gabrielli¹⁵⁶ P. Gadow³⁶ G. Gagliardi^{57b,57a} L. G. Gagnon^{17a} S. Gaid¹⁶¹ S. Galantzan¹⁵² E. J. Gallas¹²⁷
 B. J. Gallop¹³⁵ K. K. Gan¹²⁰ S. Ganguly¹⁵⁴ Y. Gao⁵² F. M. Garay Walls^{138a,138b} B. Garcia²⁹ C. García¹⁶⁴
 A. Garcia Alonso¹¹⁵ A. G. Garcia Caffaro¹⁷³ J. E. García Navarro¹⁶⁴ M. Garcia-Sciveres^{17a} G. L. Gardner¹²⁹
 R. W. Gardner³⁹ N. Garelli¹⁵⁹ D. Garg⁸⁰ R. B. Garg^{144,s} J. M. Gargan⁵² C. A. Garner¹⁵⁶ C. M. Garvey^{33a}
 P. Gaspar^{83b} V. K. Gassmann¹⁵⁹ G. Gaudio^{73a} V. Gautam¹³ P. Gauzzi^{75a,75b} I. L. Gavrilenko³⁷ A. Gavriyuk³⁷
 C. Gay¹⁶⁵ G. Gaycken⁴⁸ E. N. Gazis¹⁰ A. A. Geanta^{27b} C. M. Gee¹³⁷ A. Gekow¹²⁰ C. Gemme^{57b}
 M. H. Genest⁶⁰ A. D. Gentry¹¹³ S. George⁹⁶ W. F. George²⁰ T. Gerialis⁴⁶ P. Gessinger-Befurt³⁶
 M. E. Geyik¹⁷² M. Ghani¹⁶⁸ K. Ghorbanian⁹⁵ A. Ghosal¹⁴² A. Ghosh¹⁶⁰ A. Ghosh⁷ B. Giacobbe^{23b}
 S. Giagu^{75a,75b} T. Giani¹¹⁵ P. Giannetti^{74a} A. Giannini^{62a} S. M. Gibson⁹⁶ M. Gignac¹³⁷ D. T. Gil^{86b}
 A. K. Gilbert^{86a} B. J. Gilbert⁴¹ D. Gillberg³⁴ G. Gilles¹¹⁵ L. Ginabat¹²⁸ D. M. Gingrich^{2,e}
 M. P. Giordani^{69a,69c} P. F. Giraud¹³⁶ G. Giugliarelli^{69a,69c} D. Giugni^{71a} F. Giuli³⁶ I. Gkialas^{9,r}
 L. K. Gladilin³⁷ C. Glasman¹⁰⁰ G. R. Gledhill¹²⁴ G. Glemža⁴⁸ M. Glisic¹²⁴ I. Gnesi^{43b,t} Y. Go²⁹
 M. Goblirsch-Kolb³⁶ B. Gocke⁴⁹ D. Godin¹⁰⁹ B. Gokturk^{21a} S. Goldfarb¹⁰⁶ T. Golling⁵⁶ M. G. D. Gololo^{33g}
 D. Golubkov³⁷ J. P. Gombas¹⁰⁸ A. Gomes^{131a,131b} G. Gomes Da Silva¹⁴² A. J. Gomez Delegido¹⁶⁴
 R. Gonçalves^{131a,131c} L. Gonella²⁰ A. Gongadze^{150c} F. Gonnella²⁰ J. L. Gonski¹⁴⁴ R. Y. González Andana⁵²
 S. González de la Hoz¹⁶⁴ R. Gonzalez Lopez⁹³ C. Gonzalez Renteria^{17a} M. V. Gonzalez Rodrigues⁴⁸
 R. Gonzalez Suarez¹⁶² S. Gonzalez-Sevilla⁵⁶ L. Goossens³⁶ B. Gorini³⁶ E. Gorini^{70a,70b} A. Gorišek⁹⁴
 T. C. Gosart¹²⁹ A. T. Goshaw⁵¹ M. I. Gostkin³⁸ S. Goswami¹²² C. A. Gottardo³⁶ S. A. Gotz¹¹⁰
 M. Goughri^{35b} V. Goumarre⁴⁸ A. G. Goussiou¹³⁹ N. Govender^{33c} I. Grabowska-Bold^{86a} K. Graham³⁴
 E. Gramstad¹²⁶ S. Grancagnolo^{70a,70b} C. M. Grant^{1,136} P. M. Gravila^{27f} F. G. Gravili^{70a,70b} H. M. Gray^{17a}
 M. Greco^{70a,70b} C. Grefe²⁴ I. M. Gregor⁴⁸ K. T. Greif¹⁶⁰ P. Grenier¹⁴⁴ S. G. Grewe¹¹¹ A. A. Grillo¹³⁷
 K. Grimm³¹ S. Grinstein^{13,u} J.-F. Grivaz⁶⁶ E. Gross¹⁷⁰ J. Grosse-Knetter⁵⁵ J. C. Grundy¹²⁷ L. Guan¹⁰⁷
 C. Gubbels¹⁶⁵ J. G. R. Guerrero Rojas¹⁶⁴ G. Guerrieri^{69a,69c} F. Guescini¹¹¹ R. Gugel¹⁰¹ J. A. M. Guhit¹⁰⁷
 A. Guida¹⁸ E. Guillon¹⁶⁸ S. Guindon³⁶ F. Guo^{14a,14e} J. Guo^{62c} L. Guo⁴⁸ Y. Guo¹⁰⁷ R. Gupta⁴⁸
 R. Gupta¹³⁰ S. Gurbuz²⁴ S. S. Gurdasani⁵⁴ G. Gustavino³⁶ M. Guth⁵⁶ P. Gutierrez¹²¹
 L. F. Gutierrez Zagazeta¹²⁹ M. Gutsche⁵⁰ C. Gutschow⁹⁷ C. Gwenlan¹²⁷ C. B. Gwilliam⁹³ E. S. Haaland¹²⁶

A. Haas¹¹⁸ M. Habedank⁴⁸ C. Haber^{17a} H. K. Hadavand⁸ A. Hadeef⁵⁰ S. Hadzic¹¹¹ A. I. Hagan⁹²
 J. J. Hahn¹⁴² E. H. Haines⁹⁷ M. Haleem¹⁶⁷ J. Haley¹²² J. J. Hall¹⁴⁰ G. D. Hallewell¹⁰³ L. Halser¹⁹
 K. Hamano¹⁶⁶ M. Hamer²⁴ G. N. Hamity⁵² E. J. Hampshire⁹⁶ J. Han^{62b} K. Han^{62a} L. Han^{14c} L. Han^{62a}
 S. Han^{17a} Y. F. Han¹⁵⁶ K. Hanagaki⁸⁴ M. Hance¹³⁷ D. A. Hangal⁴¹ H. Hanif¹⁴³ M. D. Hank¹²⁹
 J. B. Hansen⁴² P. H. Hansen⁴² K. Hara¹⁵⁸ D. Harada⁵⁶ T. Harenberg¹⁷² S. Harkusha³⁷ M. L. Harris¹⁰⁴
 Y. T. Harris¹²⁷ J. Harrison¹³ N. M. Harrison¹²⁰ P. F. Harrison¹⁶⁸ N. M. Hartman¹¹¹ N. M. Hartmann¹¹⁰
 Y. Hasegawa¹⁴¹ S. Hassan¹⁶ R. Hauser¹⁰⁸ C. M. Hawkes²⁰ R. J. Hawkins³⁶ Y. Hayashi¹⁵⁴ S. Hayashida¹¹²
 D. Hayden¹⁰⁸ C. Hayes¹⁰⁷ R. L. Hayes¹¹⁵ C. P. Hays¹²⁷ J. M. Hays⁹⁵ H. S. Hayward⁹³ F. He^{62a}
 M. He^{14a,14e} Y. He¹⁵⁵ Y. He⁴⁸ Y. He⁹⁷ N. B. Heatley⁹⁵ V. Hedberg⁹⁹ A. L. Heggelund¹²⁶ N. D. Hehir^{95,a}
 C. Heidegger⁵⁴ K. K. Heidegger⁵⁴ W. D. Heidorn⁸¹ J. Heilmann³⁴ S. Heim⁴⁸ T. Heim^{17a} J. G. Heinlein¹²⁹
 J. J. Heinrich¹²⁴ L. Heinrich^{111,v} J. Hejbal¹³² A. Held¹⁷¹ S. Hellesund¹⁶ C. M. Helling¹⁶⁵ S. Hellman^{47a,47b}
 R. C. W. Henderson⁹² L. Henkelmann³² A. M. Henriques Correia³⁶ H. Herde⁹⁹ Y. Hernández Jiménez¹⁴⁶
 L. M. Herrmann²⁴ T. Herrmann⁵⁰ G. Hertel⁵⁴ R. Hertenberger¹¹⁰ L. Hervas³⁶ M. E. Hespig¹⁰¹
 N. P. Hessey^{157a} M. Hidaoui^{35b} E. Hill¹⁵⁶ S. J. Hillier²⁰ J. R. Hinds¹⁰⁸ F. Hinterkeuser²⁴ M. Hirose¹²⁵
 S. Hirose¹⁵⁸ D. Hirschbuehl¹⁷² T. G. Hitchings¹⁰² B. Hiti⁹⁴ J. Hobbs¹⁴⁶ R. Hobincu^{27e} N. Hod¹⁷⁰
 M. C. Hodgkinson¹⁴⁰ B. H. Hodgkinson¹²⁷ A. Hoecker³⁶ D. D. Hofer¹⁰⁷ J. Hofer⁴⁸ T. Holm²⁴
 M. Holzbock¹¹¹ L. B. A. H. Hommels³² B. P. Honan¹⁰² J. Hong^{62c} T. M. Hong¹³⁰ B. H. Hooberman¹⁶³
 W. H. Hopkins⁶ Y. Horii¹¹² S. Hou¹⁴⁹ A. S. Howard⁹⁴ J. Howarth⁵⁹ J. Hoya⁶ M. Hrabovsky¹²³
 A. Hrynevich⁴⁸ T. Hryn'ova⁴ P. J. Hsu⁶⁵ S.-C. Hsu¹³⁹ T. Hsu⁶⁶ M. Hu^{17a} Q. Hu^{62a} S. Huang^{64b}
 X. Huang^{14a,14e} Y. Huang¹⁴⁰ Y. Huang¹⁰¹ Y. Huang^{14a} Z. Huang¹⁰² Z. Hubacek¹³³ M. Huebner²⁴
 F. Huegging²⁴ T. B. Huffman¹²⁷ C. A. Hugli⁴⁸ M. Huhtinen³⁶ S. K. Huiberts¹⁶ R. Hulsken¹⁰⁵
 N. Huseynov¹² J. Huston¹⁰⁸ J. Huth⁶¹ R. Hyneman¹⁴⁴ G. Iacobucci⁵⁶ G. Iakovidis²⁹ I. Ibragimov¹⁴²
 L. Iconomidou-Fayard⁶⁶ J. P. Iddon³⁶ P. Iengo^{72a,72b} R. Iguchi¹⁵⁴ T. Iizawa¹²⁷ Y. Ikegami⁸⁴ N. Ilic¹⁵⁶
 H. Imam^{35a} M. Ince Lezki⁵⁶ T. Ingebretsen Carlson^{47a,47b} G. Introzzi^{73a,73b} M. Iodice^{77a} V. Ippolito^{75a,75b}
 R. K. Irwin⁹³ M. Ishino¹⁵⁴ W. Islam¹⁷¹ C. Issever^{18,48} S. Istin^{21a,w} H. Ito¹⁶⁹ R. Iuppa^{78a,78b} A. Ivina¹⁷⁰
 J. M. Izen⁴⁵ V. Izzo^{72a} P. Jacka^{132,133} P. Jackson¹ B. P. Jaeger¹⁴³ C. S. Jagfeld¹¹⁰ G. Jain^{157a} P. Jain⁵⁴
 K. Jakobs⁵⁴ T. Jakoubek¹⁷⁰ J. Jamieson⁵⁹ K. W. Janas^{86a} M. Javurkova¹⁰⁴ L. Jeanty¹²⁴ J. Jejelava^{150a,x}
 P. Jenni^{54,y} C. E. Jessiman³⁴ C. Jia^{62b} J. Jia¹⁴⁶ X. Jia⁶¹ X. Jia^{14a,14e} Z. Jia^{14c} C. Jiang⁵² S. Jiggins⁴⁸
 J. Jimenez Pena¹³ S. Jin^{14c} A. Jinaru^{27b} O. Jinnouchi¹⁵⁵ P. Johansson¹⁴⁰ K. A. Johns⁷ J. W. Johnson¹³⁷
 D. M. Jones¹⁴⁷ E. Jones⁴⁸ P. Jones³² R. W. L. Jones⁹² T. J. Jones⁹³ H. L. Joos^{55,36} R. Joshi¹²⁰
 J. Jovicevic¹⁵ X. Ju^{17a} J. J. Junggeburth¹⁰⁴ T. Junkermann^{63a} A. Juste Rozas^{13,u} M. K. Juzek⁸⁷ S. Kabana^{138e}
 A. Kaczmarek⁸⁷ M. Kado¹¹¹ H. Kagan¹²⁰ M. Kagan¹⁴⁴ A. Kahn⁴¹ A. Kahn¹²⁹ C. Kahra¹⁰¹ T. Kaji¹⁵⁴
 E. Kajomovitz¹⁵¹ N. Kakati¹⁷⁰ I. Kalaitzidou⁵⁴ C. W. Kalderon²⁹ N. J. Kang¹³⁷ D. Kar^{33g} K. Karava¹²⁷
 M. J. Kareem^{157b} E. Karentzos⁵⁴ I. Karkanas¹⁵³ O. Karkout¹¹⁵ S. N. Karpov³⁸ Z. M. Karpova³⁸
 V. Kartvelishvili⁹² A. N. Karyukhin³⁷ E. Kasimi¹⁵³ J. Katzy⁴⁸ S. Kaur³⁴ K. Kawade¹⁴¹ M. P. Kawale¹²¹
 C. Kawamoto⁸⁸ T. Kawamoto^{62a} E. F. Kay³⁶ F. I. Kaya¹⁵⁹ S. Kazakos¹⁰⁸ V. F. Kazanin³⁷ Y. Ke¹⁴⁶
 J. M. Keaveney^{33a} R. Keeler¹⁶⁶ G. V. Kehris⁶¹ J. S. Keller³⁴ A. S. Kelly⁹⁷ J. J. Kempster¹⁴⁷ P. D. Kennedy¹⁰¹
 O. Kepka¹³² B. P. Kerridge¹³⁵ S. Kersten¹⁷² B. P. Kerševan⁹⁴ L. Keszeghova^{28a} S. Ketabchi Haghightat¹⁵⁶
 R. A. Khan¹³⁰ A. Khanov¹²² A. G. Kharlamov³⁷ T. Kharlamova³⁷ E. E. Khoda¹³⁹ M. Kholodenko³⁷
 T. J. Khoo¹⁸ G. Khoriauli¹⁶⁷ J. Khubua^{150b} Y. A. R. Khwaira⁶⁶ B. Kibirige^{33g} A. Kilgallon¹²⁴ D. W. Kim^{47a,47b}
 Y. K. Kim³⁹ N. Kimura⁹⁷ M. K. Kingston⁵⁵ A. Kirchoff⁵⁵ C. Kirfel²⁴ F. Kirfel²⁴ J. Kirk¹³⁵
 A. E. Kiryunin¹¹¹ C. Kitsaki¹⁰ O. Kivernyk²⁴ M. Klassen¹⁵⁹ C. Klein³⁴ L. Klein¹⁶⁷ M. H. Klein⁴⁴
 S. B. Klein⁵⁶ U. Klein⁹³ P. Klimek³⁶ A. Klimentov²⁹ T. Klioutchnikova³⁶ P. Kluit¹¹⁵ S. Kluth¹¹¹
 E. Kneringer⁷⁹ T. M. Knight¹⁵⁶ A. Knue⁴⁹ R. Kobayashi⁸⁸ D. Kobylanskii¹⁷⁰ S. F. Koch¹²⁷ M. Kocian¹⁴⁴
 P. Kodyš¹³⁴ D. M. Koeck¹²⁴ P. T. Koenig²⁴ T. Koffas³⁴ O. Kolay⁵⁰ I. Koletsou⁴ T. Komarek¹²³
 K. Köneke⁵⁴ A. X. Y. Kong¹ T. Kono¹¹⁹ N. Konstantinidis⁹⁷ P. Kontaxakis⁵⁶ B. Konya⁹⁹ R. Kopeliansky⁴¹
 S. Koperny^{86a} K. Korcyl⁸⁷ K. Kordas^{153,z} A. Korn⁹⁷ S. Korn⁵⁵ I. Korolkov¹³ N. Korotkova³⁷
 B. Kortman¹¹⁵ O. Kortner¹¹¹ S. Kortner¹¹¹ W. H. Kostecka¹¹⁶ V. V. Kostyukhin¹⁴² A. Kotskechagia¹³⁶
 A. Kotwal⁵¹ A. Koulouris³⁶ A. Kourkoumeli-Charalampidi^{73a,73b} C. Kourkoumelis⁹ E. Kourlitis^{111,v}

O. Kovanda¹²⁴ R. Kowalewski¹⁶⁶ W. Kozanecki¹³⁶ A. S. Kozhin³⁷ V. A. Kramarenko³⁷ G. Kramberger⁹⁴
P. Kramer¹⁰¹ M. W. Krasny¹²⁸ A. Krasznahorkay³⁶ J. W. Kraus¹⁷² J. A. Kremer⁴⁸ T. Kresse⁵⁰
J. Kretzschmar⁹³ K. Kreul¹⁸ P. Krieger¹⁵⁶ S. Krishnamurthy¹⁰⁴ M. Krivos¹³⁴ K. Krizka²⁰ K. Kroeninger⁴⁹
H. Kroha¹¹¹ J. Kroll¹³² J. Kroll¹²⁹ K. S. Krowpman¹⁰⁸ U. Kruchonak³⁸ H. Krüger²⁴ N. Krumnack,⁸¹
M. C. Kruse⁵¹ O. Kuchinskaia³⁷ S. Kuday^{3a} S. Kuehn³⁶ R. Kuesters⁵⁴ T. Kuhl⁴⁸ V. Kukhtin³⁸
Y. Kulchitsky^{37,k} S. Kuleshov^{138d,138b} M. Kumar^{33g} N. Kumari⁴⁸ P. Kumari^{157b} A. Kupco¹³² T. Kupfer,⁴⁹
A. Kupich³⁷ O. Kuprash⁵⁴ H. Kurashige⁸⁵ L. L. Kurchaninov^{157a} O. Kurdyshev⁶⁶ Y. A. Kurochkin³⁷
A. Kurova³⁷ M. Kuze¹⁵⁵ A. K. Kvam¹⁰⁴ J. Kvita¹²³ T. Kwan¹⁰⁵ N. G. Kyriacou¹⁰⁷ L. A. O. Laatu¹⁰³
C. Lacasta¹⁶⁴ F. Lacava^{75a,75b} H. Lacker¹⁸ D. Lacour¹²⁸ N. N. Lad⁹⁷ E. Ladygin³⁸ A. Lafarge⁴⁰
B. Laforge¹²⁸ T. Lagouri¹⁷³ F. Z. Lahbabi^{35a} S. Lai⁵⁵ I. K. Lakomic^{86a} J. E. Lambert¹⁶⁶ S. Lammers⁶⁸
W. Lampl⁷ C. Lampoudis^{153,z} G. Lamprinoudis,¹⁰¹ A. N. Lancaster¹¹⁶ E. Lançon²⁹ U. Landgraf⁵⁴
M. P. J. Landon⁹⁵ V. S. Lang⁵⁴ O. K. B. Langrekken¹²⁶ A. J. Lankford¹⁶⁰ F. Lanni³⁶ K. Lantzsche²⁴
A. Lanza^{73a} A. Lapertosa^{57b,57a} J. F. Laporte¹³⁶ T. Lari^{71a} F. Lasagni Manghi^{23b} M. Lassnig³⁶ V. Latonova¹³²
A. Laudrain¹⁰¹ A. Laurier¹⁵¹ S. D. Lawlor¹⁴⁰ Z. Lawrence¹⁰² R. Lazaridou,¹⁶⁸ M. Lazzaroni^{71a,71b} B. Le,¹⁰²
E. M. Le Boulicaut⁵¹ L. T. Le Pottier^{17a} B. Leban^{23b,23a} A. Lebedev⁸¹ M. LeBlanc¹⁰² F. Ledroit-Guillon⁶⁰
A. C. A. Lee,⁹⁷ S. C. Lee¹⁴⁹ S. Lee^{47a,47b} T. F. Lee⁹³ L. L. Leeuw^{33c} H. P. Lefebvre⁹⁶ M. Lefebvre¹⁶⁶
C. Leggett^{17a} G. Lehmann Miotto³⁶ M. Leigh⁵⁶ W. A. Leight¹⁰⁴ W. Leinonen¹¹⁴ A. Leisos^{153,aa}
M. A. L. Leite^{83c} C. E. Leitgeb¹⁸ R. Leitner¹³⁴ K. J. C. Leney⁴⁴ T. Lenz²⁴ S. Leone^{74a} C. Leonidopoulos⁵²
A. Leopold¹⁴⁵ C. Leroy¹⁰⁹ R. Les¹⁰⁸ C. G. Lester³² M. Levchenko³⁷ J. Levêque⁴ L. J. Levinson¹⁷⁰
G. Levrini,^{23b,23a} M. P. Lewicki⁸⁷ C. Lewis¹³⁹ D. J. Lewis⁴ A. Li⁵ B. Li^{62b} C. Li,^{62a} C-Q. Li¹¹¹ H. Li^{62a}
H. Li^{62b} H. Li^{14c} H. Li^{14b} H. Li^{62b} J. Li^{62c} K. Li¹³⁹ L. Li^{62c} M. Li^{14a,14e} Q. Y. Li^{62a} S. Li^{14a,14e}
S. Li^{62d,62c,bb} T. Li⁵ X. Li¹⁰⁵ Z. Li¹²⁷ Z. Li¹⁰⁵ Z. Li^{14a,14e} S. Liang,^{14a,14e} Z. Liang^{14a} M. Liberatore¹³⁶
B. Liberti^{76a} K. Lie^{64c} J. Lieber Marin^{83e} H. Lien⁶⁸ K. Lin¹⁰⁸ R. E. Lindley⁷ J. H. Lindon² E. Lipeles¹²⁹
A. Lipniacka¹⁶ A. Lister¹⁶⁵ J. D. Little⁴ B. Liu^{14a} B. X. Liu¹⁴³ D. Liu^{62d,62c} E. H. L. Liu²⁰ J. B. Liu^{62a}
J. K. K. Liu³² K. Liu^{62d} K. Liu^{62d,62c} M. Liu^{62a} M. Y. Liu^{62a} P. Liu^{14a} Q. Liu^{62d,139,62c} X. Liu^{62a} X. Liu^{62b}
Y. Liu^{14d,14e} Y. L. Liu^{62b} Y. W. Liu^{62a} J. Llorente Merino¹⁴³ S. L. Lloyd⁹⁵ E. M. Lobodzinska⁴⁸ P. Loch⁷
T. Lohse¹⁸ K. Lohwasser¹⁴⁰ E. Loiacono⁴⁸ M. Lokajicek^{132,a} J. D. Lomas²⁰ J. D. Long¹⁶³ I. Longarini¹⁶⁰
L. Longo^{70a,70b} R. Longo¹⁶³ I. Lopez Paz⁶⁷ A. Lopez Solis⁴⁸ N. Lorenzo Martinez⁴ A. M. Lory¹¹⁰
G. Löschecke Centeno¹⁴⁷ O. Loseva³⁷ X. Lou^{47a,47b} X. Lou^{14a,14e} A. Lounis⁶⁶ P. A. Love⁹² G. Lu^{14a,14e}
M. Lu⁶⁶ S. Lu¹²⁹ Y. J. Lu⁶⁵ H. J. Lubatti¹³⁹ C. Luci^{75a,75b} F. L. Lucio Alves^{14c} F. Luehring⁶⁸ I. Luise¹⁴⁶
O. Lukianchuk⁶⁶ O. Lundberg¹⁴⁵ B. Lund-Jensen¹⁴⁵ N. A. Luongo⁶ M. S. Lutz³⁶ A. B. Lux²⁵ D. Lynn²⁹
R. Lysak¹³² E. Lytken⁹⁹ V. Lyubushkin³⁸ T. Lyubushkina³⁸ M. M. Lyukova¹⁴⁶ M. Firdaus M. Soberi⁵²
H. Ma²⁹ K. Ma,^{62a} L. L. Ma^{62b} W. Ma^{62a} Y. Ma¹²² D. M. Mac Donell¹⁶⁶ G. Maccarrone⁵³
J. C. MacDonald¹⁰¹ P. C. Machado De Abreu Farias^{83e} R. Madar⁴⁰ T. Madula⁹⁷ J. Maeda⁸⁵ T. Maeno²⁹
H. Maguire¹⁴⁰ V. Maiboroda¹³⁶ A. Maio^{131a,131b,131d} K. Maj^{86a} O. Majersky⁴⁸ S. Majewski¹²⁴ N. Makovec⁶⁶
V. Maksimovic¹⁵ B. Malaescu¹²⁸ Pa. Malecki⁸⁷ V. P. Maleev³⁷ F. Malek^{60,cc} M. Mali⁹⁴ D. Malito⁹⁶
U. Mallik⁸⁰ S. Maltezos,¹⁰ S. Malyukov,³⁸ J. Mamuzic¹³ G. Mancini⁵³ M. N. Mancini²⁶ G. Manco^{73a,73b}
J. P. Mandalia⁹⁵ I. Mandić⁹⁴ L. Manhaes de Andrade Filho^{83a} I. M. Maniatis¹⁷⁰ J. Manjarres Ramos⁹⁰
D. C. Mankad¹⁷⁰ A. Mann¹¹⁰ S. Manzoni³⁶ L. Mao^{62c} X. Mapekula^{33c} A. Marantis^{153,aa} G. Marchiori⁵
M. Marcisovsky¹³² C. Marcon^{71a} M. Marinescu²⁰ S. Marium⁴⁸ M. Marjanovic¹²¹ A. Markhoos⁵⁴
M. Markovitch⁶⁶ E. J. Marshall⁹² Z. Marshall^{17a} S. Marti-Garcia¹⁶⁴ T. A. Martin¹⁶⁸ V. J. Martin⁵²
B. Martin dit Latour¹⁶ L. Martinelli^{75a,75b} M. Martinez^{13,u} P. Martinez Agullo¹⁶⁴ V. I. Martinez Outschoorn¹⁰⁴
P. Martinez Suarez¹³ S. Martin-Haugh¹³⁵ G. Martinovicova¹³⁴ V. S. Martoiu^{27b} A. C. Martyniuk⁹⁷
A. Marzin³⁶ D. Mascione^{78a,78b} L. Masetti¹⁰¹ T. Mashimo¹⁵⁴ J. Masik¹⁰² A. L. Maslennikov³⁷
P. Massarotti^{72a,72b} P. Mastrandrea^{74a,74b} A. Mastroberardino^{43b,43a} T. Masubuchi¹⁵⁴ T. Mathisen¹⁶²
J. Matousek¹³⁴ N. Matsuzawa,¹⁵⁴ J. Maurer^{27b} A. J. Maury⁶⁶ B. Maček⁹⁴ D. A. Maximov³⁷ A. E. May¹⁰²
R. Mazini¹⁴⁹ I. Maznas¹¹⁶ M. Mazza¹⁰⁸ S. M. Mazza¹³⁷ E. Mazzeo^{71a,71b} C. Mc Ginn²⁹ J. P. Mc Gowan¹⁶⁶
S. P. Mc Kee¹⁰⁷ C. C. McCracken¹⁶⁵ E. F. McDonald¹⁰⁶ A. E. McDougall¹¹⁵ J. A. Mcfayden¹⁴⁷
R. P. McGovern¹²⁹ G. Mchedlidze^{150b} R. P. McKenzie^{33g} T. C. Mclachlan⁴⁸ D. J. McLaughlin⁹⁷

S. J. McMahon¹³⁵ C. M. Mcpartland⁹³ R. A. McPherson^{166,n} S. Mehlhase¹¹⁰ A. Mehta⁹³ D. Melini¹⁶⁴
 B. R. Mellado Garcia^{33g} A. H. Melo⁵⁵ F. Meloni⁴⁸ A. M. Mendes Jacques Da Costa¹⁰² H. Y. Meng¹⁵⁶
 L. Meng⁹² S. Menke¹¹¹ M. Mentink³⁶ E. Meoni^{43b,43a} G. Mercado¹¹⁶ C. Merlassino^{69a,69c} L. Merola^{72a,72b}
 C. Meroni^{71a,71b} J. Metcalfe⁶ A. S. Mete⁶ C. Meyer⁶⁸ J-P. Meyer¹³⁶ R. P. Middleton¹³⁵ L. Mijović⁵²
 G. Mikenberg¹⁷⁰ M. Mikestikova¹³² M. Mikuš⁹⁴ H. Mildner¹⁰¹ A. Milic³⁶ D. W. Miller³⁹ E. H. Miller¹⁴⁴
 L. S. Miller³⁴ A. Milov¹⁷⁰ D. A. Milstead^{47a,47b} T. Min^{14c} A. A. Minaenko³⁷ I. A. Minashvili^{150b} L. Mince⁵⁹
 A. I. Mincer¹¹⁸ B. Mindur^{86a} M. Mineev³⁸ Y. Mino⁸⁸ L. M. Mir¹³ M. Miralles Lopez⁵⁹ M. Mironova^{17a}
 A. Mishima¹⁵⁴ M. C. Missio¹¹⁴ A. Mitra¹⁶⁸ V. A. Mitsou¹⁶⁴ Y. Mitsumori¹¹² O. Miu¹⁵⁶ P. S. Miyagawa⁹⁵
 T. Mkrtchyan^{63a} M. Mlinarevic⁹⁷ T. Mlinarevic⁹⁷ M. Mlynarikova³⁶ S. Mobius¹⁹ P. Mogg¹¹⁰
 M. H. Mohamed Farook¹¹³ A. F. Mohammed^{14a,14e} S. Mohapatra⁴¹ G. Mokgatitswane^{33g} L. Moleri¹⁷⁰
 B. Mondal¹⁴² S. Mondal¹³³ K. Mönig⁴⁸ E. Monnier¹⁰³ L. Monsonis Romero¹⁶⁴ J. Montejo Berlingen¹³
 M. Montella¹²⁰ F. Montekali^{77a,77b} F. Monticelli⁹¹ S. Monzani^{69a,69c} N. Morange⁶⁶
 A. L. Moreira De Carvalho⁴⁸ M. Moreno Llácer¹⁶⁴ C. Moreno Martinez⁵⁶ P. Morettini^{57b} S. Morgenstern³⁶
 M. Morii⁶¹ M. Morinaga¹⁵⁴ F. Morodei^{75a,75b} L. Morvaj³⁶ P. Moschovakos³⁶ B. Moser³⁶ M. Mosidze^{150b}
 T. Moskalets⁵⁴ P. Moskvitina¹¹⁴ J. Moss^{31,dd} P. Moszkowicz^{86a} A. Moussa^{35d} E. J. W. Moyse¹⁰⁴
 O. Mtintsilana^{33g} S. Muanza¹⁰³ J. Mueller¹³⁰ D. Muenstermann⁹² R. Müller¹⁹ G. A. Mullier¹⁶² A. J. Mullin³²
 J. J. Mullin¹²⁹ D. P. Mungo¹⁵⁶ D. Munoz Perez¹⁶⁴ F. J. Munoz Sanchez¹⁰² M. Murin¹⁰² W. J. Murray^{168,135}
 M. Muškinja⁹⁴ C. Mwewa²⁹ A. G. Myagkov^{37,k} A. J. Myers⁸ G. Myers¹⁰⁷ M. Myska¹³³ B. P. Nachman^{17a}
 O. Nackenhorst⁴⁹ K. Nagai¹²⁷ K. Nagano⁸⁴ J. L. Nagle^{29,o} E. Nagy¹⁰³ A. M. Nairz³⁶ Y. Nakahama⁸⁴
 K. Nakamura⁸⁴ K. Nakkalil⁵ H. Nanjo¹²⁵ R. Narayan⁴⁴ E. A. Narayanan¹¹³ I. Naryshkin³⁷ M. Naseri³⁴
 S. Nasri^{117b} C. Nass²⁴ G. Navarro^{22a} J. Navarro-Gonzalez¹⁶⁴ R. Nayak¹⁵² A. Nayaz¹⁸ P. Y. Nechaeva³⁷
 S. Nechaeva^{23b,23a} F. Nechansky⁴⁸ L. Nedic¹²⁷ T. J. Neep²⁰ A. Negri^{73a,73b} M. Negrini^{23b} C. Nellist¹¹⁵
 C. Nelson¹⁰⁵ K. Nelson¹⁰⁷ S. Nemecek¹³² M. Nessi^{36,ee} M. S. Neubauer¹⁶³ F. Neuhaus¹⁰¹ J. Neundorf⁴⁸
 R. Newhouse¹⁶⁵ P. R. Newman²⁰ C. W. Ng¹³⁰ Y. W. Y. Ng⁴⁸ B. Ngair^{117a} H. D. N. Nguyen¹⁰⁹
 R. B. Nickerson¹²⁷ R. Nicolaidou¹³⁶ J. Nielsen¹³⁷ M. Niemeyer⁵⁵ J. Niermann⁵⁵ N. Nikiforou³⁶
 V. Nikolaenko^{37,k} I. Nikolic-Audit¹²⁸ K. Nikolopoulos²⁰ P. Nilsson²⁹ I. Ninca⁴⁸ H. R. Nindhito⁵⁶
 G. Ninio¹⁵² A. Nisati^{75a} N. Nishu² R. Nisius¹¹¹ J-E. Nitschke⁵⁰ E. K. Nkadimeng^{33g} T. Nobe¹⁵⁴
 D. L. Noel³² T. Nommensen¹⁴⁸ M. B. Norfolk¹⁴⁰ R. R. B. Norisam⁹⁷ B. J. Norman³⁴ M. Noury^{35a}
 J. Novak⁹⁴ T. Novak⁴⁸ L. Novotny¹³³ R. Novotny¹¹³ L. Nozka¹²³ K. Ntekas¹⁶⁰
 N. M. J. Nunes De Moura Junior^{83b} J. Ocariz¹²⁸ A. Ochi⁸⁵ I. Ochoa^{131a} S. Oerdek^{48,ff} J. T. Offermann³⁹
 A. Ogrodnik¹³⁴ A. Oh¹⁰² C. C. Ohm¹⁴⁵ H. Oide⁸⁴ R. Oishi¹⁵⁴ M. L. Ojeda⁴⁸ Y. Okumura¹⁵⁴
 L. F. Oleiro Seabra^{131a} S. A. Olivares Pino^{138d} G. Oliveira Correa¹³ D. Oliveira Damazio²⁹
 D. Oliveira Goncalves^{83a} J. L. Oliver¹⁶⁰ Ö. O. Öncel⁵⁴ A. P. O'Neill¹⁹ A. Onofre^{131a,131e} P. U. E. Onyisi¹¹
 M. J. Oreglia³⁹ G. E. Orellana⁹¹ D. Orestano^{77a,77b} N. Orlando¹³ R. S. Orr¹⁵⁶ V. O'Shea⁵⁹ L. M. Osojnak¹²⁹
 R. Ospanov^{62a} G. Otero y Garzon³⁰ H. Otono⁸⁹ P. S. Ott^{63a} G. J. Ottino^{17a} M. Ouchrif^{35d} F. Ould-Saada¹²⁶
 T. Ovsianikova¹³⁹ M. Owen⁵⁹ R. E. Owen¹³⁵ K. Y. Oyulmaz^{21a} V. E. Ozcan^{21a} F. Ozturk⁸⁷ N. Ozturk⁸
 S. Ozturk⁸² H. A. Pacey¹²⁷ A. Pacheco Pages¹³ C. Padilla Aranda¹³ G. Padovano^{75a,75b} S. Pagan Griso^{17a}
 G. Palacino⁶⁸ A. Palazzo^{70a,70b} J. Pampel²⁴ J. Pan¹⁷³ T. Pan^{64a} D. K. Panchal¹¹ C. E. Pandini¹¹⁵
 J. G. Panduro Vazquez⁹⁶ H. D. Pandya¹ H. Pang^{14b} P. Pani⁴⁸ G. Panizzo^{69a,69c} L. Panwar¹²⁸ L. Paolozzi⁵⁶
 S. Parajuli¹⁶³ A. Paramonov⁶ C. Paraskevopoulos⁵³ D. Paredes Hernandez^{64b} A. Pareti^{73a,73b} K. R. Park⁴¹
 T. H. Park¹⁵⁶ M. A. Parker³² F. Parodi^{57b,57a} E. W. Parrish¹¹⁶ V. A. Parrish⁵² J. A. Parsons⁴¹ U. Parzefall⁵⁴
 B. Pascual Dias¹⁰⁹ L. Pascual Dominguez¹⁵² E. Pasqualucci^{75a} S. Passaggio^{57b} F. Pastore⁹⁶ P. Patel⁸⁷
 U. M. Patel⁵¹ J. R. Pater¹⁰² T. Pauly³⁶ C. I. Pazos¹⁵⁹ J. Pearkes¹⁴⁴ M. Pedersen¹²⁶ R. Pedro^{131a}
 S. V. Peleganchuk³⁷ O. Penc³⁶ E. A. Pender⁵² G. D. Penn¹⁷³ K. E. Pensi¹¹⁰ M. Penzin³⁷ B. S. Peralva^{83d}
 A. P. Pereira Peixoto¹³⁹ L. Pereira Sanchez¹⁴⁴ D. V. Perepelitsa^{29,o} E. Perez Codina^{157a} M. Perganti¹⁰
 H. Pernegger³⁶ O. Perrin⁴⁰ K. Peters⁴⁸ R. F. Y. Peters¹⁰² B. A. Petersen³⁶ T. C. Petersen⁴² E. Petit¹⁰³
 V. Petousis¹³³ C. Petridou^{153,z} T. Petru¹³⁴ A. Petrukhin¹⁴² M. Pettee^{17a} N. E. Pettersson³⁶ A. Petukhov³⁷
 K. Petukhova¹³⁴ R. Pezoa^{138f} L. Pezzotti³⁶ G. Pezzullo¹⁷³ T. M. Pham¹⁷¹ T. Pham¹⁰⁶ P. W. Phillips¹³⁵
 G. Piacquadio¹⁴⁶ E. Pianori^{17a} F. Piazza¹²⁴ R. Piegaia³⁰ D. Pietreanu^{27b} A. D. Pilkington¹⁰²

M. Pinamonti^{69a,69c} J. L. Pinfold² B. C. Pinheiro Pereira^{131a} A. E. Pinto Pinoargote^{101,136} L. Pintucci^{69a,69c}
K. M. Piper¹⁴⁷ A. Pirttikoski⁵⁶ D. A. Pizzi³⁴ L. Pizzimento^{64b} A. Pizzini¹¹⁵ M.-A. Pleier²⁹ V. Plesanovs,⁵⁴
V. Pleskot¹³⁴ E. Plotnikova,³⁸ G. Poddar⁹⁵ R. Poettgen⁹⁹ L. Poggioli¹²⁸ I. Pokharel⁵⁵ S. Polacek¹³⁴
G. Polesello^{73a} A. Poley^{143,157a} A. Polini^{23b} C. S. Pollard¹⁶⁸ Z. B. Pollock¹²⁰ E. Pompa Pacchi^{75a,75b}
D. Ponomarenko¹¹⁴ L. Pontecorvo³⁶ S. Popa^{27a} G. A. Popeneciu^{27d} A. Poreba³⁶ D. M. Portillo Quintero^{157a}
S. Pospisil¹³³ M. A. Postill¹⁴⁰ P. Postolache^{27c} K. Potamianos¹⁶⁸ P. A. Potepa^{86a} I. N. Potrap³⁸ C. J. Potter³²
H. Potti¹ J. Poveda¹⁶⁴ M. E. Pozo Astigarraga³⁶ A. Prades Ibanez¹⁶⁴ J. Pretel⁵⁴ D. Price¹⁰² M. Primavera^{70a}
M. A. Principe Martin¹⁰⁰ R. Privara¹²³ T. Procter⁵⁹ M. L. Proffitt¹³⁹ N. Proklova¹²⁹ K. Prokofiev^{64c}
G. Proto¹¹¹ J. Proudfoot⁶ M. Przybycien^{86a} W. W. Przygoda^{86b} A. Psallidas⁴⁶ J. E. Puddefoot¹⁴⁰
D. Pudzha³⁷ D. Pyatiizbyantseva³⁷ J. Qian¹⁰⁷ D. Qichen¹⁰² Y. Qin¹³ T. Qiu⁵² A. Quadt⁵⁵
M. Queitsch-Maitland¹⁰² G. Quetant⁵⁶ R. P. Quinn¹⁶⁵ G. Rabanal Bolanos⁶¹ D. Rafanoharana⁵⁴
F. Ragusa^{71a,71b} J. L. Rainbolt³⁹ J. A. Raine⁵⁶ S. Rajagopalan²⁹ E. Ramakoti³⁷ I. A. Ramirez-Berend³⁴
K. Ran^{48,14e} N. P. Rapheeha^{33g} H. Rasheed^{27b} V. Raskina¹²⁸ D. F. Rassloff^{63a} A. Rastogi^{17a} S. Rave¹⁰¹
B. Ravina⁵⁵ I. Ravinovich¹⁷⁰ M. Raymond³⁶ A. L. Read¹²⁶ N. P. Readioff¹⁴⁰ D. M. Rebuzzi^{73a,73b}
G. Redlinger²⁹ A. S. Reed¹¹¹ K. Reeves²⁶ J. A. Reidelsturz¹⁷² D. Reikher¹⁵² A. Rej⁴⁹ C. Rembser³⁶
M. Renda^{27b} M. B. Rendel¹¹¹ F. Renner⁴⁸ A. G. Rennie¹⁶⁰ A. L. Rescia⁴⁸ S. Resconi^{71a} M. Ressegotti^{57b,57a}
S. Rettie³⁶ J. G. Reyes Rivera¹⁰⁸ E. Reynolds^{17a} O. L. Rezanova³⁷ P. Reznicek¹³⁴ H. Riani^{35d} N. Ribaric⁹²
E. Ricci^{78a,78b} R. Richter¹¹¹ S. Richter^{47a,47b} E. Richter-Was^{86b} M. Ridel¹²⁸ S. Ridouani^{35d} P. Rieck¹¹⁸
P. Riedler³⁶ E. M. Riefel^{47a,47b} J. O. Rieger¹¹⁵ M. Rijssenbeek¹⁴⁶ M. Rimoldi³⁶ L. Rinaldi^{23b,23a} T. T. Rinn²⁹
M. P. Rinnagel¹¹⁰ G. Ripellino¹⁶² I. Riu¹³ J. C. Rivera Vergara¹⁶⁶ F. Rizatdinova¹²² E. Rizvi⁹⁵
B. R. Roberts^{17a} S. H. Robertson^{105,n} D. Robinson³² C. M. Robles Gajardo^{138f} M. Robles Manzano¹⁰¹
A. Robson⁵⁹ A. Rocchi^{76a,76b} C. Roda^{74a,74b} S. Rodriguez Bosca³⁶ Y. Rodriguez Garcia^{22a}
A. Rodriguez Rodriguez⁵⁴ A. M. Rodríguez Vera¹¹⁶ S. Roe³⁶ J. T. Roemer¹⁶⁰ A. R. Roepe-Gier¹³⁷ J. Roggel¹⁷²
O. Røhne¹²⁶ R. A. Rojas¹⁰⁴ C. P. A. Roland¹²⁸ J. Roloff²⁹ A. Romaniouk³⁷ E. Romano^{73a,73b} M. Romano^{23b}
A. C. Romero Hernandez¹⁶³ N. Rompotis⁹³ L. Roos¹²⁸ S. Rosati^{75a} B. J. Rosser³⁹ E. Rossi¹²⁷ E. Rossi^{72a,72b}
L. P. Rossi⁶¹ L. Rossini⁵⁴ R. Rosten¹²⁰ M. Rotaru^{27b} B. Rottler⁵⁴ C. Rougier⁹⁰ D. Rousseau⁶⁶
D. Rousso⁴⁸ A. Roy¹⁶³ S. Roy-Garand¹⁵⁶ A. Rozanov¹⁰³ Z. M. A. Rozario⁵⁹ Y. Rozen¹⁵¹
A. Rubio Jimenez¹⁶⁴ A. J. Ruby⁹³ V. H. Ruelas Rivera¹⁸ T. A. Ruggeri¹ A. Ruggiero¹²⁷ A. Ruiz-Martinez¹⁶⁴
A. Rummeler³⁶ Z. Rurikova⁵⁴ N. A. Rusakovich³⁸ H. L. Russell¹⁶⁶ G. Russo^{75a,75b} J. P. Rutherford⁷
S. Rutherford Colmenares³² K. Rybacki⁹² M. Rybar¹³⁴ E. B. Rye¹²⁶ A. Ryzhov⁴⁴ J. A. Sabater Iglesias⁵⁶
P. Sabatini¹⁶⁴ H. F.-W. Sadrozinski¹³⁷ F. Safai Tehrani^{75a} B. Safarzadeh Samani¹³⁵ S. Saha¹ M. Sahinsoy¹¹¹
A. Saibel¹⁶⁴ M. Saimpert¹³⁶ M. Saito¹⁵⁴ T. Saito¹⁵⁴ A. Sala^{71a,71b} D. Salamani³⁶ A. Salmikov¹⁴⁴ J. Salt¹⁶⁴
A. Salvador Salas¹⁵² D. Salvatore^{43b,43a} F. Salvatore¹⁴⁷ A. Salzburger³⁶ D. Sammel⁵⁴ E. Sampson⁹²
D. Sampsonidis^{153,z} D. Sampsonidou¹²⁴ J. Sánchez¹⁶⁴ V. Sanchez Sebastian¹⁶⁴ H. Sandaker¹²⁶ C. O. Sander⁴⁸
J. A. Sandesara¹⁰⁴ M. Sandhoff¹⁷² C. Sandoval^{22b} D. P. C. Sankey¹³⁵ T. Sano⁸⁸ A. Sansoni⁵³ L. Santi^{75a,75b}
C. Santoni⁴⁰ H. Santos^{131a,131b} A. Santra¹⁷⁰ E. Sanzani^{23b,23a} K. A. Saoucha¹⁶¹ J. G. Saraiva^{131a,131d}
J. Sardain⁷ O. Sasaki⁸⁴ K. Sato¹⁵⁸ C. Sauer^{63b} F. Sauerburger⁵⁴ E. Sauvan⁴ P. Savard^{156,e} R. Sawada¹⁵⁴
C. Sawyer¹³⁵ L. Sawyer⁹⁸ I. Sayago Galvan¹⁶⁴ C. Sbarra^{23b} A. Sbrizzi^{23b,23a} T. Scanlon⁹⁷ J. Schaarschmidt¹³⁹
U. Schäfer¹⁰¹ A. C. Schaffer^{66,44} D. Schaile¹¹⁰ R. D. Schamberger¹⁴⁶ C. Scharf¹⁸ M. M. Schefer¹⁹
V. A. Schegelsky³⁷ D. Scheirich¹³⁴ F. Schenck¹⁸ M. Schernau¹⁶⁰ C. Scheulen⁵⁵ C. Schiavi^{57b,57a}
M. Schioppa^{43b,43a} B. Schlag^{144,s} K. E. Schleicher⁵⁴ S. Schlenker³⁶ J. Schmeing¹⁷² M. A. Schmidt¹⁷²
K. Schmieden¹⁰¹ C. Schmitt¹⁰¹ N. Schmitt¹⁰¹ S. Schmitt⁴⁸ L. Schoeffel¹³⁶ A. Schoening^{63b} P. G. Scholer³⁴
E. Schopf¹²⁷ M. Schott¹⁰¹ J. Schovancova³⁶ S. Schramm⁵⁶ T. Schroer⁵⁶ H.-C. Schultz-Coulon^{63a}
M. Schumacher⁵⁴ B. A. Schumm¹³⁷ Ph. Schune¹³⁶ A. J. Schuy¹³⁹ H. R. Schwartz¹³⁷ A. Schwartzman¹⁴⁴
T. A. Schwarz¹⁰⁷ Ph. Schwemling¹³⁶ R. Schwienhorst¹⁰⁸ A. Sciandra²⁹ G. Sciolla²⁶ F. Scuri^{74a}
C. D. Sebastiani⁹³ K. Sedlaczek¹¹⁶ P. Seema¹⁸ S. C. Seidel¹¹³ A. Seiden¹³⁷ B. D. Seidlitz⁴¹ C. Seitz⁴⁸
J. M. Seixas^{83b} G. Sekhniaidze^{72a} L. Selem⁶⁰ N. Semprini-Cesari^{23b,23a} D. Sengupta⁵⁶ V. Senthilkumar¹⁶⁴
L. Serin⁶⁶ L. Serkin^{69a,69b} M. Sessa^{76a,76b} H. Severini¹²¹ F. Sforza^{57b,57a} A. Sfyrla⁵⁶ Q. Sha^{14a}
E. Shabalina⁵⁵ A. H. Shah³² R. Shaheen¹⁴⁵ J. D. Shahinian¹²⁹ D. Shaked Renous¹⁷⁰ L. Y. Shan^{14a}

M. Shapiro^{17a}, A. Sharma³⁶, A. S. Sharma¹⁶⁵, P. Sharma⁸⁰, P. B. Shatalov³⁷, K. Shaw¹⁴⁷, S. M. Shaw¹⁰², A. Shcherbakova³⁷, Q. Shen^{62c,5}, D. J. Sheppard¹⁴³, P. Sherwood⁹⁷, L. Shi⁹⁷, X. Shi^{14a}, C. O. Shimmin¹⁷³, J. D. Shinner⁹⁶, I. P. J. Shipsey¹²⁷, S. Shirabe⁸⁹, M. Shiyakova^{38,gg}, J. Shlomi¹⁷⁰, M. J. Shochet³⁹, J. Shojaii¹⁰⁶, D. R. Shope¹²⁶, B. Shrestha¹²¹, S. Shrestha^{120,hh}, E. M. Shrif^{33g}, M. J. Shroff¹⁶⁶, P. Sicho¹³², A. M. Sickles¹⁶³, E. Sideras Haddad^{33g}, A. C. Sidley¹¹⁵, A. Sidoti^{23b}, F. Siegert⁵⁰, Dj. Sijacki¹⁵, F. Sili⁹¹, J. M. Silva⁵², M. V. Silva Oliveira²⁹, S. B. Silverstein^{47a}, S. Simion⁶⁶, R. Simoniello³⁶, E. L. Simpson¹⁰², H. Simpson¹⁴⁷, L. R. Simpson¹⁰⁷, N. D. Simpson⁹⁹, S. Simsek⁸², S. Sindhu⁵⁵, P. Sinervo¹⁵⁶, S. Singh¹⁵⁶, S. Sinha⁴⁸, S. Sinha¹⁰², M. Sioli^{23b,23a}, I. Siral³⁶, E. Sitnikova⁴⁸, J. Sjölin^{47a,47b}, A. Skaf⁵⁵, E. Skorda²⁰, P. Skubic¹²¹, M. Slawinska⁸⁷, V. Smakhtin¹⁷⁰, B. H. Smart¹³⁵, S. Yu. Smirnov³⁷, Y. Smirnov³⁷, L. N. Smirnova^{37,k}, O. Smirnova⁹⁹, A. C. Smith⁴¹, D. R. Smith¹⁶⁰, E. A. Smith³⁹, H. A. Smith¹²⁷, J. L. Smith¹⁰², R. Smith¹⁴⁴, M. Smizanska⁹², K. Smolek¹³³, A. A. Snesarev³⁷, S. R. Snider¹⁵⁶, H. L. Snoek¹¹⁵, S. Snyder²⁹, R. Sobie^{166,n}, A. Soffer¹⁵², C. A. Solans Sanchez³⁶, E. Yu. Soldatov³⁷, U. Soldevila¹⁶⁴, A. A. Solodkov³⁷, S. Solomon²⁶, A. Soloshenko³⁸, K. Solovieva⁵⁴, O. V. Solovyanov⁴⁰, P. Sommer³⁶, A. Sonay¹³, W. Y. Song^{157b}, A. Sopczak¹³³, A. L. Sapiro⁹⁷, F. Sopkova^{28b}, J. D. Sorenson¹¹³, I. R. Sotarriva Alvarez¹⁵⁵, V. Sothilingam^{63a}, O. J. Soto Sandoval^{138c,138b}, S. Sottocornola⁶⁸, R. Soualah¹⁶¹, Z. Soumami^{35e}, D. South⁴⁸, N. Soybelman¹⁷⁰, S. Spagnolo^{70a,70b}, M. Spalla¹¹¹, D. Sperlich⁵⁴, G. Spigo³⁶, S. Spinali⁹², D. P. Spiteri⁵⁹, M. Spousta¹³⁴, E. J. Staats³⁴, R. Stamen^{63a}, A. Stampekis²⁰, M. Standke²⁴, E. Stanecka⁸⁷, W. Stanek-Maslouska⁴⁸, M. V. Stange⁵⁰, B. Stanislaus^{17a}, M. M. Stanitzki⁴⁸, B. Stapf⁴⁸, E. A. Starchenko³⁷, G. H. Stark¹³⁷, J. Stark⁹⁰, P. Staroba¹³², P. Starovoitov^{63a}, S. Stärz¹⁰⁵, R. Staszewski⁸⁷, G. Stavropoulos⁴⁶, J. Steentoft¹⁶², P. Steinberg²⁹, B. Stelzer^{143,157a}, H. J. Stelzer¹³⁰, O. Stelzer-Chilton^{157a}, H. Stenzel⁵⁸, T. J. Stevenson¹⁴⁷, G. A. Stewart³⁶, J. R. Stewart¹²², M. C. Stockton³⁶, G. Stoicea^{27b}, M. Stolarski^{131a}, S. Stonjek¹¹¹, A. Straessner⁵⁰, J. Strandberg¹⁴⁵, S. Strandberg^{47a,47b}, M. Stratmann¹⁷², M. Strauss¹²¹, T. Strebler¹⁰³, P. Strizenec^{28b}, R. Ströhmer¹⁶⁷, D. M. Strom¹²⁴, R. Stroynowski⁴⁴, A. Strubig^{47a,47b}, S. A. Stucci²⁹, B. Stugu¹⁶, J. Stupak¹²¹, N. A. Styles⁴⁸, D. Su¹⁴⁴, S. Su^{62a}, W. Su^{62d}, X. Su^{62a}, D. Suchy^{28a}, K. Sugizaki¹⁵⁴, V. V. Sulini³⁷, M. J. Sullivan⁹³, D. M. S. Sultan¹²⁷, L. Sultanaliev³⁷, S. Sultansoy^{3b}, T. Sumida⁸⁸, S. Sun¹⁰⁷, S. Sun¹⁷¹, O. Sunneborn Gudnadottir¹⁶², N. Sur¹⁰³, M. R. Sutton¹⁴⁷, H. Suzuki¹⁵⁸, M. Svatos¹³², M. Swiatlowski^{157a}, T. Swirski¹⁶⁷, I. Sykora^{28a}, M. Sykora¹³⁴, T. Sykora¹³⁴, D. Ta¹⁰¹, K. Tackmann^{48,ff}, A. Taffard¹⁶⁰, R. Tafirout^{157a}, J. S. Tafoya Vargas⁶⁶, Y. Takubo⁸⁴, M. Talby¹⁰³, A. A. Talyshev³⁷, K. C. Tam^{64b}, N. M. Tamir¹⁵², A. Tanaka¹⁵⁴, J. Tanaka¹⁵⁴, R. Tanaka⁶⁶, M. Tanasini^{57b,57a}, Z. Tao¹⁶⁵, S. Tapia Araya^{138f}, S. Tapprogge¹⁰¹, A. Tarek Abouelfadl Mohamed¹⁰⁸, S. Tarem¹⁵¹, K. Tariq^{14a}, G. Tarna^{27b}, G. F. Tartarelli^{71a}, M. J. Tartarin⁹⁰, P. Tas¹³⁴, M. Tasevsky¹³², E. Tassi^{43b,43a}, A. C. Tate¹⁶³, G. Tateno¹⁵⁴, Y. Tayalati^{35e,ii}, G. N. Taylor¹⁰⁶, W. Taylor^{157b}, A. S. Tee¹⁷¹, R. Teixeira De Lima¹⁴⁴, P. Teixeira-Dias⁹⁶, J. J. Teoh¹⁵⁶, K. Terashi¹⁵⁴, J. Terron¹⁰⁰, S. Terzo¹³, M. Testa⁵³, R. J. Teuscher^{156,n}, A. Thaler⁷⁹, O. Theiner⁵⁶, N. Themistokleous⁵², T. Theveneaux-Pelzer¹⁰³, O. Thielmann¹⁷², D. W. Thomas⁹⁶, J. P. Thomas²⁰, E. A. Thompson^{17a}, P. D. Thompson²⁰, E. Thomson¹²⁹, R. E. Thornberry⁴⁴, Y. Tian⁵⁵, V. Tikhomirov^{37,k}, Yu. A. Tikhonov³⁷, S. Timoshenko³⁷, D. Timoshyn¹³⁴, E. X. L. Ting¹, P. Tipton¹⁷³, S. H. Tlou^{33g}, K. Todome¹⁵⁵, S. Todorova-Nova¹³⁴, S. Todt⁵⁰, L. Toffolin^{69a,69c}, M. Togawa⁸⁴, J. Tojo⁸⁹, S. Tokár^{28a}, K. Tokushuku⁸⁴, O. Toldaiev⁶⁸, R. Tombs³², M. Tomoto^{84,112}, L. Tompkins^{144,s}, K. W. Topolnicki^{86b}, E. Torrence¹²⁴, H. Torres⁹⁰, E. Torró Pastor¹⁶⁴, M. Toscani³⁰, C. Toscirri³⁹, M. Tost¹¹, D. R. Tovey¹⁴⁰, A. Traet¹⁶, I. S. Trandafir^{27b}, T. Trefzger¹⁶⁷, A. Tricoli²⁹, I. M. Trigger^{157a}, S. Trincaz-Duvoid¹²⁸, D. A. Trischuk²⁶, B. Trocmé⁶⁰, L. Truong^{33c}, M. Trzebinski⁸⁷, A. Trzupek⁸⁷, F. Tsai¹⁴⁶, M. Tsai¹⁰⁷, A. Tsiamis^{153,z}, P. V. Tsiarehka³⁷, S. Tsigaridas^{157a}, A. Tsirigotis^{153,aa}, V. Tsiskaridze¹⁵⁶, E. G. Tskhadadze^{150a}, M. Tsopoulou¹⁵³, Y. Tsujikawa⁸⁸, I. I. Tsukerman³⁷, V. Tsulaia^{17a}, S. Tsuno⁸⁴, K. Tsurii¹¹⁹, D. Tsybychev¹⁴⁶, Y. Tu^{64b}, A. Tudorache^{27b}, V. Tudorache^{27b}, A. N. Tuna⁶¹, S. Turchikhin^{57b,57a}, I. Turk Cakir^{3a}, R. Turra^{71a}, T. Turtuvshin^{38,jj}, P. M. Tuts⁴¹, S. Tzamarias^{153,z}, E. Tzovara¹⁰¹, F. Ukegawa¹⁵⁸, P. A. Ulloa Poblete^{138c,138b}, E. N. Umaka²⁹, G. Unal³⁶, A. Undrus²⁹, G. Unel¹⁶⁰, J. Urban^{28b}, P. Urquijo¹⁰⁶, P. Urrejola^{138a}, G. Usai⁸, R. Ushioda¹⁵⁵, M. Usman¹⁰⁹, Z. Uysal⁸², V. Vacek¹³³, B. Vachon¹⁰⁵, T. Vafeiadis³⁶, A. Vaitkus⁹⁷, C. Valderanis¹¹⁰, E. Valdes Santurio^{47a,47b}, M. Valente^{157a}, S. Valentinetti^{23b,23a}, A. Valero¹⁶⁴, E. Valiente Moreno¹⁶⁴, A. Vallier⁹⁰, J. A. Valls Ferrer¹⁶⁴, D. R. Van Arneman¹¹⁵, T. R. Van Daalen¹³⁹, A. Van Der Graaf⁴⁹, P. Van Gemmeren⁶, M. Van Rijnbach¹²⁶

S. Van Stroud⁹⁷ I. Van Vulpen¹¹⁵ P. Vana¹³⁴ M. Vanadia^{76a,76b} W. Vandelli³⁶ E. R. Vandewall¹²²
D. Vannicola¹⁵² L. Vannoli⁵³ R. Vari^{75a} E. W. Varnes⁷ C. Varni^{17b} T. Varol¹⁴⁹ D. Varouchas⁶⁶
L. Varriale¹⁶⁴ K. E. Varvell¹⁴⁸ M. E. Vasile^{27b} L. Vaslin⁸⁴ G. A. Vasquez¹⁶⁶ A. Vasyukov³⁸ R. Vavricka¹⁰¹
F. Vazeille⁴⁰ T. Vazquez Schroeder³⁶ J. Veatch³¹ V. Vecchio¹⁰² M. J. Veen¹⁰⁴ I. Veliscek²⁹ L. M. Veloce¹⁵⁶
F. Veloso^{131a,131c} S. Veneziano^{75a} A. Ventura^{70a,70b} S. Ventura Gonzalez¹³⁶ A. Verbitskyi¹¹¹ M. Verducci^{74a,74b}
C. Vergis⁹⁵ M. Verissimo De Araujo^{83b} W. Verkerke¹¹⁵ J. C. Vermeulen¹¹⁵ C. Vernieri¹⁴⁴ M. Vessella¹⁰⁴
M. C. Vetterli^{143,e} A. Vgenopoulos^{153,z} N. Viaux Maira^{138f} T. Vickey¹⁴⁰ O. E. Vickey Boeriu¹⁴⁰
G. H. A. Viehhauser¹²⁷ L. Vigani^{63b} M. Villa^{23b,23a} M. Villaplana Perez¹⁶⁴ E. M. Villhauer⁵² E. Vilucchi⁵³
M. G. Vincter³⁴ G. S. Virdee²⁰ A. Visibile¹¹⁵ C. Vittori³⁶ I. Vivarelli^{23b,23a} E. Voevodina¹¹¹ F. Vogel¹¹⁰
J. C. Voigt⁵⁰ P. Vokac¹³³ Yu. Volkotrub^{86b} J. Von Ahnen⁴⁸ E. Von Toerne²⁴ B. Vormwald³⁶ V. Vorobel¹³⁴
K. Vorobev³⁷ M. Vos¹⁶⁴ K. Voss¹⁴² M. Vozak¹¹⁵ L. Vozdecky¹²¹ N. Vranjes¹⁵ M. Vranjes Milosavljevic¹⁵
M. Vreeswijk¹¹⁵ N. K. Vu^{62d,62c} R. Vuillemet³⁶ O. Vujinovic¹⁰¹ I. Vukotic³⁹ S. Wada¹⁵⁸ C. Wagner¹⁰⁴
J. M. Wagner^{17a} W. Wagner¹⁷² S. Wahdan¹⁷² H. Wahlberg⁹¹ M. Wakida¹¹² J. Walder¹³⁵ R. Walker¹¹⁰
W. Walkowiak¹⁴² A. Wall¹²⁹ E. J. Wallin⁹⁹ T. Wamorkar⁶ A. Z. Wang¹³⁷ C. Wang¹⁰¹ C. Wang¹¹
H. Wang^{17a} J. Wang^{64c} R.-J. Wang¹⁰¹ R. Wang⁶¹ R. Wang⁶ S. M. Wang¹⁴⁹ S. Wang^{62b} S. Wang^{14a}
T. Wang^{62a} W. T. Wang⁸⁰ W. Wang^{14a} X. Wang^{14c} X. Wang¹⁶³ X. Wang^{62c} Y. Wang^{62d} Y. Wang^{14c}
Z. Wang¹⁰⁷ Z. Wang^{62d,51,62c} Z. Wang¹⁰⁷ A. Warburton¹⁰⁵ R. J. Ward²⁰ N. Warrack⁵⁹ S. Waterhouse⁹⁶
A. T. Watson²⁰ H. Watson⁵⁹ M. F. Watson²⁰ E. Watton^{59,135} G. Watts¹³⁹ B. M. Waugh⁹⁷ J. M. Webb⁵⁴
C. Weber²⁹ H. A. Weber¹⁸ M. S. Weber¹⁹ S. M. Weber^{63a} C. Wei^{62a} Y. Wei⁵⁴ A. R. Weidberg¹²⁷
E. J. Weik¹¹⁸ J. Weingarten⁴⁹ M. Weirich¹⁰¹ C. Weiser⁵⁴ C. J. Wells⁴⁸ T. Wenaus²⁹ B. Wendland⁴⁹
T. Wengler³⁶ N. S. Wenke¹¹¹ N. Wermes²⁴ M. Wessels^{63a} A. M. Wharton⁹² A. S. White⁶¹ A. White⁸
M. J. White¹ D. Whiteson¹⁶⁰ L. Wickremasinghe¹²⁵ W. Wiedenmann¹⁷¹ M. Wielers¹³⁵ C. Wiglesworth⁴²
D. J. Wilbern¹²¹ H. G. Wilkens³⁶ J. J. H. Wilkinson³² D. M. Williams⁴¹ H. H. Williams¹²⁹ S. Williams³²
S. Willocq¹⁰⁴ B. J. Wilson¹⁰² P. J. Windischhofer³⁹ F. I. Winkel³⁰ F. Winklmeier¹²⁴ B. T. Winter⁵⁴
J. K. Winter¹⁰² M. Wittgen¹⁴⁴ M. Wobisch⁹⁸ T. Wojtkowski⁶⁰ Z. Wolffs¹¹⁵ J. Wollrath¹⁶⁰ M. W. Wolter⁸⁷
H. Wolters^{131a,131c} M. C. Wong¹³⁷ E. L. Woodward⁴¹ S. D. Worm⁴⁸ B. K. Wosiek⁸⁷ K. W. Woźniak⁸⁷
S. Wozniowski⁵⁵ K. Wraight⁵⁹ C. Wu²⁰ M. Wu^{14d} M. Wu¹¹⁴ S. L. Wu¹⁷¹ X. Wu⁵⁶ Y. Wu^{62a} Z. Wu⁴
J. Wuerzinger^{111,v} T. R. Wyatt¹⁰² B. M. Wynne⁵² S. Xella⁴² L. Xia^{14c} M. Xia^{14b} J. Xiang^{64c} M. Xie^{62a}
X. Xie^{62a} S. Xin^{14a,14e} A. Xiong¹²⁴ J. Xiong^{17a} D. Xu^{14a} H. Xu^{62a} L. Xu^{62a} R. Xu¹²⁹ T. Xu¹⁰⁷ Y. Xu^{14b}
Z. Xu⁵² Z. Xu^{14c} B. Yabsley¹⁴⁸ S. Yacoob^{33a} Y. Yamaguchi¹⁵⁵ E. Yamashita¹⁵⁴ H. Yamauchi¹⁵⁸
T. Yamazaki^{17a} Y. Yamazaki⁸⁵ J. Yan^{62c} S. Yan⁵⁹ Z. Yan¹⁰⁴ H. J. Yang^{62c,62d} H. T. Yang^{62a} S. Yang^{62a}
T. Yang^{64c} X. Yang³⁶ X. Yang^{14a} Y. Yang⁴⁴ Y. Yang^{62a} Z. Yang^{62a} W.-M. Yao^{17a} H. Ye^{14c} H. Ye⁵⁵
J. Ye^{14a} S. Ye²⁹ X. Ye^{62a} Y. Yeh⁹⁷ I. Yeletsikh³⁸ B. K. Yeo^{17b} M. R. Yexley⁹⁷ T. P. Yildirim¹²⁷ P. Yin⁴¹
K. Yorita¹⁶⁹ S. Younas^{27b} C. J. S. Young³⁶ C. Young¹⁴⁴ C. Yu^{14a,14e} Y. Yu^{62a} M. Yuan¹⁰⁷ R. Yuan^{62d,62c}
L. Yue⁹⁷ M. Zaazoua^{62a} B. Zabinski⁸⁷ E. Zaid⁵² Z. K. Zak⁸⁷ T. Zakareishvili¹⁶⁴ N. Zakharchuk³⁴
S. Zambito⁵⁶ J. A. Zamora Saa^{138d,138b} J. Zang¹⁵⁴ D. Zanzi⁵⁴ O. Zaplatilek¹³³ C. Zeitnitz¹⁷² H. Zeng^{14a}
J. C. Zeng¹⁶³ D. T. Zenger Jr.²⁶ O. Zenin³⁷ T. Ženiš^{28a} S. Zenz⁹⁵ S. Zerradi^{35a} D. Zerwas⁶⁶ M. Zhai^{14a,14e}
D. F. Zhang¹⁴⁰ J. Zhang^{62b} J. Zhang⁶ K. Zhang^{14a,14e} L. Zhang^{62a} L. Zhang^{14c} P. Zhang^{14a,14e} R. Zhang¹⁷¹
S. Zhang¹⁰⁷ S. Zhang⁴⁴ T. Zhang¹⁵⁴ X. Zhang^{62c} X. Zhang^{62b} Y. Zhang^{62c,5} Y. Zhang⁹⁷ Y. Zhang^{14c}
Z. Zhang^{17a} Z. Zhang⁶⁶ H. Zhao¹³⁹ T. Zhao^{62b} Y. Zhao¹³⁷ Z. Zhao^{62a} Z. Zhao^{62a} A. Zhemchugov³⁸
J. Zheng^{14c} K. Zheng¹⁶³ X. Zheng^{62a} Z. Zheng¹⁴⁴ D. Zhong¹⁶³ B. Zhou¹⁰⁷ H. Zhou⁷ N. Zhou^{62c}
Y. Zhou^{14c} Y. Zhou⁷ C. G. Zhu^{62b} J. Zhu¹⁰⁷ X. Zhu^{62d} Y. Zhu^{62c} Y. Zhu^{62a} X. Zhuang^{14a} K. Zhukov³⁷
N. I. Zimine³⁸ J. Zinsser^{63b} M. Ziolkowski¹⁴² L. Živković¹⁵ A. Zoccoli^{23b,23a} K. Zoch⁶¹ T. G. Zorbas¹⁴⁰
O. Zormpa⁴⁶ W. Zou⁴¹ and L. Zwalinski³⁶

(ATLAS Collaboration)

¹Department of Physics, University of Adelaide, Adelaide, Australia²Department of Physics, University of Alberta, Edmonton, Alberta, Canada^{3a}Department of Physics, Ankara University, Ankara, Türkiye

- ^{3b}*Division of Physics, TOBB University of Economics and Technology, Ankara, Türkiye*
⁴*LAPP, Université Savoie Mont Blanc, CNRS/IN2P3, Annecy, France*
⁵*APC, Université Paris Cité, CNRS/IN2P3, Paris, France*
- ⁶*High Energy Physics Division, Argonne National Laboratory, Argonne, Illinois, USA*
⁷*Department of Physics, University of Arizona, Tucson, Arizona, USA*
⁸*Department of Physics, University of Texas at Arlington, Arlington, Texas, USA*
⁹*Physics Department, National and Kapodistrian University of Athens, Athens, Greece*
¹⁰*Physics Department, National Technical University of Athens, Zografou, Greece*
¹¹*Department of Physics, University of Texas at Austin, Austin, Texas, USA*
¹²*Institute of Physics, Azerbaijan Academy of Sciences, Baku, Azerbaijan*
- ¹³*Institut de Física d'Altes Energies (IFAE), Barcelona Institute of Science and Technology, Barcelona, Spain*
^{14a}*Institute of High Energy Physics, Chinese Academy of Sciences, Beijing, China*
^{14b}*Physics Department, Tsinghua University, Beijing, China*
^{14c}*Department of Physics, Nanjing University, Nanjing, China*
^{14d}*School of Science, Shenzhen Campus of Sun Yat-sen University, China*
^{14e}*University of Chinese Academy of Science (UCAS), Beijing, China*
¹⁵*Institute of Physics, University of Belgrade, Belgrade, Serbia*
- ¹⁶*Department for Physics and Technology, University of Bergen, Bergen, Norway*
^{17a}*Physics Division, Lawrence Berkeley National Laboratory, Berkeley, California, USA*
^{17b}*University of California, Berkeley, California, USA*
¹⁸*Institut für Physik, Humboldt Universität zu Berlin, Berlin, Germany*
- ¹⁹*Albert Einstein Center for Fundamental Physics and Laboratory for High Energy Physics, University of Bern, Bern, Switzerland*
- ²⁰*School of Physics and Astronomy, University of Birmingham, Birmingham, United Kingdom*
^{21a}*Department of Physics, Bogazici University, Istanbul, Türkiye*
^{21b}*Department of Physics Engineering, Gaziantep University, Gaziantep, Türkiye*
^{21c}*Department of Physics, Istanbul University, Istanbul, Türkiye*
- ^{22a}*Facultad de Ciencias y Centro de Investigaciones, Universidad Antonio Nariño, Bogotá, Colombia*
^{22b}*Departamento de Física, Universidad Nacional de Colombia, Bogotá, Colombia*
- ^{23a}*Dipartimento di Fisica e Astronomia A. Righi, Università di Bologna, Bologna, Italy*
^{23b}*INFN Sezione di Bologna, Italy*
²⁴*Physikalisches Institut, Universität Bonn, Bonn, Germany*
- ²⁵*Department of Physics, Boston University, Boston, Massachusetts, USA*
²⁶*Department of Physics, Brandeis University, Waltham, Massachusetts, USA*
^{27a}*Transilvania University of Brasov, Brasov, Romania*
- ^{27b}*Horia Hulubei National Institute of Physics and Nuclear Engineering, Bucharest, Romania*
^{27c}*Department of Physics, Alexandru Ioan Cuza University of Iasi, Iasi, Romania*
^{27d}*National Institute for Research and Development of Isotopic and Molecular Technologies, Physics Department, Cluj-Napoca, Romania*
^{27e}*National University of Science and Technology Politehnica, Bucharest, Romania*
^{27f}*West University in Timisoara, Timisoara, Romania*
^{27g}*Faculty of Physics, University of Bucharest, Bucharest, Romania*
- ^{28a}*Faculty of Mathematics, Physics and Informatics, Comenius University, Bratislava, Slovak Republic*
^{28b}*Department of Subnuclear Physics, Institute of Experimental Physics of the Slovak Academy of Sciences, Kosice, Slovak Republic*
- ²⁹*Physics Department, Brookhaven National Laboratory, Upton, New York, USA*
- ³⁰*Universidad de Buenos Aires, Facultad de Ciencias Exactas y Naturales, Departamento de Física, y CONICET, Instituto de Física de Buenos Aires (IFIBA), Buenos Aires, Argentina*
³¹*California State University, Fresno, California, USA*
- ³²*Cavendish Laboratory, University of Cambridge, Cambridge, United Kingdom*
^{33a}*Department of Physics, University of Cape Town, Cape Town, South Africa*
^{33b}*iThemba Labs, Western Cape, South Africa*
^{33c}*Department of Mechanical Engineering Science, University of Johannesburg, Johannesburg, South Africa*
- ^{33d}*National Institute of Physics, University of the Philippines Diliman, Quezon City, Metro Manila, Philippines*
^{33e}*University of South Africa, Department of Physics, Pretoria, South Africa*
^{33f}*University of Zululand, KwaDlangezwa, South Africa*
^{33g}*School of Physics, University of the Witwatersrand, Johannesburg, South Africa*

- ³⁴*Department of Physics, Carleton University, Ottawa, Ontario, Canada*
- ^{35a}*Faculté des Sciences Ain Chock, Réseau Universitaire de Physique des Hautes Energies—Université Hassan II, Casablanca, Morocco*
- ^{35b}*Faculté des Sciences, Université Ibn-Tofail, Kénitra, Morocco*
- ^{35c}*Faculté des Sciences Semlalia, Université Cadi Ayyad, LPHEA-Marrakech, Morocco*
- ^{35d}*LPMR, Faculté des Sciences, Université Mohamed Premier, Oujda, Morocco*
- ^{35e}*Faculté des Sciences, Université Mohammed V, Rabat, Morocco*
- ^{35f}*Institute of Applied Physics, Mohammed VI Polytechnic University, Ben Guerir, Morocco*
- ³⁶*CERN, Geneva, Switzerland*
- ³⁷*Affiliated with an institute covered by a cooperation agreement with CERN*
- ³⁸*Affiliated with an international laboratory covered by a cooperation agreement with CERN*
- ³⁹*Enrico Fermi Institute, University of Chicago, Chicago, Illinois, USA*
- ⁴⁰*LPC, Université Clermont Auvergne, CNRS/IN2P3, Clermont-Ferrand, France*
- ⁴¹*Nevis Laboratory, Columbia University, Irvington, New York, USA*
- ⁴²*Niels Bohr Institute, University of Copenhagen, Copenhagen, Denmark*
- ^{43a}*Dipartimento di Fisica, Università della Calabria, Rende, Italy*
- ^{43b}*INFN Gruppo Collegato di Cosenza, Laboratori Nazionali di Frascati, Italy*
- ⁴⁴*Physics Department, Southern Methodist University, Dallas, Texas, USA*
- ⁴⁵*Physics Department, University of Texas at Dallas, Richardson, Texas, USA*
- ⁴⁶*National Centre for Scientific Research “Demokritos,” Agia Paraskevi, Greece*
- ^{47a}*Department of Physics, Stockholm University, Stockholm, Sweden*
- ^{47b}*Oskar Klein Centre, Stockholm, Sweden*
- ⁴⁸*Deutsches Elektronen-Synchrotron DESY, Hamburg and Zeuthen, Germany*
- ⁴⁹*Fakultät Physik, Technische Universität Dortmund, Dortmund, Germany*
- ⁵⁰*Institut für Kern- und Teilchenphysik, Technische Universität Dresden, Dresden, Germany*
- ⁵¹*Department of Physics, Duke University, Durham, North Carolina, USA*
- ⁵²*SUPA—School of Physics and Astronomy, University of Edinburgh, Edinburgh, United Kingdom*
- ⁵³*INFN e Laboratori Nazionali di Frascati, Frascati, Italy*
- ⁵⁴*Physikalisches Institut, Albert-Ludwigs-Universität Freiburg, Freiburg, Germany*
- ⁵⁵*II. Physikalisches Institut, Georg-August-Universität Göttingen, Göttingen, Germany*
- ⁵⁶*Département de Physique Nucléaire et Corpusculaire, Université de Genève, Genève, Switzerland*
- ^{57a}*Dipartimento di Fisica, Università di Genova, Genova, Italy*
- ^{57b}*INFN Sezione di Genova, Italy*
- ⁵⁸*II. Physikalisches Institut, Justus-Liebig-Universität Giessen, Giessen, Germany*
- ⁵⁹*SUPA—School of Physics and Astronomy, University of Glasgow, Glasgow, United Kingdom*
- ⁶⁰*LPSC, Université Grenoble Alpes, CNRS/IN2P3, Grenoble INP, Grenoble, France*
- ⁶¹*Laboratory for Particle Physics and Cosmology, Harvard University, Cambridge, Massachusetts, USA*
- ^{62a}*Department of Modern Physics and State Key Laboratory of Particle Detection and Electronics, University of Science and Technology of China, Hefei, China*
- ^{62b}*Institute of Frontier and Interdisciplinary Science and Key Laboratory of Particle Physics and Particle Irradiation (MOE), Shandong University, Qingdao, China*
- ^{62c}*School of Physics and Astronomy, Shanghai Jiao Tong University, Key Laboratory for Particle Astrophysics and Cosmology (MOE), SKLPPC, Shanghai, China*
- ^{62d}*Tsung-Dao Lee Institute, Shanghai, China*
- ^{62e}*School of Physics and Microelectronics, Zhengzhou University, China*
- ^{63a}*Kirchhoff-Institut für Physik, Ruprecht-Karls-Universität Heidelberg, Heidelberg, Germany*
- ^{63b}*Physikalisches Institut, Ruprecht-Karls-Universität Heidelberg, Heidelberg, Germany*
- ^{64a}*Department of Physics, Chinese University of Hong Kong, Shatin, N.T., Hong Kong, China*
- ^{64b}*Department of Physics, University of Hong Kong, Hong Kong, China*
- ^{64c}*Department of Physics and Institute for Advanced Study, Hong Kong University of Science and Technology, Clear Water Bay, Kowloon, Hong Kong, China*
- ⁶⁵*Department of Physics, National Tsing Hua University, Hsinchu, Taiwan*
- ⁶⁶*IJCLab, Université Paris-Saclay, CNRS/IN2P3, 91405, Orsay, France*
- ⁶⁷*Centro Nacional de Microelectrónica (IMB-CNM-CSIC), Barcelona, Spain*
- ⁶⁸*Department of Physics, Indiana University, Bloomington, Indiana, USA*
- ^{69a}*INFN Gruppo Collegato di Udine, Sezione di Trieste, Udine, Italy*
- ^{69b}*ICTP, Trieste, Italy*
- ^{69c}*Dipartimento Politecnico di Ingegneria e Architettura, Università di Udine, Udine, Italy*
- ^{70a}*INFN Sezione di Lecce, Lecce, Italy*
- ^{70b}*Dipartimento di Matematica e Fisica, Università del Salento, Lecce, Italy*

- ^{71a}INFN Sezione di Milano, Milano, Italy
^{71b}Dipartimento di Fisica, Università di Milano, Milano, Italy
^{72a}INFN Sezione di Napoli, Napoli, Italy
^{72b}Dipartimento di Fisica, Università di Napoli, Napoli, Italy
^{73a}INFN Sezione di Pavia, Pavia, Italy
^{73b}Dipartimento di Fisica, Università di Pavia, Pavia, Italy
^{74a}INFN Sezione di Pisa, Pisa, Italy
^{74b}Dipartimento di Fisica E. Fermi, Università di Pisa, Pisa, Italy
^{75a}INFN Sezione di Roma, Roma, Italy
^{75b}Dipartimento di Fisica, Sapienza Università di Roma, Roma, Italy
^{76a}INFN Sezione di Roma Tor Vergata, Roma, Italy
^{76b}Dipartimento di Fisica, Università di Roma Tor Vergata, Roma, Italy
^{77a}INFN Sezione di Roma Tre, Italy
^{77b}Dipartimento di Matematica e Fisica, Università Roma Tre, Roma, Italy
^{78a}INFN-TIFPA, Trento, Italy
^{78b}Università degli Studi di Trento, Trento, Italy
⁷⁹Universität Innsbruck, Department of Astro and Particle Physics, Innsbruck, Austria
⁸⁰University of Iowa, Iowa City, Iowa, USA
⁸¹Department of Physics and Astronomy, Iowa State University, Ames, Iowa, USA
⁸²Istinye University, Sariyer, Istanbul, Türkiye
^{83a}Departamento de Engenharia Elétrica, Universidade Federal de Juiz de Fora (UFJF), Juiz de Fora, Brazil
^{83b}Universidade Federal do Rio De Janeiro COPPE/EE/IF, Rio de Janeiro, Brazil
^{83c}Instituto de Física, Universidade de São Paulo, São Paulo, Brazil
^{83d}Rio de Janeiro State University, Rio de Janeiro, Brazil
^{83e}Federal University of Bahia, Bahia, Brazil
⁸⁴KEK, High Energy Accelerator Research Organization, Tsukuba, Japan
⁸⁵Graduate School of Science, Kobe University, Kobe, Japan
^{86a}AGH University of Krakow, Faculty of Physics and Applied Computer Science, Krakow, Poland
^{86b}Marian Smoluchowski Institute of Physics, Jagiellonian University, Krakow, Poland
⁸⁷Institute of Nuclear Physics Polish Academy of Sciences, Krakow, Poland
⁸⁸Faculty of Science, Kyoto University, Kyoto, Japan
⁸⁹Research Center for Advanced Particle Physics and Department of Physics, Kyushu University, Fukuoka, Japan
⁹⁰L2IT, Université de Toulouse, CNRS/IN2P3, UPS, Toulouse, France
⁹¹Instituto de Física La Plata, Universidad Nacional de La Plata and CONICET, La Plata, Argentina
⁹²Physics Department, Lancaster University, Lancaster, United Kingdom
⁹³Oliver Lodge Laboratory, University of Liverpool, Liverpool, United Kingdom
⁹⁴Department of Experimental Particle Physics, Jožef Stefan Institute and Department of Physics, University of Ljubljana, Ljubljana, Slovenia
⁹⁵School of Physics and Astronomy, Queen Mary University of London, London, United Kingdom
⁹⁶Department of Physics, Royal Holloway University of London, Egham, United Kingdom
⁹⁷Department of Physics and Astronomy, University College London, London, United Kingdom
⁹⁸Louisiana Tech University, Ruston, Louisiana, USA
⁹⁹Fysiska institutionen, Lunds universitet, Lund, Sweden
¹⁰⁰Departamento de Física Teórica C-15 and CIAFF, Universidad Autónoma de Madrid, Madrid, Spain
¹⁰¹Institut für Physik, Universität Mainz, Mainz, Germany
¹⁰²School of Physics and Astronomy, University of Manchester, Manchester, United Kingdom
¹⁰³CPPM, Aix-Marseille Université, CNRS/IN2P3, Marseille, France
¹⁰⁴Department of Physics, University of Massachusetts, Amherst, Massachusetts, USA
¹⁰⁵Department of Physics, McGill University, Montreal, Quebec, Canada
¹⁰⁶School of Physics, University of Melbourne, Victoria, Australia
¹⁰⁷Department of Physics, University of Michigan, Ann Arbor, Michigan, USA
¹⁰⁸Department of Physics and Astronomy, Michigan State University, East Lansing, Michigan, USA
¹⁰⁹Group of Particle Physics, University of Montreal, Montreal, Quebec, Canada
¹¹⁰Fakultät für Physik, Ludwig-Maximilians-Universität München, München, Germany
¹¹¹Max-Planck-Institut für Physik (Werner-Heisenberg-Institut), München, Germany
¹¹²Graduate School of Science and Kobayashi-Maskawa Institute, Nagoya University, Nagoya, Japan
¹¹³Department of Physics and Astronomy, University of New Mexico, Albuquerque, New Mexico, USA

- ¹¹⁴*Institute for Mathematics, Astrophysics and Particle Physics,
Radboud University/Nikhef, Nijmegen, Netherlands*
- ¹¹⁵*Nikhef National Institute for Subatomic Physics and University of Amsterdam, Amsterdam, Netherlands*
- ¹¹⁶*Department of Physics, Northern Illinois University, DeKalb, Illinois, USA*
- ^{117a}*New York University Abu Dhabi, Abu Dhabi, United Arab Emirates*
- ^{117b}*United Arab Emirates University, Al Ain, United Arab Emirates*
- ¹¹⁸*Department of Physics, New York University, New York, New York, USA*
- ¹¹⁹*Ochanomizu University, Otsuka, Bunkyo-ku, Tokyo, Japan*
- ¹²⁰*The Ohio State University, Columbus OH, United States of America*
- ¹²¹*Homer L. Dodge Department of Physics and Astronomy,
University of Oklahoma, Norman, Oklahoma, USA*
- ¹²²*Department of Physics, Oklahoma State University, Stillwater, Oklahoma, USA*
- ¹²³*Palacký University, Joint Laboratory of Optics, Olomouc, Czech Republic*
- ¹²⁴*Institute for Fundamental Science, University of Oregon, Eugene, Oregon, USA*
- ¹²⁵*Graduate School of Science, Osaka University, Osaka, Japan*
- ¹²⁶*Department of Physics, University of Oslo, Oslo, Norway*
- ¹²⁷*Department of Physics, Oxford University, Oxford, United Kingdom*
- ¹²⁸*LPNHE, Sorbonne Université, Université Paris Cité, CNRS/IN2P3, Paris, France*
- ¹²⁹*Department of Physics, University of Pennsylvania, Philadelphia, Pennsylvania, USA*
- ¹³⁰*Department of Physics and Astronomy, University of Pittsburgh, Pittsburgh, Pennsylvania, USA*
- ^{131a}*Laboratório de Instrumentação e Física Experimental de Partículas—LIP, Lisboa, Portugal*
- ^{131b}*Departamento de Física, Faculdade de Ciências, Universidade de Lisboa, Lisboa, Portugal*
- ^{131c}*Departamento de Física, Universidade de Coimbra, Coimbra, Portugal*
- ^{131d}*Centro de Física Nuclear da Universidade de Lisboa, Lisboa, Portugal*
- ^{131e}*Departamento de Física, Universidade do Minho, Braga, Portugal*
- ^{131f}*Departamento de Física Teórica y del Cosmos, Universidad de Granada, Granada, Spain*
- ^{131g}*Departamento de Física, Instituto Superior Técnico, Universidade de Lisboa, Lisboa, Portugal*
- ¹³²*Institute of Physics of the Czech Academy of Sciences, Prague, Czech Republic*
- ¹³³*Czech Technical University in Prague, Prague, Czech Republic*
- ¹³⁴*Charles University, Faculty of Mathematics and Physics, Prague, Czech Republic*
- ¹³⁵*Particle Physics Department, Rutherford Appleton Laboratory, Didcot, United Kingdom*
- ¹³⁶*IRFU, CEA, Université Paris-Saclay, Gif-sur-Yvette, France*
- ¹³⁷*Santa Cruz Institute for Particle Physics, University of California Santa Cruz,
Santa Cruz, California, USA*
- ^{138a}*Departamento de Física, Pontificia Universidad Católica de Chile, Santiago, Chile*
- ^{138b}*Millennium Institute for Subatomic physics at high energy frontier (SAPHIR), Santiago, Chile*
- ^{138c}*Instituto de Investigación Multidisciplinario en Ciencia y Tecnología, y Departamento de Física,
Universidad de La Serena, Chile*
- ^{138d}*Universidad Andres Bello, Department of Physics, Santiago, Chile*
- ^{138e}*Instituto de Alta Investigación, Universidad de Tarapacá, Arica, Chile*
- ^{138f}*Departamento de Física, Universidad Técnica Federico Santa María, Valparaíso, Chile*
- ¹³⁹*Department of Physics, University of Washington, Seattle, Washington, USA*
- ¹⁴⁰*Department of Physics and Astronomy, University of Sheffield, Sheffield, United Kingdom*
- ¹⁴¹*Department of Physics, Shinshu University, Nagano, Japan*
- ¹⁴²*Department Physik, Universität Siegen, Siegen, Germany*
- ¹⁴³*Department of Physics, Simon Fraser University, Burnaby, British Columbia, Canada*
- ¹⁴⁴*SLAC National Accelerator Laboratory, Stanford, California, USA*
- ¹⁴⁵*Department of Physics, Royal Institute of Technology, Stockholm, Sweden*
- ¹⁴⁶*Departments of Physics and Astronomy, Stony Brook University, Stony Brook, New York, USA*
- ¹⁴⁷*Department of Physics and Astronomy, University of Sussex, Brighton, United Kingdom*
- ¹⁴⁸*School of Physics, University of Sydney, Sydney, Australia*
- ¹⁴⁹*Institute of Physics, Academia Sinica, Taipei, Taiwan*
- ^{150a}*E. Andronikashvili Institute of Physics, Iv. Javakhishvili Tbilisi State University, Tbilisi, Georgia*
- ^{150b}*High Energy Physics Institute, Tbilisi State University, Tbilisi, Georgia*
- ^{150c}*University of Georgia, Tbilisi, Georgia*
- ¹⁵¹*Department of Physics, Technion, Israel Institute of Technology, Haifa, Israel*
- ¹⁵²*Raymond and Beverly Sackler School of Physics and Astronomy, Tel Aviv University, Tel Aviv, Israel*
- ¹⁵³*Department of Physics, Aristotle University of Thessaloniki, Thessaloniki, Greece*
- ¹⁵⁴*International Center for Elementary Particle Physics and Department of Physics, University of Tokyo,
Tokyo, Japan*

- ¹⁵⁵*Department of Physics, Tokyo Institute of Technology, Tokyo, Japan*
¹⁵⁶*Department of Physics, University of Toronto, Toronto, Ontario, Canada*
^{157a}*TRIUMF, Vancouver, British Columbia, Canada*
^{157b}*Department of Physics and Astronomy, York University, Toronto, Ontario, Canada*
¹⁵⁸*Division of Physics and Tomonaga Center for the History of the Universe, Faculty of Pure and Applied Sciences, University of Tsukuba, Tsukuba, Japan*
¹⁵⁹*Department of Physics and Astronomy, Tufts University, Medford, Massachusetts, USA*
¹⁶⁰*Department of Physics and Astronomy, University of California Irvine, Irvine, California, USA*
¹⁶¹*University of Sharjah, Sharjah, United Arab Emirates*
¹⁶²*Department of Physics and Astronomy, University of Uppsala, Uppsala, Sweden*
¹⁶³*Department of Physics, University of Illinois, Urbana, Illinois, USA*
¹⁶⁴*Instituto de Física Corpuscular (IFIC), Centro Mixto Universidad de Valencia—CSIC, Valencia, Spain*
¹⁶⁵*Department of Physics, University of British Columbia, Vancouver, British Columbia, Canada*
¹⁶⁶*Department of Physics and Astronomy, University of Victoria, Victoria, British Columbia, Canada*
¹⁶⁷*Fakultät für Physik und Astronomie, Julius-Maximilians-Universität Würzburg, Würzburg, Germany*
¹⁶⁸*Department of Physics, University of Warwick, Coventry, United Kingdom*
¹⁶⁹*Waseda University, Tokyo, Japan*
¹⁷⁰*Department of Particle Physics and Astrophysics, Weizmann Institute of Science, Rehovot, Israel*
¹⁷¹*Department of Physics, University of Wisconsin, Madison, Wisconsin, USA*
¹⁷²*Fakultät für Mathematik und Naturwissenschaften, Fachgruppe Physik, Bergische Universität Wuppertal, Wuppertal, Germany*
¹⁷³*Department of Physics, Yale University, New Haven, Connecticut, USA*

^aDeceased.

^bAlso at Department of Physics, King's College London, London, United Kingdom.

^cAlso at Institute of Physics, Azerbaijan Academy of Sciences, Baku, Azerbaijan.

^dAlso at Lawrence Livermore National Laboratory, Livermore, USA.

^eAlso at TRIUMF, Vancouver, British Columbia, Canada.

^fAlso at Department of Physics, University of Thessaly, Greece.

^gAlso at An-Najah National University, Nablus, Palestine.

^hAlso at Department of Physics, University of Fribourg, Fribourg, Switzerland.

ⁱAlso at Department of Physics, Westmont College, Santa Barbara, USA.

^jAlso at Departament de Física de la Universitat Autònoma de Barcelona, Barcelona, Spain.

^kAlso at Affiliated with an institute covered by a cooperation agreement with CERN.

^lAlso at The Collaborative Innovation Center of Quantum Matter (CICQM), Beijing, China.

^mAlso at Università di Napoli Parthenope, Napoli, Italy.

ⁿAlso at Institute of Particle Physics (IPP), Canada.

^oAlso at University of Colorado Boulder, Department of Physics, Colorado, USA.

^pAlso at Borough of Manhattan Community College, City University of New York, New York, New York, USA.

^qAlso at National Institute of Physics, University of the Philippines Diliman (Philippines), Philippines.

^rAlso at Department of Financial and Management Engineering, University of the Aegean, Chios, Greece.

^sAlso at Department of Physics, Stanford University, Stanford, California, USA.

^tAlso at Centro Studi e Ricerche Enrico Fermi, Italy.

^uAlso at Institutio Catalana de Recerca i Estudis Avancats, ICREA, Barcelona, Spain.

^vAlso at Technical University of Munich, Munich, Germany.

^wAlso at Yeditepe University, Physics Department, Istanbul, Türkiye.

^xAlso at Institute of Theoretical Physics, Ilia State University, Tbilisi, Georgia.

^yAlso at CERN, Geneva, Switzerland.

^zAlso at Center for Interdisciplinary Research and Innovation (CIRI-AUTH), Thessaloniki, Greece.

^{aa}Also at Hellenic Open University, Patras, Greece.

^{bb}Also at Center for High Energy Physics, Peking University, China.

^{cc}Also at Department of Physics, Stellenbosch University, South Africa.

^{dd}Also at Department of Physics, California State University, Sacramento, USA.

^{ee}Also at Département de Physique Nucléaire et Corpusculaire, Université de Genève, Genève, Switzerland.

^{ff}Also at Institut für Experimentalphysik, Universität Hamburg, Hamburg, Germany.

^{gg}Also at Institute for Nuclear Research and Nuclear Energy (INRNE) of the Bulgarian Academy of Sciences, Sofia, Bulgaria.

^{hh}Also at Washington College, Chestertown, Maryland, USA.

ⁱⁱAlso at Institute of Applied Physics, Mohammed VI Polytechnic University, Ben Guerir, Morocco.

^{jj}Also at Institute of Physics and Technology, Mongolian Academy of Sciences, Ulaanbaatar, Mongolia.